UNIVERSITI TEKNOLOGI MARA

MOLECULAR INTERACTIONS AND BEHAVIOR OF KRATOM ALKALOIDS-MITRAGYNINE, 7-HYDROXYMITRAGYNINE, AND MITRAGYNINE PSEUDOINDOXYL-IN DPPC LIPID BILAYERS: A MOLECULAR DYNAMICS SIMULATION STUDY

NUR SYAHIRUNELISA BINTI MOHD ZUBRI

MSc

February 2026

UNIVERSITI TEKNOLOGI MARA

MOLECULAR INTERACTIONS AND BEHAVIOR OF KRATOM ALKALOIDS-MITRAGYNINE, 7-HYDROXYMITRAGYNINE, AND MITRAGYNINE PSEUDOINDOXYL-IN DPPC LIPID BILAYERS: A MOLECULAR DYNAMICS SIMULATION STUDY

NUR SYAHIRUNELISA BINTI MOHD ZUBRI

Thesis submitted in fulfilment
of the requirements for the degree of
Master of Science

Faculty of Pharmacy

February 2026

CONFIRMATION BY PANEL OF EXAMINERS

I certify that a Panel of Examiners has met on 03 June 2025 to conduct the final examination of Nur Syahirunehsa Binti Mohd Zubri on her Master of Science thesis entitled "Molecular Interactions and Behavior of Kratom Alkaloids- Mitragynine, 7-Hydroxymitragynine, and Mitragynine Pseudoindoxyl-in DPPC Lipid Bilayers: A Molecular Dynamics Simulation Study" in accordance with Universiti Teknologi MARA Act 1976 (Akta 173). The Panel of Examiner recommends that the student be awarded the relevant degree. The Panel of Examiners was as follows:

Mahmathi Karuppannan, PhD
Associate Professior
Faculty of Pharmacy
Universiti Teknologi MARA
(Chairman)

Zafirah Liyana Abdullah, PhD
Senior Lecturer
Faculty of Pharmacy
Universiti Teknologi MARA
(Internal Examiner)

Khairul Bariyyah Abd Halim, PhD
Senior Lecturer
Kuliyyah of Science
International Islamic University Malaysia
(External Examiner)

PROFESOR DR HJH. ZURAEDA IBRAHIM
Dean
Institute of Postgraduates Studies
Universiti Teknologi MARA
Date: 20 February 2026

AUTHOR'S DECLARATION

I declare that the work in this thesis was carried out in accordance with the regulations of Universiti Teknologi MARA. It is original and is the results of my own work, unless otherwise indicated or acknowledged as referenced work. This thesis has not been submitted to any other academic institution or non-academic institution for any degree or qualification.

I, hereby, acknowledge that I have been supplied with the Academic Rules and Regulations for Post Graduate, Universiti Teknologi MARA, regulating the conduct of my study and research.

Name of Student	Nur Syahirunelisa binti Mohd Zubri
Student ID. No.	2023715661
Program	Master of Science - PH780
Faculty	Faculty of Pharmacy
Thesis Title	Molecular Interactions and Behavior of Kratom Alkaloids- Mitragynine, 7-Hydroxymitragynine, and Mitragynine Pseudoindoxyl-in DPPC Lipid Bilayers: A Molecular Dynamics Simulation Study

Signature of student

Date February 2026

ABSTRACT

Kratom *(Mitragyna speciosa)*, a tropical plant native to Southeast Asia, has gained global attention for its potential therapeutic effects, particularly as an alternative to classical opioids for pain management and opioid withdrawal. Its primary alkaloids—mitragynine, 7-hydroxymitragynine, and mitragynine pseudoindoxyl— exhibit analgesic properties through partial agonism at u- opioid receptors, with a lower risk of respiratory depression compared to traditional opioids. However, despite its widespread use, kratom remains controversial due to limited clinical data and regulatory concerns which hindered its acceptance in mainstream medicine. To address this gap, we employed molecular dynamics (MD) simulations to investigate the interactions of kratom alkaloids with DPPC lipid bilayers, a model system for biological membranes. The simulations reveal that all three alkaloids exhibit amphiphilic behavior, able to rapidly diffuse into the hydrophobic core and localize near the lipid phosphate groups. The preference position allows the alkaloids for the hydrogen bonding with both lipid headgroups and water molecules at the interface. Mitragynine demonstrates the fastest diffusion into the bilayer, followed by 7-hydroxymitragynine and mitragynine pseudoindoxyl. However, at higher concentrations, molecular aggregation in the aqueous environment delays or prevents penetration of the alkaloids into the bilayer, particularly for 7-hydroxymitragynine. These findings highlight the critical role of molecular assembly in modulating membrane interactions and provide insights into the factors influencing the bioavailability and pharmacological efficacy of kratom alkaloids. This study represents a significant step toward understanding the membrane interactions of kratom alkaloids, offering a foundation for future experimental validation and rational drug design. By elucidating the mechanisms underlying their behavior in lipid bilayers, this study contributes to the growing body of knowledge on kratom's therapeutic potential and safety profile. These insights could inform the development of safer and more effective opioid analogs, addressing the ongoing need for alternatives to classical opioids in pain management and addiction treatment.

ACKNOWLEDGEMENT

First and foremost, I wish to thank Allah for giving me the opportunity to embark on my MSc and for completing this long and challenging journey successfully.

I would like to express my deepest gratitude to my supervisor, Dr Siti Azma Jusoh, for her invaluable guidance, insightful advice, and constant support throughout this research journey. Their expertise and encouragement have been instrumental in the completion of this thesis.

My appreciation extends to the members of the Bioinformatics Lab at the Faculty of Pharmacy, UiTM Puncak Alam, for providing the facilities and assistance crucial to my research. I am especially grateful to my colleagues and friends, Nur Aqasyah Amran, Nur Alya Amirah Azhar and Nur Hannani Ahmad Rozani for their help with this project and for their constant support throughout my master's journey.

I would like to express my heartfelt gratitude to my co-supervisor, Dr. Nazahiyah Rodzli, for her invaluable guidance and continuous support throughout my research. I am also deeply thankful to Dr. Fatahiya Mohamed Tap for generously providing access to a GPU computer, which was crucial for running simulations and completing my study. A thanks goes to Dr. Zafirah Liyana Abdullah for her teaching and helping me with essential skills and techniques that significantly contributed to the success of this work.

My deepest gratitude goes to my parents Mohd Zubri Jaafar and
for their unwavering support and for providing me with a solid education. To my siblings, Nur Syahirunnisa' and Ahmad Emir Erfan, thank you for being my constant cheerleaders and for your unwavering love, support, and encouragement. Your belief in me has been a source of strength and motivation throughout this journey.

Finally, I dedicate this thesis to my parents and family for their vision and determination to educate me. This piece of victory is dedicated to all of you. Alhamdulillah.

TABLE OF CONTENTS

LIST OF TABLES

LIST OF FIGURES

LIST OF ABBREVIATIONS

Abbreviations

ATB	Automated Topology Builder
AMBER	Assisted Model Building with Energy Refinement
AMPA	a-Amino-3-hydroxy-5-methyl-4-isoxazolepropionic acid receptor
DPPC	Dipalmitoylphosphatidylcholine
CADD	Computer-Aided Drug Design
CB2	Cannabinoid Receptor Type 2
CHARMM	Chemistry at Harvard Macromolecular Mechanics
DOR	Delta Opioid Receptor
DEA	Drug Enforcement Administration
FDA	Food and Drug Administration
GABAB	Gamma-Aminobutyric Acid B receptor
GPCR	G-protein-coupled receptor
GROMACS	Groningen Machine for Chemical Simulations
HLM	Human Liver Microsomes
KOR	Kappa Opioid Receptor
MD	Molecular Dynamic
MOR	Mu Opioid Receptor
MLM	Mouse Liver Microsomes

NMBA	N-Methyl-D-Aspartate receptor
7-OH	7-hydroxymitragynine
MP	Mitragynine pseudoindoxyl
NAMD	Nanoscale Molecular Dynamics
PBC	Periodic Boundary Condition
PDB	Protein Data Bank
RMSD	Root Mean Square Deviation
SPC	Simple Point Charge
WHO	World Health Organization

CHAPTER 1
INTRODUCTION

1.1 Research Background

Mitragyna speciosa, also known as kratom, is a plant native to Southeast Asia that has grown in popularity in many Western countries, largely as an alternative to illegal opioids (Brown et al., 2017). Traditionally, kratom is consumed by local users—particularly rural farmers, laborers, and indigenous communities—for its medicinal benefits, such as analgesic effects, pain relief, mood enhancement, improved physical endurance, and as an energy stimulant (Hossain et al., 2021; Veltri & Grundmann, 2019). Kratom contains at least 50 types of alkaloids, including mitragynine, the unique active compound to kratom representing the highest amount in the leaf extract (Kruegel & Grundmann, 2018; Todd et al., 2020). There are studies reporting the evidence of the kratom's alkaloid interacting with opioid receptors to produce analgesic effects, making it useful for managing chronic pain conditions (Kruegel et al., 2019) with users claiming it helps alleviate withdrawal symptoms and reduce dependency on prescription painkillers or illicit drugs (Todd et al., 2020).

Despite its widespread use, the U.S. Food and Drug Administration (FDA) has not approved kratom for medical purposes (Ellis et al., 2020). The U.S. Drug Enforcement Administration (DEA) previously considered classifying kratom as an illegal substance but ultimately suspended the decision following public opposition, particularly from heavy consumers and advocacy groups (Todd et al., 2020). Over the past decade, kratom use has surged in the United States, with many users advocating its effectiveness in managing physical pain, mood disorders, and anxiety. For some users, kratom has served as a viable alternative where conventional treatments have either failed or caused intolerable side effects. A significant number of users have turned to kratom as a means to reduce or discontinue the use of prescription or illicit opioids, making it particularly relevant in the context of the ongoing opioid crisis (Kruegel et al., 2019).

However, despite its potential benefits, kratom use is associated with several side effects and health risks. Common adverse effects include nausea, vomiting, constipation, dizziness, and dry mouth, particularly when consumed in high doses (Veltri & Grundmann, 2019; Warner et al., 2016). Some users experience drowsiness and impaired motor coordination, increasing the risk of accidents or injuries (Brown et al., 2017). Long-term or excessive use may lead to dependence and withdrawal symptoms such as irritability, muscle pain, insomnia, and mood disturbances (Kruegel et al., 2019). Additionally, cases of increased heart rate, high blood pressure, and liver toxicity have been reported, raising concerns about kratom's safety profile (Hassan et al., 2023). However, limited data on controlled clinical studies were conducted to validate kratom's therapeutic effects or assess its long-term risks. Moreover, kratom is primarily distributed through unregulated online markets and is often used without medical supervision, raising concerns about product quality, contamination, and potential misuse (Kruegel et al., 2019). Given the lack of standardized regulations and scientific research, further studies are needed to better understand the pharmacological effects, safety, and potential medical applications of kratom.

In Malaysia, kratom has been added to the Poison Schedule List since the introduction of the Poison Act 1952 (Malaysia Poison Act, 1952). In the 2003 amendment to the Act, mitragynine, an alkaloid found in kratom leaves, was classified as a poisonous substance in both the First and Third Schedules due to its psychotropic properties. Despite legal measures to categorize kratom as a poisonous substance under the Poisons Act 1952, the users of kratom still increases. The Poisons Act is not to curb consumption and addiction, but rather to regulate the possession and distribution of poisonous substances (S. Khalil et al., 2020). On the other hand, Thailand has adopted a more lenient stance, decriminalizing kratom in 2021 for medicinal and personal use—a significant departure from its earlier prohibition under the 1943 Kratom Act (Charoenratana et al., 2021). Similarly, kratom remains a legal commodity in Indonesia, though its regulation has garnered increased attention. Following the 2019 discovery of 12 tons of kratom intended for export, especially in Palangkaraya, Central Kalimantan, Indonesia authorities have stepped up security measures to oversee its trade (S. Khalil et al., 2020).

Among the alkaloids of kratom (Todd et al., 2020), mitragynine and 7-hydroxymitragynine have been heavily investigated by FDA (Ellis et al., 2020). Mitragynine represents 66% by mass of crude alkaloid extracts and 7-

hydroxymitragynine constitutes <1% of the total alkaloid content in the leaves (Anand & Hosanagar, 2022). Both alkaloids are mainly responsible for kratom's effects (Prozialeck et al., 2012) and primary opioid-like components (Obeng et al., 2020). In human embryonic kidney 293 (HEK) cells, both compounds were shown to strongly interact with the ^t-opioid receptor (MOR) as partial agonists, while also weak competitive agonists for the /(-opioid receptor (KOR) and 5-opioid receptor (DOR) (Ellis et al., 2020; Kruegel et al., 2019). Another kratom alkaloid, mitragynine pseudoindoxyl, displays strong interaction for MOR and DOR, but shows moderate affinity for KOR in *in vitro* study (Varadi et al., 2016). Fentanyl, a synthetic opioid, is a potent agonist of the *i* -opioid receptor (MOR), reported to be over 50-fold stronger than morphine (Manabe et al., 2019). Its high lipophilicity allows it to rapidly partition from the solvent into membrane lipids, facilitating direct binding to the MOR orthosteric pocket via the lipid bilayer (Sutcliffe et al., 2022; Vo et al., 2021). Similarly, mitragynine has been identified as a partial MOR agonist, exhibiting opioid-like effects while differing in its binding dynamics and pharmacological profile. Studies suggest that while fentanyl remains the most potent MOR agonist, mitragynine demonstrates significant activity, surpassing morphine in some models (Matsumoto et al., 2004; Takayama et al., 2002). Given the rising interest in kratom as a potential alternative to traditional opioids, understanding its interaction with lipid bilayers and MOR activation is crucial in assessing both its therapeutic potential and safety profile.

MD simulations have been used extensively in drug development (Swift et al., 2016; Sztain et al., 2021; Tang et al., 2021). This computational method provides insight at the atomic level of small molecule interactions with target receptors and other molecules in the system such as lipids and water molecules (Ismail & Jusoh, 2017; Jusoh & Helms, 2011; Swift et al., 2016). By leveraging on the capabilities of MD simulations coupled with wet lab experiments, target specific drugs can be designed with reduced early development cost in shorter duration compared to conventional drug development.

Drugs and drug-like plant extracts interact with plasma membranes to reach the intracellular target locations. Understanding drug-membrane permeability is crucial in order to understand the mechanism of action of drug binding to target receptors (Hossain et al., 2021; Kopec et al., 2013). The physicochemical properties determine the efficiency of the compounds to cross the barrier of phospholipid bilayers. In the case of opioids, fentanyl and morphine have been shown to use different routes to bind the opioid receptors (Sutcliffe et al., 2022; Vo et al., 2021). In addition, a cannabinoid was

also reported to directly enter the binding pocket of the cannabinoid CB2 receptor via the lipid membranes (Hurst et al., 2010).

In this study, MD simulations was employed to investigate the behavior and interactions of kratom alkaloids—mitragynine, 7-hydroxymitragynine, and mitragynine pseudoindoxyl—with DPPC lipid bilayers, which served as a model for the cell membrane. The main goal was to study the permeability of these alkaloids and their interactions with lipid bilayers, providing insights into their mechanisms of action and potential therapeutic applications. This study advances our understanding of the alkaloids mechanisms of action and lays the groundwork for the development of safer and more effective opioid analogs, for alternatives in the pain and drug addiction issues.

1.2 Problem Statement

In Malaysia, kratom is often linked to issues such as misuse among teenagers, involvement in the black market, and the smuggling of its leaves to other countries. Classified as a psychoactive substance, kratom falls under the Poisons Act 1952, which regulates its sale and distribution. Despite this classification, the cultivation of kratom is neither explicitly prohibited nor deemed illegal (S. Khalil et al., 2020). Furthermore, the illegal export of kratom has become increasingly prevalent, especially as its market value continues to rise (Domnic et al., 2021). This surge is largely driven by the fact that processing and selling kratom products are explicitly prohibited under Malaysian law.

Despite growing interest in the pharmacological potential of these alkaloids, research data on the molecular mechanisms governing their interaction, especially with cell membranes remain poorly understood. This lack of knowledge significantly hampers the ability to predict their bioavailability, efficacy, and potential toxicity in biological systems. Addressing this knowledge gap is essential for advancing the development of safe and effective therapeutics of kratom alkaloids.

1.3 Research Objectives

This study aims to investigate the behavior of kratom alkaloids (mitragynine, 7-hydroxymitragynine, and mitragynine pseudoindoxyl) in DPPC lipid bilayers,

elucidating how alkaloid type and concentration (number of alkaloids per system) influence the permeability and interactions with the membrane.

1. To construct atomistic model systems of kratom alkaloids in DPPC lipid bilayers based on different concentration (number of alkaloid) in both homogeneous (single type of alkaloid) and heterogeneous (mixed type of alkaloid) systems.
2. To perform MD simulations to the alkaloid-DPPC model systems.
3. To quantify the behavior of the alkaloids within the DPPC lipid bilayer using computational analyses based on permeability and binding interactions.

1.4 Significant of the Study

The molecular interactions between kratom alkaloids—mitragynine, 7-hydroxymitragynine, and mitragynine pseudoindoxyl—with DPPC lipid bilayers hold great potential for enhancing our understanding of the pharmacological effects of these compounds. The significance of this study lies in its contribution to bridging the critical knowledge gap regarding the molecular interactions between kratom alkaloids and lipid bilayers, which serve as model systems for cell membranes. Despite increasing interest in the pharmacological potential of these alkaloids, limited data on how they interact at the membrane level has hindered the ability to predict their bioavailability, efficacy, and potential toxicity.

This study directly addresses this problem by employing MD simulations to unravel the positioning, penetration depth, and dynamic interactions of mitragynine, 7-hydroxymitragynine, and mitragynine pseudoindoxyl within DPPC lipid bilayers. The findings highlight how these alkaloids differentially interact with membrane components, affecting membrane structure and dynamics—critical factors influencing drug absorption and distribution. By providing atomic-level insights into their membrane interactions, this study advances the understanding of how kratom alkaloids behave in biological systems, thereby aiding in the prediction of their pharmacokinetic and pharmacodynamic properties. Indirectly, these insights contribute to the safer and more effective therapeutic application of kratom alkaloids, supporting drug design efforts while also guiding future experimental studies to validate these computational findings.

1.5 Scope and Limitation

Among more 50 known kratom alkaloids, the study only investigated the three alkaloids: mitragynine, 7-hydroxymitragynine and mitragynine pseudoindoxyl. The goal of the study is to understand the molecular interactions of these alkaloids with membrane lipid bilayer using MD simulation method. However, it is important to note the limitation of the method: (1) Simplified model systems: The models often simplify biological environments, potentially limiting the accuracy of the findings. (2) Methodological constraints: MD simulations rely on force fields and modeling approximations that may not fully represent molecular behavior, while the limited temporal and spatial scales of simulations restrict their comprehensiveness. (3) Biological validation: Although MD simulations reveal important molecular insights, the observed interactions and their physiological implications require experimental validation to confirm accuracy. (4) Timescale limitations: Traditional MD simulations are computationally demanding and limited in duration, but modern advancements in hardware, particularly the use of graphics processing units (GPUs) designed for gaming and graphics, significantly accelerate simulations, allowing more extensive analyses. Despite these challenges, MD simulations remain a powerful tool for exploring the complex interactions between kratom alkaloids and lipid bilayers.

CHAPTER 2
LITERATURE REVIEW

2.1 Introduction of Kratom

Mitragyna speciosa, commonly known as the kratom, is a tropical plant native to the rainforests of Southeast Asia. It thrives in warm, humid environments and isnaturally found in countries such as Thailand, Malaysia, Indonesia, and Papua New Guinea. This tree is predominantly cultivated for its leaves, which have been traditionally valued for their medicinal, cultural, and recreational uses (Ahmad & Aziz, 2012). The leaves of kratom are often consumed in various ways—either chewed fresh, brewed into a tea, or dried and smoked—depending on regional practices and intended effects. Belonging to the Rubiaceae family, the same botanical group as coffee plants, *Mitragyna speciosa* is particularly renowned for its unique pharmacological properties. For centuries, communities in Thailand and neighboring regions have recognized kratom's stimulating effects in low doses, which enhance endurance and productivity, as well as its pain-relieving and sedative properties in higher doses (Kim et al., 2012). Traditionally, laborers and farmers in Southeast Asia have used kratom to combat fatigue and increase stamina, while others have relied on its analgesic effects to manage pain and discomfort. Beyond its medicinal applications, kratom has also played a role in social and cultural settings, often used in traditional ceremonies or communal gatherings. Despite its long history of use, scientific research on kratom's bioactive compounds, particularly mitragynine and 7-hydroxymitragynine, continues to evolve, aiming to better understand its pharmacokinetics, mechanisms of action, and potential therapeutic benefits. Table 2.1 provides the taxonomic classification of *Mitragyna speciosa* based on data from the Global Biodiversity Information Facility (GBIF), categorizing it within the broader context of plant taxonomy to highlight its botanical lineage and classification.

Table 2.1
Taxonomic Classification for *Mitragyna Speciosa* According To The Global Biodiversity Information Facility (GBIF)

Kingdom	Plantae
Phylum	Tracheophyta
Class	Magnoliopsida
Order	Gentianales
Family	Rubiaceae
Genus	Mitragyna Korth
Species	*Mitragyna speciosa* (Korth.) Havil

Note: Kratom Book: Health and Socio-Economic Prospects, (Maharani & Prasetyo, 2022)

Historically, kratom played a vital role in the lives of laborers in rural Southeast Asia, especially in Malaysia and Thailand (Tanguay, 2011), where its leaves were used as an herbal remedy for treating common ailments such as diarrhea, fever, and minor wounds (Assanangkornchai et al., 2007). Peasant workers and manual laborers frequently consumed kratom as a natural energizer, often chewing the leaves or drinking kratom-infused teas to combat fatigue and improve endurance while performing strenuous physical tasks in the sweltering heat (Shijun Lu et al., 2009). The leaf s ability to enhance productivity and maintain stamina has made it a long-standing narcotic panacea for those engaged in physically demanding work. Despite its cultural and medicinal significance, the use of kratom is officially prohibited in Malaysia. However, its traditional utilization continues unabated in some communities, primarily due to its perceived therapeutic benefits and role in socioeconomic practices.

In Malaysia, morphine users have turned to kratom as a substitute to help reduce their dependence on opioid drugs, with several studies reporting kratom's potential as an effective treatment for opiate addiction (Singh et al., 2014; Vicknasingam et al., 2010). Similarly, reports from the United States indicate that kratom and its primary alkaloid, mitragynine, are being used as alternative therapies for heroin addiction, suggesting a broader global interest in its application for managing substance dependence (Ahmad & Aziz, 2012; Vicknasingam et al., 2010; Singh et al., 2015). These findings underscore kratom's therapeutic promise in mitigating addiction-related challenges while also offering new avenues for research into its role as a harm-reduction agent.

One of the most fascinating aspects of kratom is its dose-dependent dual effects. At lower doses, kratom acts as a mild stimulant, inducing sensations of energy, heightened focus, and increased alertness, which are particularly favored for enhancing physical and mental activity. In contrast, higher doses produce opioid-like effects, including sedation, pain relief, and relaxation, which mimic those of more traditional narcotics like morphine (Hassan et al., 2013). These effects are largely influenced by the variety of the kratom plant, specifically the vein color of the leaves. The red vein leaf, highly favored in Thailand, is well-known for its stronger potency, making it a popular choice among traditional users for its robust effects (Suwanlert, 1975; Saingam et al., 2012). Despite its widespread use, kratom has not acquired the severe negative stigma associated with substances like opium, as it is viewed as less harmful in its traditional context. However, habitual use can lead to a gradual increase in consumption over time, particularly among regular users as opposed to those who consume it occasionally (Vicknasingam et al., 2010; Singh et al., 2014).

Notably, kratom use is associated with minimal adverse effects when consumed responsibly. Early observations by Lee (1957) reported no severe physical or psychological symptoms even among chronic users, with only mild withdrawal symptoms upon cessation, such as minor discomfort. Users of kratom have frequently expressed experiencing positive sensations, describing feelings of elation, strength, and enhanced physical capabilities (Suwanlert, 1975). Additionally, it has been documented that kratom users report an increased capacity for work, a heightened sexual desire, and a general boost in physical activity (Vicknasingam et al., 2010). A study by Ahmad and Aziz (2012) further highlights kratom's broad spectrum of effects, which include feelings of relaxation, contentment, light-headedness, and mild sedation. Some users also describe sensations of being energized and alert, along with experiences of euphoria and improved sexual performance, although mild side effects such as feeling hot and sweaty may occur. These effects are typically short-lived, lasting between 1 to 6 hours (Ahmad & Aziz, 2012), making kratom an attractive natural remedy with manageable effects for its users.

2.1.1 Benefit of Kratom

Preclinical findings support anecdotal evidence that kratom can be beneficial for treating pain and mental health conditions (Prevete et al., 2022). Studies conducted *in vitro* and *in vivo* have demonstrated that kratom and its alkaloids produce analgesic and antinociceptive effects, as indicated by increased latency in response to the hot plate or tail-flick tests and in models of inflammatory pain induced by acetic acid (Wilson et al., 2020). Additionally, kratom has shown anti-allodynic efficacy in neuropathic pain models (Farkas et a1, 2022; Foss et al., 2020). Preclinical models also suggest that kratom has antidepressant, anxiolytic, stress-relieving (Chen et al., 2022; Idayu et al., 2011; Vazquez Lopez et al., 2017), and antipsychotic properties (Vijeepallam et al., 2016). Furthermore, kratom and its alkaloids exhibit gastroprotective, anti-inflammatory (Chittrakarn et al., 2018; Salim et al., 2022), antibacterial (Juanda et al., 2019), antioxidant, antimutagenic, and anticancer activities (Prevete et al., 2022). For example, a recent study found that mitragynine and speciociliatine acted as chemo-sensitizers for cisplatin and inhibited cell proliferation in nasopharyngeal carcinoma (Domnic et al., 2021). Another study showed that mitragynine inhibits acetylcholinesterase, an enzyme involved in Alzheimer's disease (Innok et al., 2021). Kratom may also have lipolytic effects and antidiabetic actions by inhibiting enzymes such as a-glucosidase and pancreatic lipase when combined with the diabetes drug acarbose (Limcharoen et al., 2022). Additionally, preclinical evidence suggests kratom's potential in treating alcohol use disorder, withdrawal, and alcohol- seeking behavior (Gutridge et al., 2021; Vijeepallam et al., 2016); opioid dependence and withdrawal without causing anxiety while improving cognitive performance; and methamphetamine craving and addiction.

2.1.2 Therapeutic Effects of Kratom Alkaloids

As the use of kratom has risen significantly in the Western world over the past 15 years (Prozialeck et al., 2012), there has been a notable increase in research efforts aimed at identifying and characterizing the active pharmacological agents present in kratom. This surge in interest is driven by the desire to better understand the potential therapeutic applications and the underlying mechanisms through which kratom exerts

its effects. To date, more than 50 distinct compounds have been isolated from kratom, with extensive research confirming that many of these compounds possess substantial pharmacological activity (Ellis et al., 2020; Prozialeck et al., 2012). As the body of knowledge surrounding the chemical and pharmacological properties of kratom continues to grow, these findings have made kratom a subject of considerable scientific investigation.

The medicinal chemistry and pharmacognosy of kratom have been comprehensively reviewed by Adkins et al. (2011), who highlighted the diverse range of compounds present in the plant and their significant pharmacological activities. Within the body of research, a table has been compiled that provides detailed chemical structures of some of the most extensively studied kratom derived compounds, as well as a summary of their major pharmacological effects. Among these compounds, the mitragynine analogs are the most thoroughly characterized and have emerged as the primary active agents driving kratom's pharmacological profile. These mitragynine analogs are defined by the presence of an indole ring structure, which, in certain respects, bears structural similarity to yohimbine, a compound known for its own pharmacological properties.

Research has demonstrated that mitragynine and its analogs produce a wide array of pharmacological effects, both in experimental models (*in vitro*) and living organisms (*in vivo*), signifying their versatility and potency. The following sections of research will delve deeper into the specific significance of these compounds, particularly in relation to their primary pharmacological effects, such as their remarkable potential for analgesia and their role in alleviating opioid withdrawal symptoms. These two effects are of paramount interest, as they suggest that mitragynine and related alkaloids may offer therapeutic benefits for individuals suffering from chronic pain or opioid dependence. As these compounds continue to be studied, their potential as safer alternatives to traditional opioid-based treatments and as adjuncts to current opioid withdrawal therapies is increasingly recognized.

In addition to their established roles in providing analgesia and mitigating opioid withdrawal symptoms, kratom alkaloids exhibit a diverse range of pharmacological effects, which could significantly expand their potential medical applications. Remarkably, these compounds possess both stimulant and sedative properties, with their effects influenced by factors such as dosage and method of administration,

highlighting the nuanced and multifaceted nature of their pharmacological behavior (Prozialeck et al., 2012).

Ongoing research into kratom continues to focus on elucidating the full spectrum of effects these alkaloids produce, unraveling their intricate mechanisms of action, and assessing the safety and therapeutic potential of kratom-based treatments. By gaining a deeper understanding of these unique bioactive compounds, kratom holds the potential to pave the way for groundbreaking innovations in therapeutic strategies. These strategies could extend beyond pain relief and addiction recovery to encompass broader medical applications.

2.1.3 Abused of Kratom

In the mid-twentieth century, kratom use in Southeast Asia expanded as a substitute for opioids to treat various conditions such as diarrhea, cough, pain, and depression. It was also used to alleviate opioid withdrawal symptoms in chronic users who temporarily lacked access to opioid or were attempting to quit opioids, alcohol, and other addictive substances (Singh et al., 2014; Swogger et al., 2015; Vicknasingam et al., 2010). By the 1990s, kratom consumption began to spread beyond Southeast Asia, possibly due to increased migration from the region to Europe and the United States. This growth was further facilitated by the dissemination of information and marketing on the internet. By 2016, it was estimated that several million consumers in the US were purchasing kratom products from over 10,000 retail outlets, with the annual market valued at approximately 207 million US dollars (Botanical Education Alliance, 2016). For decades in Southeast Asia, and more recently in the US, kratom has been utilized as a substitute for opioids to relieve pain, alleviate opioid withdrawal symptoms, and maintain abstinence from highly addictive opioids (Henningfield, 2018). In the US, it seems that most kratom use does not align with the abuse-related purposes outlined by the FDA in its abuse potential assessment guidance (FDA 2017, p. 4), which include "euphoria, hallucinations and other perceptual distortions, alterations in cognition, and changes in mood" (Singh et al., 2015).

In the northern states of Malaysia, the rural Malay community often used kratom to address minor health issues such as diabetes and hypertension (Hassan et al., 2013; Singh et al., 2015). Kratom misuse in this region is a socioeconomically influenced

issue rooted in rural Malay traditions, leading to the perception that kratom is safe for various uses (Singh et al., 2014, 2015). It was claimed to have effects similar to both opium and cocaine and was used to alleviate opioid withdrawal symptoms during opium shortages in Malaysia (Singh et al., 2015). However, frequent and prolonged use of kratom can ultimately result in dependance, withdrawal, and cravings in humans (Singh etal., 2014, 2015).

2.1.4 Toxicity of Kratom

Given that patients experiencing kratom toxicity often present initially in the emergency department, conducting a comprehensive primary survey is of utmost importance to assess critical factors such as airway patency, breathing adequacy, and circulatory stability. Developing a broad and inclusive differential diagnosis is equally critical, as the presenting symptoms can significantly differ based on the amount of kratom consumed, the route of administration, and potential co-ingestion of other substances. Recognizing the variable clinical presentation is essential for effective triage and management.

Furthermore, one of the challenges in identifying kratom misuse lies in the lack of routine detection through standard drug screening methods. Conventional toxicology panels do not test for kratom or its active compounds, leaving clinicians reliant on detailed patient history and self-reporting to confirm exposure (Jentsch & Pippin, 2024). This highlights the necessity of maintaining a high index of suspicion when evaluating patients with unclear or atypical toxicological profiles. Additionally, public health education on kratom's effects and potential risks can empower healthcare providers to identify its misuse more effectively and develop appropriate management strategies. There are no established, evidence-based guidelines for treating kratom toxicity.

Symptoms of kratom toxicity can vary depending on the dose ingested and any alterations to the substance. Kratom's physiological effects are dose-dependent, with lower doses producing stimulant-like effects and higher doses resulting in opioid-like effects. Toxicity generally occurs when doses exceed 8 grams (Babu et al., 2008; Singh et al., 2015). Kratom use can affect multiple organ systems, with reported cases of hepatotoxicity, seizures, coma, lung injury, kidney injury, and cardiotoxicity (Eggleston et al., 2019). Pregnant patients using kratom also risk their neonates developing neonatal abstinence syndrome (Davidson et al., 2019). Evaluations should be based on the

patient's presenting symptoms. It is advisable for healthcare providers to contact their local poison control center for guidance and assistance when kratom ingestion is suspected or confirmed (Mackay & Abrahams, 2018).

At higher doses, kratom toxicity can resemble opioid overdose. Although naloxone is a known reversal agent for opioid overdose, its effectiveness for kratom toxicity is not well-established. However, some reports suggest potential benefits, and certain studies have recommended its use. Cases of acute drug-induced hepatitis due to kratom toxicity have also been documented, with N-acetylcysteine being used for treatment (Jentsch & Pippin, 2024; Overbeek et al., 2019; Rech et al., 2015), similar to other instances of drug-induced hepatitis. For patients who experience seizures after kratom ingestion, standard seizure management with anti-epileptics is necessary (Mousa et al., 2018).

Previous studies have demonstrated the toxic effects of mitragynine at high doses. It has been reported that a single oral of mg/kg of mitragynine can cause mortality in rats, while a dose of 40mg/kg shows no mice to assess the acute toxicity of mitragynine, oral doses of 1300 and 2000 mg/kg led to death, preceded by symptoms such as convulsions, restless, and tremors (Annuar et al., 2024). Conversely, an oral dose of 175 mg/kg showed no adverse effects or behavioral abnormalities, including no decrease in food intake or body weight loss. The lethal dose (LD50) for oral administration of *Mitragyna spesiosa* alkaloid and methanolic extracts were 173.20 mg/kg and 4.90 mg/kg, respectively (Annuar et al., 2024; Wantana et al., 2007). Observed signs of toxicity included tremors, paralysis, fatigue, lethargy, apnea, convulsions, and ultimately death.

Kratom, a psychoactive herb, has become widely used due to its easy availability and opiate-like effects. Although it is often used to help individuals wean off opiate addictions, misuse, or abuse of kratom can lead to numerous toxic effects. These adverse effects range from renal and liver failure to cardiac toxicity. Some negative effects can be reversed with medical intervention, while others result in long-term damage that remains resistant even to invasive treatments. For example, a patient was admitted to the intensive care unit after being found unresponsive due to a cerebrovascular accident, rhabdomyolysis, and renal failure. This patient had initially used kratom recreationally but eventually escalated to abusive doses. Although the patient survived, suffering multiple complications including transient reversible nonischemic cardiomyopathy, they were discharged in a neurologically stable but became dependent on hemodialysis

at a young age. Rhabdomyolysis is a rare complication of kratom use that has not been well documented.

2.1.5 Side Effects of Kratom

To assess the range of symptoms linked to kratom toxicity, a 2019 retrospective analysis of cases reported to the National Poison Data System and the New York City Office of the Chief Medical Examiner revealed a diverse array of clinical manifestations (Eggleston et al., 2019). The most frequently observed symptom was agitation, reported in 18.6% of cases, followed by tachycardia in 16.9%, drowsiness in 13.6%, and confusion in 8.1% (Eggleston et al., 2019). More severe neurological effects included seizures in 6.1% of cases and hallucinations in 4.8%, with 2.3% of patients advancing to a comatose state. The toxicity appeared to correlate with higher doses, particularly when consumption of kratom powder surpassed 8 grams. Additionally, the study identified kratom as a contributing factor in at least four fatalities. Based on these findings, the researchers emphasized that kratom products represent a significant public health concern and cautioned against assuming their safety, despite their legal availability in many regions.

Case studies have identified that kratom use can lead to injuries across a broad spectrum of organ systems (Table 2.2). Examples include kidney damage (Ilmie et al., 2015), cardiotoxic effects and arrhythmias (Abdullah et al., 2019; Lu et al., 2014), thyroid dysfunction such as hypothyroidism (Sheleg & Collins, 2011), lung complications like acute respiratory distress syndrome (ARDS) (Eastlack et al., 2020; Pathak et al., 2014), neonatal abstinence syndrome (Davidson et al., n.d.; Murthy & Clark, 2019), and liver damage (Fernandes et al., 2019; Kapp et al., 2011; Waters et al., 2018). Among these, hepatic injury appears to be particularly prevalent, frequently manifesting as a cholestatic hepatitis pattern akin to other drug-induced liver injuries, characterized by elevated transaminase levels (commonly exceeding 100 units/L), elevated alkaline phosphatase (>200 units/L), and increased total bilirubin (>1.2 mg/dL). Neurological complications have also been reported, including acute brain injuries, coma (Nelsen et al., 2010), and the occurrence of seizures in both acute and chronic contexts (Eastlack et al., 2020). Prolonged kratom use has been associated with long-term cognitive deficits, particularly in chronic users (Eastlack et al., 2020).

Table 2.2
Spectrum of Organ System Involvement and Related Injuries Linked to Kratom Usage.

Organ system	Presentation signs and conditions
Hepatic	Acute liver failure, hepatitis, transaminitis, intrahepatic
Endocrine	Hypothyroidism, hypogonadism
Renal	Acute kidney injury
Cardiac	Cardiotoxicity, arrhythmia
Pulmonary	Acute lung injury, ARDS
Obstetric	Neonatal abstinence syndrome
Neurological	Acute brain injury, seizure, coma, cognitive impairment

Source: (Eastlack et al., 2020)

In some severe instances, kratom toxicity has resulted in fatalities. Reports from the Centers for Disease Control and Prevention (CDC) indicate a growing number of kratom-related deaths, with 152 cases documented between 2016 and 2017 (Eastlack et al., 2020; Kuehn, 2019). Notably, polysubstance abuse has been identified as a significant risk factor contributing to both toxicity and mortality, occurring in approximately 87% of reported cases (Corkery et al., 2019). This has led to the prevailing notion that fatalities solely attributable to kratom ingestion are extremely rare, if not implausible. However, a 2019 study examining kratom-associated deaths in Colorado revealed that 4 out of 15 fatalities reported between 1999 and 2017 were due exclusively to mitragynine toxicity, as confirmed by comprehensive toxicological and biochemical analyses (Gershman et al., 2019). Despite these findings, it is widely believed that most kratom-related deaths result from a combination of factors, including kratom toxicity compounded by adulterants, contaminants in the kratom product, or concurrent consumption of other illicit substances.

2.2 Alkaloids of Kratom

The pharmacology of kratom is intricate and multifaceted, as more than 50 distinct alkaloids have been identified in the leaves of the plant. The concentration of these alkaloids is influenced by a wide range of factors, including the geographical region where the kratom is cultivated, the specific time at which the plant is harvested, and the age of the plant at the time of harvest (Ellis et al., 2020). While these numerous alkaloids contribute to the overall chemical profile of kratom, the two primary compounds currently garnering significant scientific and medicinal interest are the

indole alkaloids—mitragynine and 7-hydroxymitragynine. These alkaloids are believed to function as partial agonists, selectively interacting with the opioid receptors in the brain, a mechanism that has opened avenues for understanding their potential therapeutic effects and risks.

Typical kratom products, in the form of powders or capsules, are known to contain approximately 2% mitragynine by weight. In contrast, 7-hydroxymitragynine is generally found in much lower concentrations, either absent or present at trace levels, generally ranging from 0.01% to 0.02% (Veltri & Grundmann, 2019). Of these two active compounds, mitragynine plays a particularly prominent role, both due to its chemical abundance in kratom leaves and its notable pharmacological activity. Several mitragynine-derived pseudoindoxyl alkaloids have also been found, exhibiting similar pharmacological characteristics that differ significantly from classical opioids such as morphine, heroin, or fentanyl (Yamamoto et al., 1999). These differences in mechanisms of action underline why mitragynine is studied as a potential alternative to traditional opioids, especially regarding its effect profile on the central nervous system. While the scientific exploration of kratom's pharmacology is still unfolding, its complex mix of therapeutic, psychoactive, and sociocultural roles continues to make it an intriguing subject for researchers and communities alike. Its historical and present- day use reflects both its potential as a natural remedy and the nuanced challenges associated with its regulation and integration into modern health practices. Table 2.3 provides a comparison of the kratom alkaloids mitragynine, 7-hydroxymitragynine, and mitragynine pseudoindoxyl, highlighting their sources, potency, and pharmacological effects.

Table 2.3
Comparison of Mitragynine, 7-Hydroxymitragynine, and Mitragynine Pseudoindoxyl: Sources, Potency, and Pharmacological Effects

Property	Mitragynine	7-hydroxymitragynine	Mitragynine pseudoindoxyl
Source	Most abundant alkaloid in Kratom (60-70%) (Hennmgfield,2018)	Minor alkaloid in Kratom (<2%) (Kruegeletal., 2016)	Metabolite of mitragynine (not naturally abundant) (Varadietal.,2016)

Property	Mitragynine	7-hydroxymitragynine	Mitragynine pseudoindoxyl
Chemical Structure	Tryptamine-based indole alkaloid (Kruegeletal.,2016)	Similar to mitragynine with a hydroxy 1 group at the 7th position (Kruegeletal.,2016)	Derived from mitragynine with an "indoxyl" group (Varadietal.,2016)
Receptor Activity	Partial agonist at u-opioid receptor and *5*-opioid receptors (Kruegeletal.,2016)	Potent agonist at u-opioid receptor (Kruegeletal.,2016)	Potent u-opioid receptor agonist and 6-opioid receptor antagonist (Varadietal.,2016)
Pharmacological Effects	Mild to moderate analgesic, stimulant at low doses, sedative at high doses (Henmngfield, 2018)	Strong analgesic effects, much more potent than mitragynine (Kruegeletal.,2016)	Very strong analgesic with less respiratory depression risk compared to traditional opioids. (Varadietal.,2016)
Potency	Less potent compared to 7-hydroxymitragynine and mitragynine pseudoindoxyl (Kruegeletal.,2016)	10-20 times more potent than mitragynine; 4-5 times more potent than morphine (Varadietal.,2016)	More potent than both mitragynine and 7-hydroxymitragynine (Varadietal.,2016)
Abundance in Kratom	High (Henningfield, 2018)	Low (Kruegel et al., 2016)	Not typically found naturally in high amounts (Varadi etal.,2016)
Side Effects	Mildness may include nausea, dizziness, and sedation. (Henningfield, 2018)	Not typically found naturally in high amounts (Kruegel et al, 2016)	Lower risk of respiratory depression than traditional opioids, but still potent (Varadietal.,2016)
Usage	Traditional use for mild pain relief, mood enhancement, and energy boost (Henningfield, 2018)	Used for potent pain relief, higher risk for addiction and side effects. (Kruegel et al, 2016)	Potential for pain management with reduced risk of respiratory depression (Varadi et al., 2016)

In addition to kratom powders and capsules, a traditional preparation of kratom involves brewing the leaves into a tea. Research has shown that this method of consumption can provide greater systemic exposure to mitragynine, the most abundant

and significant alkaloid present in the plant (Cinosi et al., 2015). This increased bioavailability of mitragynine through tea consumption makes kratom an even more compelling subject of pharmacological inquiry. Further studies have confirmed that mitragynine, as well as its oxidation product 7-hydroxymitragynine and mitragynine pseudoindoxyl—a rearranged derivative with a spiro-pseudoindoxyl structure resulting from a skeletal transformation of 7-hydroxymitragynine—demonstrate significant opioid-like antinociceptive properties (Kamble et al., 2020).

Notably, these alkaloids are considered G-protein-biased u-opioid receptor (MOR) agonists, as they activate opioid receptors in a way that may differ from traditional opioid drugs, possibly offering analgesic effects while mitigating some of the risks associated with full opioid receptor activation (Chakraborty et al., 2021). This unique pharmacodynamic profile places mitragynine and related compounds in a different category of opioid-like substances that merit further study, particularly in terms of their potential for pain management and opioid addiction treatment. The chemical structures of 20 kratom alkaloids are depicted in Figure 2.1.

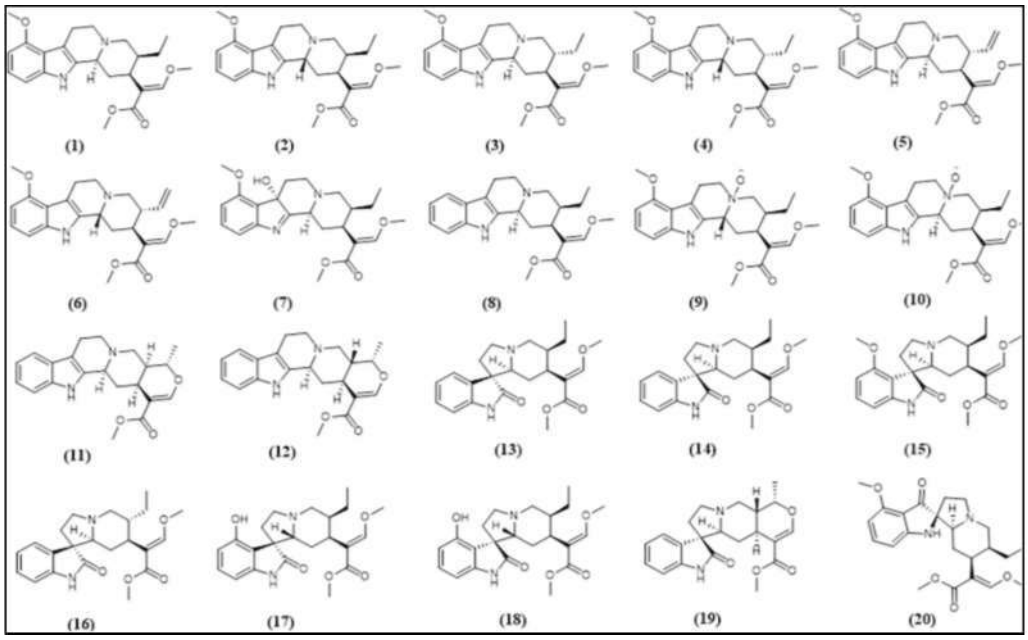

Figure 2.1 Chemical Structures of Selected Kratom Alkaloids. (1) mitragynine, (2) speciociliatine, (3) speciogynine, (4) mitraciliatine, (5) paynantheine, (6) isopaynantheine, (7) 7-hydroxymitragynine, (8) corynantheidine, (9) speciociliatine n-oxide, (10) mitragynine n-oxide, (11) tetrahydroalstonine, (12) ajmalicine, (13) corynoxine, (14) corynoxine B, (15) mitragynine oxindole B, (16) isorynchophylline, (17) isospeciofoline, (18) speciofoline, (19) mitraphylline, (20) mitragynine pseudoindoxyl.
Source: (Hanapi et al., 2021)

2.2.1 Mitragynine

Mitragynine is the main alkaloid and is unique to *Mitragyna speciosa*, accounting for approximately 66% of total alkaloids (Ahmad & Aziz, 2012). In animal studies, mitragynine did not lead to dependence or increased self-administration. In fact, it even decreased the prior administration of morphine. On the other hand, 7-OH showed a potential for dependence liability (Veltri & Grundmann, 2019) . Finding from *in vivo* and *in vitro* studies of mitragynine have indicated that it has an antinociceptive activity via supraspinal opioid receptors, and that its action is predominantly mediated by mu and 5-receptor subtypes (Matsumoto et al., 2004). Rush et al., in 2019 (Rush et al., 2019), stated that a connection between mitragynine's effects and P-glycoprotein, a multidrug transporter responsible for influencing the way xenobiotics are processed in the body. This transporter plays a crucial role in mediating drug interactions between different medications (Meireles et al., 2019).

Mitragynine is a complex indole alkaloid with the molecular formula $C_{23}H_{30}N_2O_4$, characterized by an indole ring, a quinuclidine nucleus, and various functional groups that contribute to its pharmacological effects. It primarily interacts with the brain's opioid receptors, especially the u-opioid receptor, playing a significant role in pain relief and mood regulation. Additionally, mitragynine influences other receptor systems, adding to its multifaceted pharmacological profile (Henningfield, 2018). At lower doses, mitragynine acts as a stimulant, boosting alertness, energy, and sociability. In contrast, higher doses produce effects akin to opioids, inducing a sense of calm and euphoria (Kruegel & Grundmann, 2018). Traditionally, kratom leaves have been utilized for their stimulant properties to combat fatigue and for their analgesic effects to alleviate pain. In contemporary therapeutic research, mitragynine is being explored for its potential to treat chronic pain, alleviate opioid withdrawal symptoms, and possibly address other conditions such as anxiety and depression (Singh et al., 2014).

Deuteration of mitragynine appears to have minimal impact on its metabolism in vitro. Previous studies hypothesized that a deuterated analogue would exhibit slower metabolism due to kinetic isotope effects. To test this, researchers synthesized mitragynine-d9, an analogue fully deuterated at its O-methyl groups and compared its stability with the non-deuterated mitragynine in human liver microsomes (HLM) and mouse liver microsomes (MLM). Surprisingly, the stability of the deuterated and non-

deuterated versions was the same. This finding suggests that demethylation is only a minor pathway in the hepatic metabolism of mitragynine. Demethylated metabolites may accumulate slowly in the urine or be formed outside the liver, and the previously reported metabolites are unlikely to explain the hypothesized role of a liver-formed metabolite in mitragynine's analgesic activity (Kruegel et al., 2019).

2.2.2 7-hydroxymitragynine

The importance of 7-hydroxymitragynine as an active metabolite of mitragynine and a significant mediator of its analgesic effect was reported based on the critical *in vivo* link indicating the pharmacological relevance (Kruegel et al., 2019). The report also showed that mitragynine was metabolically converted to 7-hydroxymitragynine *in vivo,* where both alkaloids were found in the plasma and the brain. The study also demonstrated in mice that 7-hydroxymitragynine contributes to the analgesic activity of mitragynine as a metabolite when comparing the pain response of substances given at equianalgesic subcutaneous doses. Then, they confirmed this by measuring concentrations of 7-hydroxymitragynine in the brain, which is consistent with 7-hydroxymitragynine being the main mediator of central analgesic activity. To clarify the significance of 7-hydroxymitragynine as a mitragynine metabolite in man, pharmacokinetic studies will be necessary, where the interspecies variations in the metabolic processes must be carefully taken into consideration.

Overall, the information provided by this study can be exploited to develop novel kratom-based pain treatments, A promising framework for the creation of functionally biased opioid modulators, which may have better therapeutic profiles as analgesics, includes the Mitragyna alkaloid scaffold. The therapeutic window for analgesic-respiratory depression would be desired and broad based on the pharmacological profile of 7-hydroxymitragynine as a partial G-protein biased agonist at the 5-opioid receptor. Besides that, with known metabolites failing to account for the observation's suggestion of an active metabolite, researchers began investigating alternative metabolic pathways that might produce such a compound. They looked into known chemical transformations of indole alkaloids, including mitragynine, under oxidative conditions. For instance, 2,3-disubstituted indoles are known to undergo functionalization under oxidation/halogenation conditions, resulting in 3-substituted

indolenines (Kruegel et al., 2019). Specifically, mitragynine is oxidized by [bis(trifluoroacetoxy)iodo] benzene (PIFA) to yield 7-hydroxymitragynine. In their synthetic explorations of the mitragynine scaffold, they also discovered that singlet oxygen and potassium peroxymonosulfate (Oxone) are effective oxidants for converting mitragynine into 7-hydroxymitragynine (Kruegel et al., 2019; Takayama et al., 2002). Consequently, researchers hypothesized that the 2-3 indole double bond targeted by these chemical oxidants might also be a site for oxidation by cytochrome P450 enzymes (CYPs), producing 7-hydroxymitragynine as a metabolite.

2.2.3 Mitragynine pseudoindoxyl

The effects of mitragynine pseudoindoxyl on electrically stimulated contractions in guinea pig ileum and mouse vas deferens, as well as its binding inhibited the contractions in both tissues in a concentration-dependent manner. In the ileum, the effective concentration was in the nanomolar range, comparable to the concentrations reported for the u-opioid receptor agonist [D-Ala^2, Met-Phe^4, Gly-ol^5] enkephalin (DAMGO), and was 100- and 20- fold lower than those of mitragynine and morphine, respectively. In the vas deferens, its effective concentration was 35 times lower than that of morphine. The inhibitory action in the ileum was countered by the non-selective opioid receptor antagonist naloxone and the u-receptor antagonist naloxonazine, while in the vas deferens, it was antagonized by the 5-receptor antagonist naltrindole.

Mitragynine pseudoindoxyl exhibited binding affinities similar to DAMGO and naltrindole at u-and 5-receptors, respectively, but had negligible affinity for *K*-receptors. This study shows that mitragynine pseudoindoxyl, a novel alkaloid structurally distinct from other opioid agonists, acts on opioid receptors, resulting in potent inhibition of electrically stimulated contraction in the ileum via 5-opioid receptor-receptors and in mouse vas deferens via 5-receptors (Yamamoto et al., 1999).

In summary, research has provided the first comprehensive *in vitro* and *in vivo* studies on mitragynine pseudoindoxyl. This compound functions as a \i agonist and *5* antagonist with a preference for G-protein-mediated signaling pathways *in vitro,* and it demonstrated potent antinociceptive effects *in vivo.* Due to its combined \i agonism and antagonism, mitragynine pseudoindoxyl may bypass several significant issues associated with opioid therapy. In the mouse model, it showed no reward or aversion

and exhibited reduced antinociceptive tolerance, physical dependance, respiratory depression, and inhibition of gastrointestinal transit. Chemical modifications to this scaffold revealed key structure-activity relationship (SAR) features distinct from the mitragynine template. Specifically, analogs modified at the C-9 position displayed varying efficacies in *in vivo* functional assays and enhanced potencies *in vivo* (Varadietal., 2016).

2.3 Mechanism of Action

The mechanism of action of kratom involves its active alkaloids, particularly mitragynine and 7-hydroxymitragynine, interacting with multiple receptor systems within the body. These compounds primarily target the opioid receptors in the central nervous system, functioning as partial agonists at u-opioid receptors to deliver kratom's well-known effects, including pain relief, sedation, and euphoria (Kruegel & Grundmann, 2018; Warner et al., 2016). In addition to their opioid-related activity, kratom's alkaloids influence the adrenergic, serotonergic, and dopaminergic systems, which contribute to mood regulation, stress alleviation, and calming effects (Hemby et al., 2018; White, 2018). Kratom also acts on muscarinic receptors, affecting gastrointestinal motility and often reducing bowel movements (Kruegel & Grundmann, 2018). These diverse pharmacological interactions highlight Kratom's potential in managing pain and mood disorders. However, its ability to activate opioid receptors over time raises serious concerns about dependence, tolerance, and the risk of addiction, emphasizing the importance of cautious and regulated use (Cinosi et al., 2015; Varadi etal., 2016).

Mitragynine has an estimated half-life of about 3 hours. When ingested orally, it demonstrates linear pharmacokinetics with biphasic elimination (Trakulsrichai et al., 2015). The precise mechanism by which these metabolites interact with specific receptors remains unclear, and the diverse range of kratom alkaloids and their potential pharmacological properties complicates the assessment of its overall physiological effects (Philipp et al., 2011). A key distinction between opioids and kratom alkaloids is their pharmacological and structural differences (Jentsch & Pippin, 2024). While kratom alkaloids, like opioids, initiate G-protein-coupled receptor (GPCR) signaling, they do not activate the beta-arrestin pathway (Varadi et al., 2016). This distinction is

significant because the beta-arrestin pathway is associated with adverse symptoms in opioid use, such as respiratory depression, sedation, and constipation. Due to the selective action of kratom alkaloids and their lack of beta-arrestin pathway activation, kratom is considered a promising substance for pain management (Jentsch & Pippin, 2024; Varadi et al., 2016).

2.3.1 Interaction with Opioid Receptor

Kratom extracts, including alcoholic, water, and alkaloid-enriched varieties, along with its main alkaloid, mitragynine, have shown significant central analgesic effects in both rodents and humans. These effects were largely counteracted by non-selective opioid antagonists such as naloxone or naltrexone in most cases (Hanapi et al., 2021; Matsumoto et al., 1996). These findings indicate that the central analgesic effects of kratom and mitragynine are mainly mediated through opioid receptors (Ramanathan et al., 2021). According to Takayama et al. (2002) were the first to report on the interaction of mitragynine related indole alkaloi 7-hydroxymitragynine, corynantheidine, and speciociliatine— with u-opioid receptors derived from guinea pigs. However, corynantheidine was subsequently found to inhibit morphine-induces twitch contraction in guinea pig ileum, demonstrating selective binding affinity to the u-opioid receptor. This suggests that corynantheidine functions as a selective u-opioid receptor antagonist. From these findings, the following can be postulated: 1) The S- orientation at the C-3 position of mitragynine is crucial for its opioid-agonistic activity; 2) Oxidation at the indole B-ring enhances opioid-agonistic activity; 3) The absence of the Nb lone pair at the C-ring eliminates opioid agonistics activity; 4) The removal of the 9-methoxy group abolishes opioid-agonistic activity (Hanapi et al., 2021).

Over the past five years, extensive studies have been conducted on the interactions of kratom alkaloids with human opioid receptors through various *in vitro* and *in vivo* assays. Kruegel et al. examined the binding affinity and functionality of mitragynine, 7-hydroxymitragynine, speciociliatine, speciogynine, and paynantheine at human *i* (hMOR), *5* (hDOR), and *K* (hKOR) opioid receptors (Kruegel et al., 2019). They employed radioligand displacement and bioluminescence resonance energy transfer (BRET) functional assays in their investigation (Kruegel et al., 2016). The antinociceptive effects of speciociliatine, 7-hydroxymitragynine, mitragynine, and

morphine were completely counteracted by naltrexone. In this study, speciociliatine demonstrated opioid agonistic activity at hMOR, a result that contrasts with the findings of Kruegel et al. (2016), which reported weak antagonistic activity of this compound at hMOR *in vitro*. This also differed from Takayama et al. (2002), who reported that speciociliatine had negligible opioid agonistic activity in a guinea pig ileum model (Takayama et al., 2002). These discrepancies may arise from the different assays used to evaluate speciociliatine's functional effects. Nevertheless, based on both *in vitro* and *in vivo* functional assays, it can be hypothesized that the R orientation at the C-3 position of speciociliatine enhances its interaction with hMOR, leading to improved antinociceptive activity compared to mitragynine.

2.3.2 Neurological Effects of Kratom

The neurological effects of kratom involve a range of biological activities that impact the central nervous system. The alkaloids in kratom, particularly mitragynine, have gained scientific interest due to their effects on brain function. In 1932, researchers discovered that mitragynine influenced the autonomic nervous system by facilitating impulse transmission in both the cranio-sacral and sympathetic divisions. It also stimulated the medulla, likely affecting motor centers (Grewal, 1932).

Kratom has shown antidepressant activity in behavioral studies (Arking et al., 2014). Mitragynine was found to activate the GABAB receptor in a conditioned place preference test in rats (Kumarnsit et al., 2007). It also displayed weak antagonist activity at a-amino-3-hydroxy-5-methyl-4-isoxazolepropionic acid receptor (AMPA) and NMDA receptors, which are involved in neurotransmission. Additionally, kratom was observed to affect the hypothalamic-pituitary-adrenal (HPA) axis, increasing the production of neurotransmitters like serotonin, noradrenaline, and dopamine. The complex effects of kratom may be due to its interaction with multiple brain receptors, including adrenergic, serotonergic, and dopaminergic receptors (Kruegel & Grundmann, 2018).

Studies on animals have shown mixed effects on cognitive function. Chronic mitragynine injections (5-15 mg/kg) for 28 days reduced locomotor activity and object recognition in mice (Apryani et al., 2010). However, acute oral administration of kratom extract did not affect short-term memory or motor coordination but increased

exploratory behavior. In a human study, frequent kratom use (more than three glasses of kratom juice per day) did not impair motor skills, memory, attention, or executive function (Singh Ph.D. et al., 2019). Some research suggests that long-term use of kratom, morphine, or THC can impair spatial learning and memory. However, the methanolic extract of kratom (100-1000 mg/kg) has been reported to enhance learning in a passive avoidance test, although it did not significantly affect long-term memory consolidation (Iman et al., 2021). Kratom extract also influenced synaptic activity in the hippocampus, promoting short-term potentiation but inhibiting long-term potentiation (LTP), which may impact learning and memory processing.

2.4 Cell Membrane

The cell membrane, also known as the plasma membrane, is one of the most critical structures in biology, serving as the boundary between the cell and its external environment. It acts as a selective barrier, regulating the movement of substances in and out of the cell, allowing essential nutrients and ions to enter while preventing the passage of harmful substances (Alberts et al., 2013). This selective permeability is crucial for maintaining homeostasis and ensuring proper cellular function. The membrane also provides structural support, maintaining the cell's shape and protecting it from mechanical stress, particularly in animal cells that lack a rigid cell wall (Lodish etal., 2016).

The cell membrane is equipped with receptors and signaling molecules that facilitate communication between the cell and its environment. These receptors detect external signals, such as hormones or neurotransmitters, and trigger intracellular responses through signal transduction, which is vital for coordinating cellular activities (Alberts et al., 2013). The membrane also facilitates the transport of molecules through passive diffusion, active transport, and processes like endocytosis and exocytosis, ensuring the uptake of nutrients and the removal of waste (Lodish et al., 2016).

2.4.1 Structure Cell Membrane

The cell membrane's structure is described by the fluid mosaic model, which emphasizes its dynamic and flexible nature. Composed of a lipid bilayer with embedded

proteins, cholesterol, and carbohydrates, the membrane can adapt to changes in the environment, ensuring its functionality (Alberts et al., 2015). In specialized cells, such as those in mitochondria and chloroplasts, the membrane plays a key role in energy conversion processes, such as ATP production and photosynthesis (Lodish et al., 2016). The membrane also acts as a protective barrier, shielding the cell from toxins, pathogens, and mechanical damage, while contributing to immune responses by displaying antigens (Cooper & Hausman, 2019). Its adaptability allows cells to maintain homeostasis under varying conditions, ensuring survival and proper function. The fluid mosaic model (Figure 2.2), introduced by Singer and Nicolson in 1972 (Singer & Nicolson, 1972), describes biological membranes as dynamic structures composed of diverse components, including lipids, proteins, and carbohydrates.

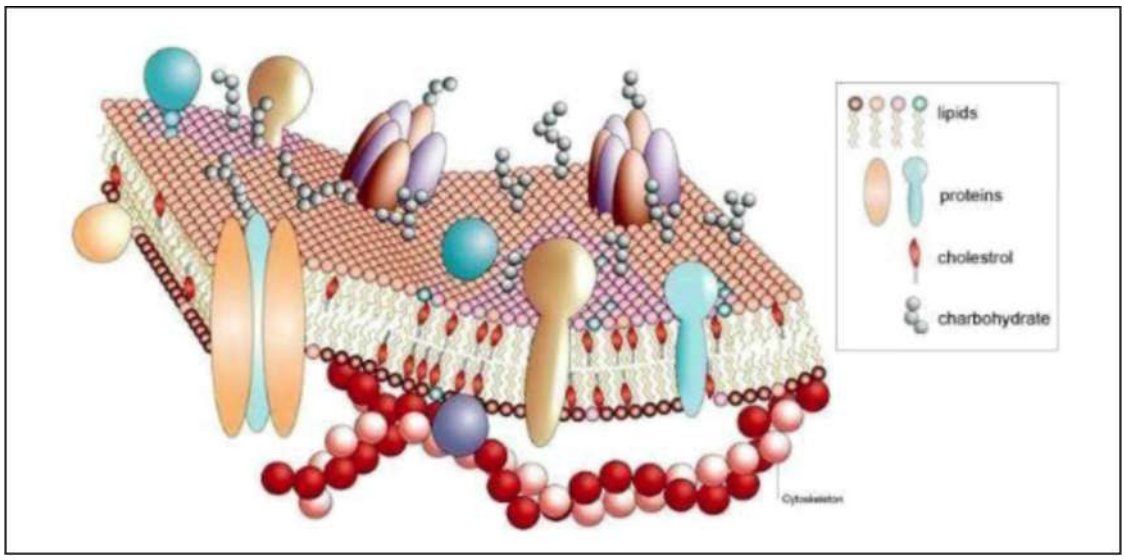

Figure 2.2 The Fluid-mosaic Model of the Cell Membrane Source: (Singer & Nicolson, 1972)

Phospholipid bilayers have been extensively researched as models for biological membranes. However, under physiological conditions of temperature and hydration, they exist in a fluid liquid crystalline (LR) state with a high degree of disorder, making it challenging to determine their detailed structure using standard techniques like X-ray diffraction. Instead, structural information can be gathered from various sources, such as the average orientation of CH-bond vectors at different carbon positions in the fatty acid chain derived from nuclear magnetic resources (NMR) order parameters, the average position along the z-axis of selectively deuterated carbon atoms obtained from

neutron diffraction, and the z-dependent electron density profile carbon atoms obtained from X-ray diffraction. Among lipids, phosphatidylcholine (DPPC) has the most extensive experimental structural data. DPPC consists of two saturated 16-carbon fatty acid chains connected by a glycerol backbone with a zwitterionic headgroup (Feller et al., 1997).

2.4.2 Drug Interactions with Cell Membrane

Most drugs are developed to target membrane proteins because the malfunction of these proteins is linked to many diseases (Knobloch et al., 2015; Yildirim et al., 2007). For instance, some drugs are specifically designed to block channel activities or inhibit protein binding (Cohen, 2002). The interactions of drugs with the membranes surrounding proteins are often overlooked. Membrane proteins need a proper membrane environment to maintain their structural and functional integrity. Natural membranes are complex systems made up of various components, including lipids, carbohydrates, and proteins. Although there are common characteristics in membranes from similar organisms, the exact composition can vary between different organisms (Dowhan, 1997; Escribaetal., 2008).

The impact of drugs on membrane structure and function is often overlooked in drug-related studies, despite its importance. Similarly, the effects of drug-induced changes in membrane properties on the function of embedded membrane proteins are seldom examined. This oversight is partly due to the membrane's complexity, making systematic investigations difficult. Additionally, experiments using whole cells or natural cell membrane patches are typically time-consuming, costly, and unsuitable for routine screening. Furthermore, non-specific drug-membrane interactions, where the drug binds to the membrane, reduce the amount of free drug available, potentially decreasing treatment efficacy (Knobloch et al., 2015; McLure et al., 2000; Nagar & Korzekwa, 2012; Smith et al., 2010). Therefore, it is crucial to investigate the role of the membrane in drug interactions for a comprehensive understanding.

Drugs interact with membranes. In traditional pharmacology, the interaction of a drug with lipid bilayer membranes is considered and optimized to enhance its ability to reach intracellular targets. Thus, studying drug-membrane interactions has always been important for drug design from both biophysical and biochemical perspectives.

Recently, it has been acknowledged that certain drugs, as well as natural plant extracts functioning as drugs, may exert their effects through interactions with the lipid bilayer membrane. This can involve disrupting membrane integrity, aiding the delivery of co-administered drugs, increasing bilayer permeability, binding to lipid signaling molecules, targeting transmembrane proteins after dissolving in the membrane, or modifying membrane protein conformation by changing the biophysical properties of the lipid bilayer, all without directly binding to specific proteins (Kopec et al., 2013).

Peetla et al. (Peetla et al., 2009) demonstrated that lipid extracts from drug-resistant and drug-sensitive cells exhibited notably different pressure-area isotherms, reflecting distinct biophysical properties of the membranes. Lipids from membranes resistant to the anti-cancer drug doxorubicin displayed significantly more rigid phase behavior compared to lipids from drug-sensitive cells. These resistant lipids also showed stronger interactions with the drug, suggesting that the resistance mechanism likely involves the drug interacting with the membrane. *In vivo,* this interaction would trap the drug within the lipid bilayer, effectively lowering the concentration of free drug. Similar findings were reported for the drug moxifloxacin, which exhibited stronger hydrophobic interactions with Langmuir monolayers compared to ciprofloxacin. This correlates to a higher cellular accumulation of moxifloxacin in vivo (Knobloch et al., 2015; Michotetal., 2005).

2.5 MD Simulations

MD Simulation is an advanced computer method for analyzing the time-dependent behaviour of biomolecules and macromolecular structure in a realistic setting. It is a computer program that is used to investigate the physical dynamics of atoms and molecules. The program is based on the classical mechanics to integrate the motion equations for a large number of atoms or residues over time, revealing structural, energetic and dynamic features of the system (Brooks et al., 1983). The fundamental idea is to use Newton's equations of motion to represent the interactions of atoms and molecules throughout time. This is performed by computing the forces applied on each atom or molecule and then using these forces to update the location and velocity of each atom or molecule at each time step. The simulation typically starts with a starting arrangement of atoms and molecules and proceeds for a certain number of time steps.

The final arrangement of atoms and molecules may be studied further to learn more about system features including structure, dynamics, and thermodynamics. MD simulations are being utilized in the fields such as biochemistry, biophysics and structural biology for studying various aspects, such as conformational changes, binding interactions and functional processes. Additionally, they have been employed to explore the properties of intricate systems like protein-ligand interactions, protein-protein interaction and macromolecular assemblies (Duan et al., 2003).

MD simulations offer a key advantage by furnishing precise insights into atomic-level behavior within a system, encompassing details like atom or residue positions, velocities and stresses across time. These simulations are also invaluable for exploring how diverse environmental factors impact a system, including temperature, pressure, pH and solvent condition (MacKerell et al., 1998). However, it's important to acknowledge the limitations inherent to MD simulations. Notably, they demand substantial computational resources and their outcomes hinge on the accuracy of the chosen force field for representing atomic interaction. Moreover, MD simulations have a limit exceeding the simulation's reach.

2.5.1 Molecular Force Fields

MD simulations rely on the application of Newton's equations of the motion. Essentially, this simulation method emulates the behavior of atoms in reality by utilizing a specific potential energy function. This energy function serves as the basis for computing the forces that act on each atom, considering the position of the surrounding atoms. Newton's laws guide how these forces drive the atoms' movements. In every time step, the forces influencing each atom are calculated through a molecular mechanics forces field. Newton's second law defines the relationship between force (F), atom mass (m) and acceleration (a).

$$F = ma \tag{2.1}$$

Simulating a molecular system requires the development of a computational model to calculate the system's energy based on the positions of all particles. This involves accounting for bonded interactions within polyatomic molecules as well as non-bonded interactions between particles. These interactions are defined by a force

field, a collection of mathematical functions that collectively represent the system's potential energy. The force field typically includes terms for intramolecular forces, which describe covalently bonded interactions, and intermolecular forces, which account for non-bonded interactions.

$$V(n, \quad ...r_N) \underset{-\wedge bonded}{} + \underset{-\wedge non\text{-}bonded}{} \tag{2.2}$$

A force field serves as a mathematical representation in MD simulations, describing the interactions between atoms or molecules. It defines the potential energy of the system based on the positions and velocities of its constituent atoms or molecules. By calculating the forces acting on each atom or molecule, the force field facilitates the continuous update of their positions and velocities throughout the simulation. This approach enables the study of molecular movement, activity, and behavior in each environment.

The atoms within a system engage in numerous interactions with each other, which can be categorized into two types: bonded and non-bonded interactions. Bonded interactions refer to interaction between atoms that are connected by covalent bonds. These interactions involve only a limited number of neighboring atoms and can be computed efficiently in (N) time for N atoms. On the other hand, non-bonded interactions occur between atoms that are not linked by covalent bonds. These interactions arise from various sources, such as electrostatic potential, Lennard-Jones potential due to van der Waals forces and others (Waidyasooriya et al., 2017). Figure 2.4 shows the bonded and non-bonded in MD simulations.

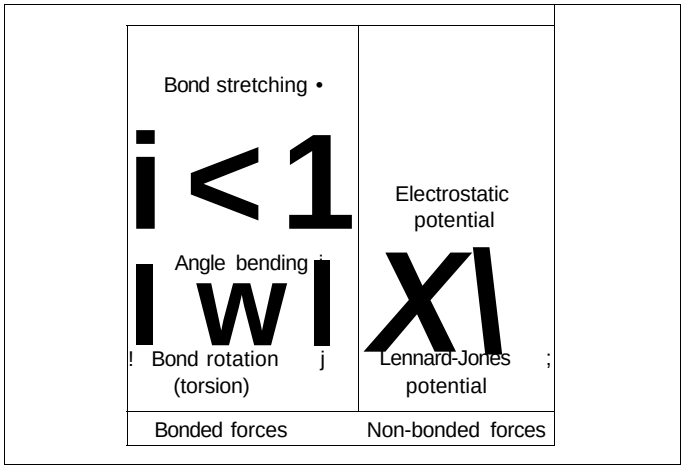

Figure 2.3 Bonded and Non-bonded Forces in Molecular Dynamic Simulations Source: (Waidyasooriya et al., 2017)

2.5.2 Periodic Boundary Condition

The computational speed of available hardware imposes a constraint on the size of molecular systems that can be simulated over practical timescales. Due to the finite number of atoms in a simulation, an artificial boundary must be introduced to limit the number of molecules. However, these boundaries can lead to surface effects by excluding interactions with particles outside the simulation box. To mitigate these artifacts, periodic boundary conditions (PBCs) are commonly employed in MD simulations (Allen et al., 1989). This approach replicates an infinite bulk system by allowing molecules at one edge of the simulation box to interact seamlessly with those at the opposite edge.

However, the primary challenge with periodicity is that simulated molecules and the structure they form often appear fragment at the edges of the unit cell. To address these issues, specific solutions have been designed for scenarios. For individual molecules, techniques have been developed to ensure that the molecule remains intact even when it crosses the periodic boundary (Bruininks et al., 2023). Correcting broken molecules offers the added benefit of enabling the use of widely available Euclidean geometric algorithms for analyzing molecular properties (Bruininks et al., 2023).

2.5.3 Long-Range Interaction

The handling of nonbonded interactions, particularly long-range electrostatic interactions, in MD simulations of liquids and solutions has been extensively studied over the past decade (Mark & Nilsson, 2002). These molecular dynamics (MD) studies assessed the impact of various approaches to handle nonbonded interactions in pure water. Pure water was a logical choice of the test system when comparing different methods for truncating nonbonded interactions. A system composed solely of water molecules, particularly with the molecules treated as rigid, proved to be the ideal choice since all forces within the system were exclusively nonbonded interactions (Mark & Nilsson, 2002).

In a large system containing N atoms, the number of bonded interactions to be calculated is relatively small, as it scales linearly with N. In contrast, non-bonded interactions are significantly more computationally demanding, as each atom can

potentially interact with every other atom, causing the number of non-bonded interactions to scale with N^2. Due to limited computational resources and the finite size of the simulation cell, non-bonded interactions must be truncated in practice. Historically, this challenge was addressed using the cut-off method, where interactions are calculated only within a specific distance, beyond which the interaction potential is set to zero.

The size of the simulation cell imposes a limitation on the cut-off distance due to periodic boundary conditions. If the cut-off distance is too large, a molecule may interact with multiple periodic images of another molecule. To avoid this, the cut-off distance must be less than half of the shortest unit cell vector (M. P. Allen et al., 1989). For the Lennard-Jones potential, which involves short-range interactions proportional to r^{-6}, the cut-off can be applied well below the symmetry distance. However, the Coulomb potential for electrostatic interactions, which scales as r^{-1}, is more challenging to truncate due to its long-range nature. Applying the same cut-off approach to Coulomb interactions can result in significant artifacts. These issues can be mitigated by either shifting the force function to zero or smoothly switching off the force at the cut-off radius.

Modern simulations address these challenges using advanced techniques to account for long-range electrostatic interactions. One widely used method is a variation of Ewald summation, which calculates the energy of an infinite lattice system. In this study, the Particle Mesh Ewald (PME) method (Essmann et al., 1995) was employed. PME improves upon the original Ewald summation by dividing the pairwise interactions into components handled in real space and Fourier space. By incorporating the fast Fourier transform (FFT) algorithm (Darden et al., 1993; Essmann et al., 1995), PME achieves computational efficiency that scales as *N log N*, making it suitable for large-scale systems.

2.5.4 Equilibration in Molecular Dynamic Simulation

In molecular dynamics (MD) simulations, thermodynamic ensembles define the specific conditions under which a system evolves, ensuring that the simulation accurately represents real-world physical behaviors. The selection of an appropriate ensemble depends on the properties and constraints of the system being studied. Two

of the most commonly employed ensembles in MD simulations are the NVT and NPT ensembles, each maintaining different physical parameters constant throughout the simulation.

The NVT ensemble (canonical or isothermal-isochoric ensemble) maintains a constant Number of particles (N), Volume (V), and Temperature (T). It is frequently used during the equilibration phase to stabilize the system's temperature before further analysis. In this phase, the system is allowed to evolve under controlled thermal conditions until the temperature reaches a steady state. The length of the equilibration period depends on factors such as molecular complexity and system composition. The NVT ensemble is particularly useful when temperature control is crucial before transitioning to other ensembles that regulate additional parameters such as pressure (Allen & Tildesley, 2017; Frenkel & Smit, 2023).

On the other hand, the NPT ensemble (isothermal-isobaric ensemble) maintains a constant Number of particles (N), Pressure (P), and Temperature (T). This ensemble is widely used to simulate conditions that closely resemble experimental environments, where both temperature and pressure must be regulated. Unlike the NVT ensemble, the NPT ensemble allows the system's volume to fluctuate in response to pressure changes, making it essential for accurately modeling biological systems, membrane behavior, or materials under varying pressure conditions. To maintain stable pressure, specialized algorithms known as barostats, such as the Parrinello-Rahman or Berendsen barostat, are employed to dynamically adjust the system's volume and ensure equilibrium in both temperature and pressure (Berendsen et al., 1984; Frenkel & Smit, 2023).

2.6 MD Simulations Software

Various software packages have made MD simulations more accessible and efficient, each suited to different research needs. The table below presents some of the most commonly used MD simulation software, detailing their typical applications and accessibility. Some of the software is available for free, with each one specializing in slightly different areas. These tools provide researchers with a variety of options to select from based on the specific needs of their studies.

Table 2.4
Common Software Used for MD Simulation

Software	Distributions	Maintained by
GROMACS	Open-source	University of Groningen, Netherlands
LAMMPS	Open-source	Sandia National Laboratories
CHARMM	Commercial	Martin Karplus and others (Academic version), Biovia (Commercial version
AMBER	Commercial	David Case, Rutgers University, and others
NAMD	Commercial	Klaus Schulten, University of Illinois at Urbana-Champaign
DESMOND	Commercial	D. E. Shaw Research
DL_POLY	Commercial	W. Smith and T.R. Forester, Daresbury Laboratory
ACEMD	Commercial	Accelera Solutions
Material studio	Commercial	Biovia

Source: (Katiyar & Jha, 2018)

2.6.1 GROMACS

GROMACS stands out as one of the most widely utilized MD simulation software packages (Berendsen et al., 1995; Lange et al., 2010). The program initially developed by the Department of Biophysics and Chemistry at Groningen University in the Netherlands, was designed primarily for studying the folding and interactions of biomolecules like proteins, nucleic acids, and lipids (Hess et al., 2008). Over time, significant algorithmic enhancements were made, enabling GROMACS to efficiently simulate the Newtonian motion of systems containing anywhere from hundreds to millions of particles. Its application has since broadened to include fields such as liquid crystals, polymers, and various biological macromolecules. GROMACS supports multiple established force fields, including CHARMM, AMBER, OPLS-AA, and GROMOS, and employs MD and stochastic dynamics methods to simulate molecular motion, analyze internal interactions, and study conformational changes. The software features a user-friendly visual trajectory program and a wide array of built-in tools for trajectory analysis, eliminating the need for custom scripts for standard analyses. Additionally, GROMACS is compatible with Windows, Unix, Linux, and other operating systems. Furthermore, GROMACS is free to download, with extensive application tutorials available online. Table 2.5 shows GROMACS features compared to other MD programs.

Table 2.5
Comparison GROMACS with Other MD Simulation Software.

Feature	GROMACS	AMBER	NAMD	LAMMPS	References
Performance & Speed	Highly optimized for speed, especially on GPUs	Slower than GROMACS but accurate for FEP	Good parallelization for large systems	Scales well, but slower for biomolecules	(Abraham et al., 2015)
Force Fields	Supports AMBER, CHARMM, GROMOS, OPLS-AA	Best for AMBER force fields	Works well with CHARMM & AMBER	Flexible, supports custom force fields	(Case et al., 2023; J. C. Phillips et al., 2005)
Best for	Biomolecular simulations (proteins, lipids, DNA)	Proteins, nucleic acids, small molecules	Large biomolecular systems	Materials science, polymers, solid-state	(Eastman et al., 2017)
Free Energy Calculations	Supports TI, BAR, FEP, MM/PBSA, MM/GBSA	Best accuracy for alchemical FEP	Supports FEP, but not as optimized	Not commonly used for free energy	(Mobley & Dill, 2009)
GPU Acceleration	Excellent GPU acceleration	Has GPU support but less optimized	Good GPU support	Can use GPU, but depends on the model	(Harvey et al., 2009)
Ease of Use	User-friendly, good documentation	Requires paid license for some tools	More difficult to set up for beginners	Complex but flexible for advanced users	(Eastman et al., 2017)
Parallel Scaling	Efficient for medium-sized systems	Not the best for large-scale simulations	Best for large-scale simulations	Excellent for highly parallel computations	(A. Q. Phillips et al, 2020)

The GROMOS parameter set is based on the GROMOS 54A7 united-atom force field. The researcher created criteria that are consistent with GROMOS 54A7 for a variety of lipid types. Computationally, these offer an advantage because united-atom lipids are significantly more efficient than all-atom lipids in most software implementations, compared to protein force fields, where the extra hydrogens have far less impact. Saturated and unsaturated phosphatidylcholine lipids were the first to be parametrized, as with other force fields. There are also characteristics for bacterial lipids with branched fatty acids in their lipid chains, cyclo-propane moieties, lipopolysaccharide, and for hopanoids and sterols. The parametric modelling is consistent with GROMOS 54A7 in approach and atom types, enabling lipid-protein or lipid-ligand simulations, but the number of various lipids available and evaluated for this force field is quite restricted.

Furthermore, GROMACS stands out as a highly utilized open source in the field of chemistry. Its main application involves conducting dynamic simulations of

biomolecules. The software offers an extensive range of calculation options, as well as tools for preparation and thorough analysis of these simulations (Abraham et al., 2015). Numerous implementations exhibit exceptional performance by using a substantial number of processors within the supercomputing environment. However, a central emphasis in the evolution of GROMACS lies in embracing the economic principle that resources are limited. Regardless of the abundance of available cores, the primary goal is to minimize resource consumption, thereby enabling the execution of a greater number of simulations, such as those facilitated by ensemble methods. The objective of GROMACS is to attain optimal performance and efficiency on all hardware configurations, striving for both exceptional theoretical capability and practical real-world throughput. This pursuit aims to maximize resource utilization, acknowledging the limitations of scarce resources.

2.6.2 Simulation of Lipid Bilayer System

Characterizing membrane properties at the microscopic scale remains a significant challenge due to the complexity of membrane composition. Over the years, experimental techniques such as NMR spectroscopy and X-ray diffraction (Petrache et al., 1998; Nagle & Tristram-Nagle, 2000), alongside simulation studies of membrane lipids, have been conducted in parallel. These combined efforts have enabled the development of robust theoretical models to describe lipid bilayers. Current force fields for simple lipid bilayers have proven highly effective in reproducing structural properties observed in experiments, such as density profiles, heat of vaporization, and lipid chain order parameters (Gompper & Schick, 2008). Among these, the widely-used "Berger lipid" parameter set stands out due to its reliability in simulating phospholipids. At physiological temperatures, the majority of phospholipids in biological membranes naturally form the La phase, enabling essential cellular processes such as membrane transport and protein function. However, certain phospholipids, such as DPPC, exhibit a propensity to remain in the gel phase under physiological conditions due to their specific physical properties. This behavior highlights the importance of carefully selecting simulation parameters, such as temperature, to ensure an accurate representation of the membrane's phase behavior and dynamic properties in computational studies.

In the gel phase, the hydrocarbon chains of lipids exhibit a highly ordered arrangement, often adopting a cone-like structure. For DPPC (dipalmitoylphosphatidylcholine), the transition temperature from the liquid-crystalline (La) phase to the gel phase (LP) occurs at 42°C (315 K). This property makes DPPC a widely studied lipid species in both experimental and computational research. Numerous experimental studies, such as those by Nagle and Tristram-Nagle (2000), and computational studies, including the work of Tieleman et al. (1997), have extensively utilized DPPC to investigate membrane properties and dynamics due to its well-characterized behavior (Nagle & Tristram-Nagle, 2000). Given its prominence in lipid bilayer research. Its well-documented phase transition and behavior under different conditions provided a reliable foundation for studying lipid membrane interactions (refer to Figure 2.2). This choice ensures that the findings are comparable with prior studies and enhances the robustness of the simulations in addressing the research objectives.

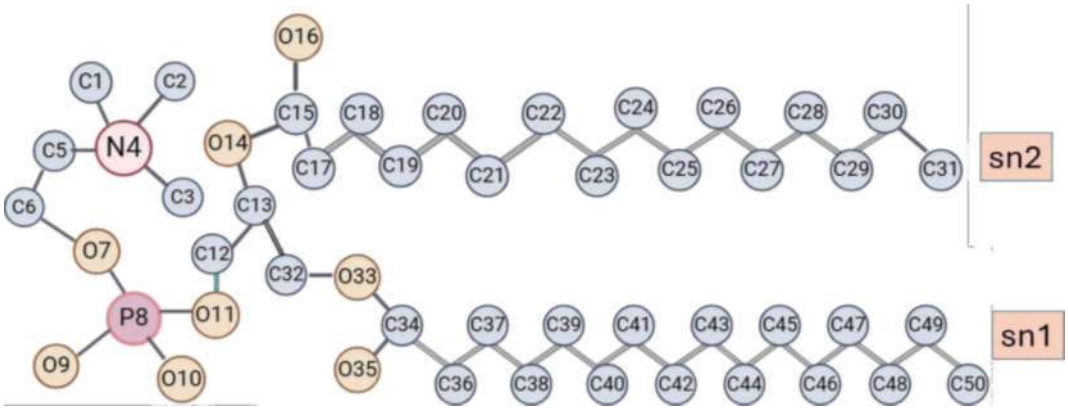

Figure 2.4 Molecular Structure and Atom Assignments for DPPC. Chemical Symbols are Carbon (C), Nitrogen (N), Oxygen (O) and Phosphorus (P).
Source: (Berger et al., 1997)

The selection of the water model is closely tied to the force field parameters used for the lipid model, as compatibility ensures accurate and reliable simulation outcomes. In the GROMACS simulation software, the Berger lipid force field (Berger et al., 1997) is a widely used parameter set for MD simulations of lipid bilayers. For simulations involving Berger lipids, the simple point charge (SPC) water model (van Buuren et al., 1993) is highly recommended. This preference arises from the optimization of reduced Lennard-Jones (LJ) interactions between the oxygen atom of

water (OW) and the CH2/CH3 groups of lipids, specifically tailored for compatibility with the Berger lipid parameters (Berger et al., 1997). To ensure realistic bilayer dynamics and prevent unwanted artifacts related to periodic boundary conditions (PBC), it is crucial to include a sufficient number of water molecules in the simulation box. Adequate hydration not only stabilizes the bilayer but also mimics the natural physiological environment, allowing for the accurate characterization of lipid-water interactions and membrane properties. This careful alignment of force field, water model, and simulation conditions ensures reliable and reproducible results in lipid bilayer studies.

2.6.3 Applications of MD Simulations in Drug Discovery

MD simulations play a crucial role in drug discovery, particularly in studying ligand-lipid interactions. These interactions are essential for understanding drug absorption, membrane permeability, and the mechanism of action for drugs targeting membrane-associated proteins such as G-protein-coupled receptors (GPCRs), ion channels, and transporters (Latorraca et al., 2017). MD simulations allow researchers to investigate how small molecules interact with lipid bilayers, providing insights into partitioning, diffusion, and conformational changes induced by drug molecules within membrane environments (Bertrand et al., 2020).

MD simulations have played a crucial role in modern drug discovery by providing insights into biomolecular interactions, leading to the successful development of several drugs. For instance, MD simulations were instrumental in the development of Nirmatrelvir (Paxlovid) by analyzing the binding stability and conformational flexibility of inhibitors targeting the SARS-CoV-2 main protease (Douangamath et al., 2020). Similarly, Oseltamivir (Tamiflu) was optimized using MD simulations to study conformational changes in the influenza neuraminidase active site, improving drug efficacy (Wang et al., 2011). In cancer therapy, Imatinib (Gleevec) was refined by leveraging MD simulations to identify key interactions stabilizing the drug in the BCR-ABL tyrosine kinase active site (Redaelli et al., 2012). Moreover, Raltegravir, an HTV-1 integrase inhibitor, was enhanced through MD studies that examined the enzyme's flexibility and optimized the drug's active site interactions (Hare et al., 2010). Additionally, Remdesivir, an antiviral targeting the RNA-dependent RNA polymerase

(RdRp) of SARS-CoV-2, benefited from MD simulations that elucidated its binding dynamics and structural stability (Yin et al., 2020). These examples highlight the significant impact of MD simulations in refining lead compounds, predicting binding affinities, and optimizing drug-target interactions, making them an essential tool in modern drug discovery.

Beyond traditional drug discovery, MD simulations have made significant contributions to lipid-related studies, particularly in understanding drug-membrane interactions and lipid-based drug delivery systems. For example, MD has been widely used to investigate the permeability of small molecules across lipid bilayers, elucidating passive diffusion mechanisms that influence drug absorption and bioavailability (Sharifian Gh., 2021). Additionally, antimicrobial peptide (AMP) research has leveraged MD simulations to uncover their membrane-disrupting mechanisms, guiding the design of novel antibiotics (Yeaman & Yount, 2003). Moreover, MD has been instrumental in studying the role of specific lipid compositions in modulating membrane protein function, such as ion channels and transporters, which are key drug targets (Stansfeld & Sansom, 2011). These advancements underscore the critical role of MD simulations in both drug discovery and lipid research, enabling a deeper understanding of molecular interactions and aiding in the development of innovative therapeutics.

Hydrogen bond analysis is a crucial aspect of MD simulations, providing insights into molecular stability and interactions. These bonds occur when a hydrogen atom covalently attached to an electronegative atom (such as oxygen or nitrogen) forms an interaction with another electronegative atom (Cardoso & Mendanha, 2021). In proteins, hydrogen bonds between the backbone and amide nitrogen are essential for stabilizing secondary structures, ensuring structural integrity and functionality. By monitoring atomic positions at each time step, researchers can assess the frequency and strength of hydrogen bonds, identifying key molecular predictors of binding interactions (Sharma et al., 2020). These findings play a significant role in drug discovery, aiding in the rational design of inhibitors and antiviral compounds by optimizing molecular interactions for enhanced efficacy.

CHAPTER 3
MATERIALS & METHODS

MD simulation is the main methodology employed in this study to study the behavior of kratom alkaloids in membrane lipid bilayers. The workflow of the steps involves preparing the input structure, equilibrating the system, simulation runs, and trajectory analyses (Figure 3.1).

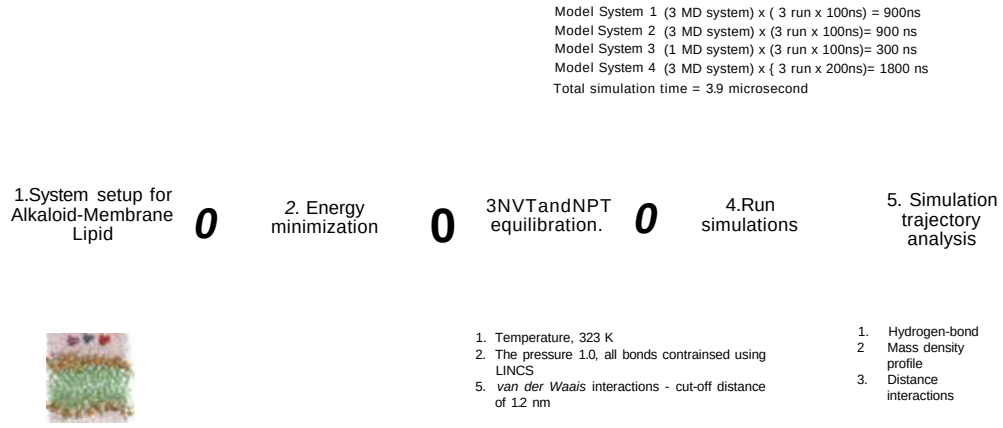

Figure 3.1 Workflow of MD Simulations.

3.1 Alkaloid Structure Preparation

The structural details of the three primary kratom alkaloids—mitragynine, 7-hydroxymitragynine (7-OH), and mitragynine pseudoindoxyl (MP) were obtained from the PubChem database (Bolton et al., 2008) (https://pubchem.ncbi.nlm.nih.gov/). Specifically, the PubChem IDs for these compounds is 3034396, 44301524, and 44301701, respectively.

Automated Topology Builder and Repository (ATB) website (Malde et al., 2011) was employed to protonate the alkaloid molecules. The ATB is a valuable resource for generating GROMACS topology files, which are essential for conducting MD simulations. These simulations have provided valuable insights into the dynamic behavior and interactions of kratom alkaloids within various molecular environments. Using ATB, the net charge of each alkaloid was carefully defined to reflect its state

under different physiological conditions. Each alkaloid was modeled in both its neutral and protonated states, capturing the diverse forms they may adopt across varying pH levels. The neutral state, with a net charge of zero, represented the uncharged form of the alkaloids, while the protonated state was assigned a +1 charge to reflect their ionized form. This approach ensured a comprehensive exploration of alkaloid-lipid interactions, enhancing our understanding of their behavior in biological membranes. The structure of alkaloids in Figure 3.2

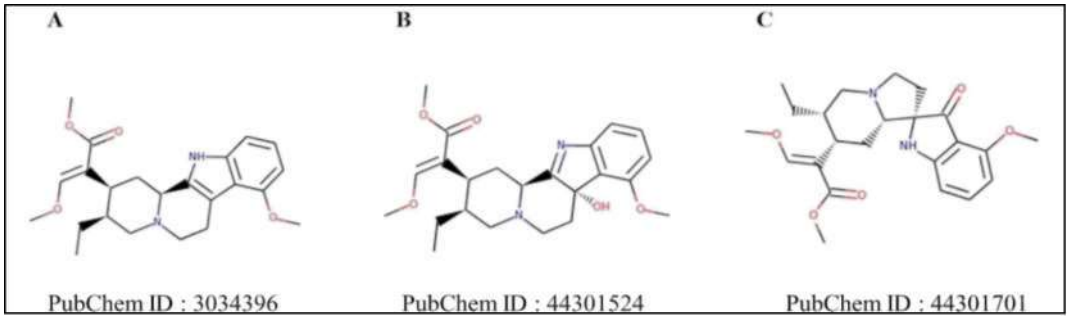

Figure 3.2 2D Structures of The Studied Kratom Alkaloids. The Structure of Protonated (A) Mitragynine, (B) 7-OH And (C) MP.

3.1.1 Preparation of the DPPC Lipid Bilayer

The starting configurations for the pre-equilibrated lipid bilayer were obtained from previously published research by Jusoh and Helms (2011) (Jusoh & Helms, 2011). This bilayer consisted of a total of 128 dipalmitoylphosphatidylcholine (DPPC) lipid molecules, with 64 lipids arranged in the upper leaflet and 64 in the lower leaflet (Lemkul, 2019), serving as a stable and well-characterized model system for studying lipid interactions. To accommodate the bilayer along with an explicit water environment, a simulation box was carefully designed with dimensions by increasing the size of the box. This setup ensured sufficient space for the lipid bilayer to maintain its structural integrity while allowing for the necessary hydration and dynamic interactions with surrounding water molecules, thereby creating a physiologically relevant simulation environment.

3.2 Model Development for the Alkaloid-DPPC Lipid Bilayer Systems

The first model system, Model System 1 served as the baseline for understanding the fundamental interactions of an individual alkaloid molecule with the lipid membrane. In all model systems, the kratom alkaloids molecule was positioned in aqueous water environment, 2.0 nm above the DPPC lipid head-group.

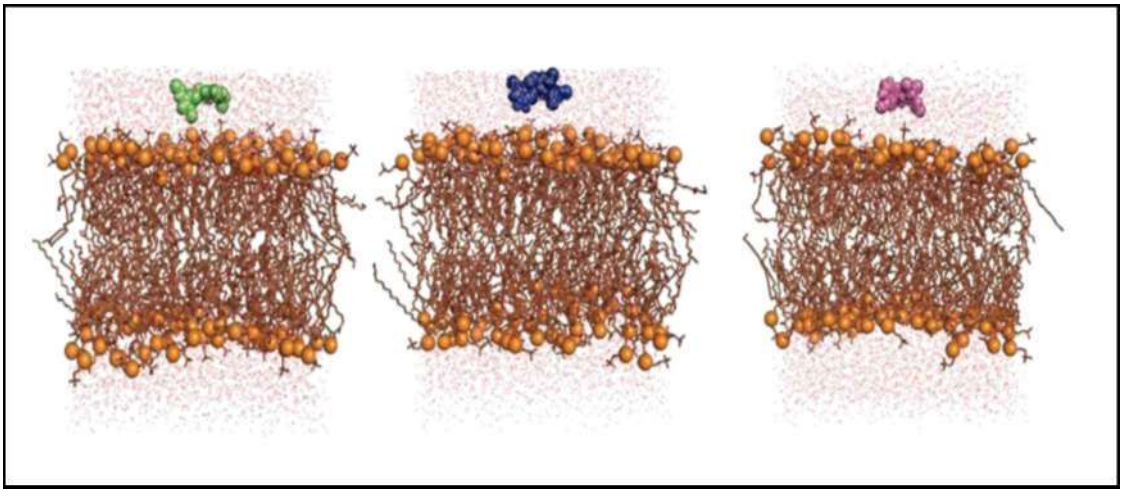

Figure 3.3 Model System 1 - Alkaloid-DPPC Lipid Bilayer. The Model System Contains One Molecule of Alkaloid: (A) Mitragynine (Green Spheres), (B) 7-OH (Blue Spheres) and (C) MP (Magenta Spheres).

The second model system, Model System 2 incorporates three molecules of the same alkaloid in the DPPC lipid bilayer. The model system is designed to explore the possibility of cooperative effects among identical alkaloids interacting with the lipid environment. This model may provide insights into concentration-dependent behaviors and possible aggregation tendencies.

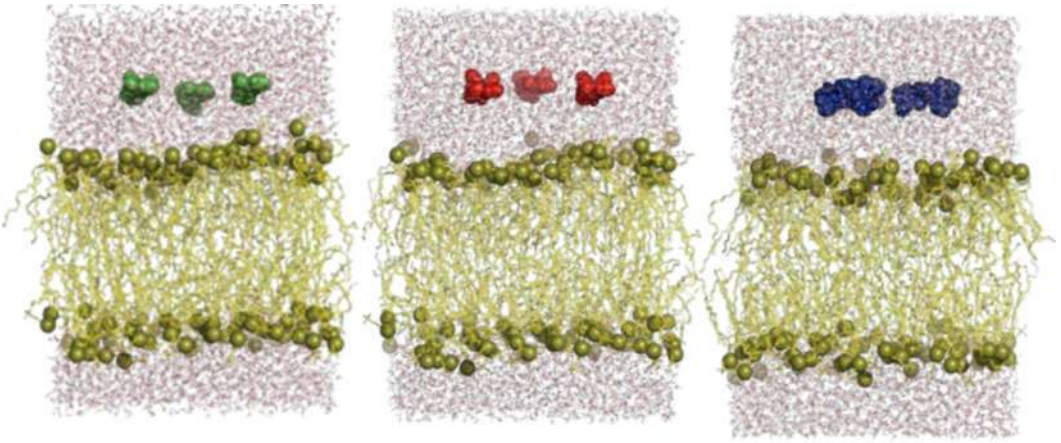

Figure 3.4 Model System 2 - Alkaloid-DPPC Lipid Bilayer. The Model System Contains 3 Molecules of the Same Alkaloids: (A) Mitragynine (Green Spheres), (B) 7-OH (Red Spheres) and (C) MP (Blue Sphere)

The third model system, Model System 3 consists of three molecules of different types of alkaloids. This configuration was set up to evaluate interactions of different types of alkaloids, shedding light on the potential variability in binding modes and structural adaptations of the lipids when exposed to a mix of alkaloids.

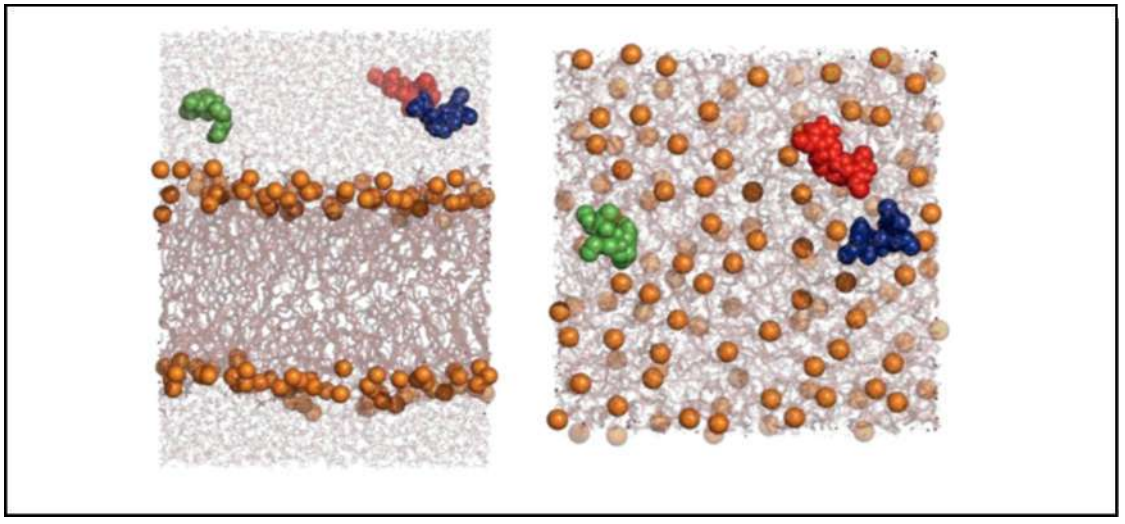

Figure 3.5 Model System 3 - Alkaloid-DPPC Lipid Bilayer. The Model System Contains Three Different Molecules of Alkaloid: Mitragynine (Green Spheres), 7-OH (Red Spheres) and MP (Blue Sphere).

The final system, Model System 4 features six different kratom alkaloids in a single DPPC lipid bilayer system. This model simulated high alkaloid concentrations to

mimic natural kratom extracts and assess their collective effects on membrane dynamics.

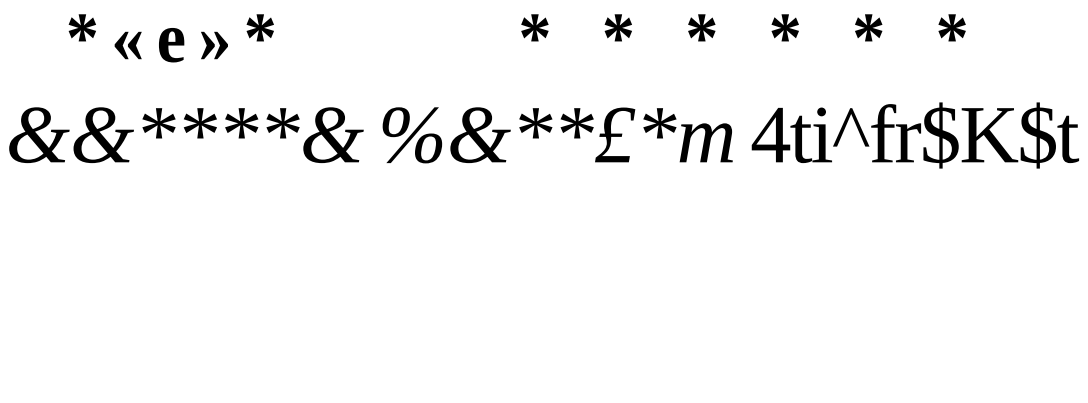

Figure 3.6 Model System 4 - Alkaloid-DPPC Lipid Bilayer. The Model System Contains 6 Molecules of Alkaloid: (A) Mitragynine (Green Spheres), (B) 7-OH (Red Spheres) and (C) MP (Blue Sphere)

3.3 MD Simulations

In each model system, alkaloid molecules were strategically placed in the water phase at a minimum distance of 10 A from both the nearest lipid headgroup and the edges of the box to avoid steric interference. The systems were further hydrated with a total of 6169 water molecules. To maintain electrical neutrality, counterions (Na+ and C1-) were introduced to balance the overall system charge. This setup ensured a stable and realistic environment for the simulations.

MD simulations were conducted using the GROMACS software suite, version 2021.5 (Abraham et al., 2015; Berendsen et al., 1995; Malde et al., 2011), an advanced tool designed for simulating and analyzing biomolecular systems. The GROMOS-54A7 force field (Abraham et al., 2015; Poger et al., 2010) was utilized to parameterize the atomic interactions, ensuring reliable simulation of the molecular systems. Additionally, a modified version of the 54A7 parameter set was implemented, incorporating the Berger lipid parameters (Berger et al., 1997) for accurately modeling the DPPC lipid molecules. This modification enhances the force field's ability to describe lipid bilayer systems with greater fidelity.

The SPC (Simple Point Charge) model was added to the DPPC lipid bilayer (Tieleman & Berendsen, 1996), a standard water model widely used for its simplicity and computational efficiency. The setup of the initial simulation systems involved meticulous preparation, including energy minimization and equilibration steps. Specifically, energy minimization was conducted using the steepest descent algorithm for 1000 steps to eliminate steric clashes and optimize the system's initial configuration. Following this, the systems were equilibrated under canonical (NVT) conditions to stabilize temperature, and then under isothermal-isobaric (NPT) conditions to equilibrate pressure.

Long-range electrostatic interactions, the Particle Mesh Ewald (PME) method (Darden et al., 1993) was employed, with a cutoff radius set to 1.2 nm, ensuring accurate treatment of Coulombic interactions while maintaining computational efficiency. Similarly, a 1.2 nm cutoff distance was applied for van der Waals interactions, balancing precision and computational cost. Constraints on bonds involving hydrogen atoms were enforced using the LINCS (Linear Constraint Solver) algorithm (Hess et al., 1997), enhancing the stability of the system and allowing for longer timesteps. Periodic boundary conditions were applied in all directions to mimic an infinite system, eliminating edge effects and ensuring realistic interactions.

The temperature of the system, specifically for the DPPC lipid bilayer, was carefully controlled and stabilized at 323 K using a temperature coupling time constant (TT) of 0.1 ps. This choice of temperature is relevant to study the behavior of the lipid bilayer in its fluid phase, closely resembling physiological conditions. The production simulations were carried out under the NPT ensemble, which maintains constant particle number, pressure, and temperature throughout the simulation, replicating realistic thermodynamic conditions. Each production run spanned 100 nanoseconds, employing a timestep of 2 femtoseconds to capture the dynamic behavior of the molecules in fine detail. The MD simulations were performed on a high-performance computing system running Ubuntu 22.04.3 LTS (64-bit) with 64 GB of RAM and 5 TB of disk storage. The system was equipped with an Intel® Core™ i9-7940X CPU (3.10 GHz, 14 cores, 28 threads) and dual NVIDIA TITAN V GPUs (GVlOO architecture), providing robust computational power for accelerated molecular simulations.

To ensure statistical reliability and reduce the potential influence of random fluctuations, each set of simulations was repeated in triplicate (Table 3.1), with three

independent production runs conducted per system. This approach allowed for comprehensive statistical analysis, yielding robust and reproducible results.

Table 3.1
List of MD Simulation Production Runs for the Alkaloid-DPPC Lipid Bilayer Model Systems Performed in This Study. Three Replicates were Conducted for Each System.

	Alkaloid	Total atoms in the system	Box size (x-y-z)	Duration nanosecond (ns)
Model System 1	Mitragynine	24943	x= 6.675 y= 6.701 z= 8.000	100 (x 3)
	7-OH	24942	x= 6.675 y= 6.701 z= 8.000	100 (x3)
	MP	24941	x= 6.675 y= 6.701 z= 8.000	100 (x3)
Model System 2	Mitragynine	25054	x= 6.675 y= 6.701 z= 8.000	100 (x3)
	7-OH	25057	x= 6.675 y= 6.701 z= 8.000	100 (x3)
	MP	26569	x= 6.675 y= 6.701 z= 8.000	100 (x3)
Model System 3	Mitragynine, 7-OH and MP	25046	x= 6.675 y= 6.701 z= 8.000	100 (x3)
Model System 4	Mitragynine	31297	x= 6.675 y= 6.701 z= 9.000	200 (x3)
	7-OH	31297	x= 6.675 y= 6.701 z= 9.000	200 (x3)
	MP	31272	x= 6.675 y= 6.701 z= 9.000	200 (x3)
				Total= 3.9 microseconds ((is)

3.4 Trajectory Analyses

Key analyses in lipid bilayer MD simulations include area per lipid, membrane thickness, deuterium order parameters and mass density profiles. These metrics help validate the simulation's accuracy by comparing results to experimental data and provide detailed information about membrane organization, phase behavior, and interactions with embedded molecules (e.g., proteins, drugs). In addition, for the interaction behavior between the alkaloid and lipid bilayer, distance and hydrogen bond analyses were also conducted from the MD simulation trajectories.

3.4.1 Intermolecular Distance

The interaction between the alkaloid and the DPPC lipid bilayer was quantitatively analyzed by computing the average distance between the center of mass

(COM) of the alkaloid and the headgroup region of DPPC lipids. This measurement was carried out using the gmx distance tool. To ensure accurate representation of the lipid headgroup, the distance was specifically calculated between the COM of the alkaloid molecule and the C1-C11 carbon atoms of the DPPC headgroup (Figure 2.4).

3.4.2 Area per Lipid and Membrane Thickness

Area per lipid and membrane thickness are essential for validating MD simulations, as they reflect bilayer packing and structural integrity, ensuring force fields accurately capture lipid interactions. These parameters provide insights into membrane phase behavior (e.g., gel vs. liquid-crystalline) and functional properties like permeability and mechanical stability. In this work, the calculation for the area per lipid and the bilayer thickness were analyzed with the GridMAT-MD program. This grid-based analysis tool was developed for analyzing membrane systems using MD trajectories (Allen, 2009).

The area per lipid is defined as the average lateral space occupied by a single lipid molecule, which serves as a fundamental indicator of bilayer packing and phase behavior. When simulations reproduce experimentally measured values (e.g., -0.60-0.65 nm^2 for DPPC in the liquid-crystalline phase) (Nagle & Tristram-Nagle, 2000), it validates the force field's ability to capture intermolecular interactions, such as headgroup repulsion and acyl chain packing. The formula to compute the area per lipid is as below:

$$Aii \wedge id \_ \wedge \wedge r^{2xLxXLy} \qquad (31)$$

Where *LxandLy* are the lateral dimension of the simulation box in the xy-plane, and the factor of 2 accounts for the two leaflets of the bilayer. *Ntotai* is refers to the total number of lipid molecules in the entire lipid bilayer system. This formula accounts for the fact that the lipid area *{LxandLy)* is divided by the number of lipids in one leaflet *{Ntotai /2).* The result reflects the average space occupied by a single lipid in the plane of the membrane.

Membrane thickness, typically measured as the distance between the phosphate groups of opposing leaflets, reflects the bilayer's structural integrity and hydrophobic

core organization. A thickness consistent with experimental data (e.g., -3.5 - 4.0 nm for DPPC) (Nagle & Tristram-Nagle, 2000) ensures that the simulated bilayer accurately models key biophysical features, such as permeability and mechanical stability. These metrics are interdependent: a larger area per lipid often correlates with reduced thickness due to looser packing, while a smaller area per lipid implies tighter packing and increased thickness. Together, they provide insights into the bilayer's phase (e.g., gel vs. liquid-crystalline) and response to perturbations, such as temperature changes or the incorporation of molecules like cholesterol or drugs. The formula for the membrane thickness calculation is as below:

$$\text{Membrane Thickness} = (\ |(\ Z,upper\ )\text{-}\{Zlower)\backslash) \qquad (3.2)$$

Where $Zu_{pp}er$ is the average z-coordinate of the phosphate groups in the upper leaflet, and *Zhwer* is the average z-coordinate of the phosphate groups in the lower leaflet. This measurement reflects the distance between the hydrophilic headgroups of the bilayer.

3.4.3 Mass Density Profile

The membrane density analysis is typically divided into several distinct groups, including lipid headgroups, acyl chains (which may be further categorized into glycerol, methylene, and terminal methyl groups), as well as ligand and solvent. The ligand and solvent groups are standard and do not require additional processing. To define index groups for membrane density analysis in GROMACS, the gmx makendx tool was utilized. During the interactive selection process, specific atoms are assigned to distinct membrane components. The lipid headgroups are selected, comprising atoms from CI to Oil. Likewise, the glycerol group (C12, C13, 014, C15, 016, C32, 033, C34, 035) and ester group (CI, C2, C3, N4 to Oil) are categorized into a separate index group. The acyl chains are determined by excluding both the headgroup and glycerol ester groups. Each of these groups can then be analyzed separately using the gmx density module, while ligand and solvent (SOL) are already included in the index file. The membrane density in GROMACS can be analyzed using the gmx density tool, which calculates the mass, charge, or number density of specified groups along a chosen axis, typically the bilayer normal (e.g., the z-axis) (Moradi et al., 2019). By defining index

groups for lipid headgroups, acyl chains, solvent, and ligands, gmx density provides insights into membrane organization, lipid distribution, and structural properties.

3.4.4 Deuterium Order Parameter

The deuterium order parameter (SCD) is shown as a function of the carbon atom positions along the acyl chains of DPPC lipid bilayers, providing insights into the structural ordering and orientation of the lipid tails (Leekumjorn & Sum, 2006; Lemkul, 2019). In this study, the sn-1 chain includes carbon atoms C34 and C36-C50, while the sn-2 chain consists of carbon atoms C15 and C17-C31. This numbering highlights the specific carbon atoms analyzed along each acyl chain of DPPC lipids, allowing for a detailed assessment of how lipid tail flexibility and order vary along the bilayer. By examining the SCD values across these carbon positions, it becomes possible to evaluate the degree of lipid tail alignment with the bilayer normal. The formula deuterium order parameter calculation is as below:

$$S_{CD} = -_2(3\cos^2 0\text{-}l) \quad (3.3)$$

Where 9 is the angle between the C-D bond vector and the bilayer normal, and the angle brackets () denote an ensemble average over time and molecules.

3.4.5 Hydrogen Bonds

Hydrogen bonds were calculated using the gmx hbond tool in GROMACS, employing geometric criteria to define the interactions. A hydrogen bond was identified based on the presence of three key atoms: a donor (an electronegative atom such as nitrogen or oxygen covalently bonded to a hydrogen), a hydrogen atom (the hydrogen covalently bonded to the donor), and an acceptor (another electronegative atom like nitrogen or oxygen interacting with the hydrogen). The analysis used a distance cutoff of 3.5 A between the donor and acceptor atoms and an angle cutoff of 30° for the donor-hydrogen-acceptor angle. The gmx hbond tool processed the trajectory files to calculate hydrogen bonds across the entire system or between specific molecular groups, providing outputs such as the number of hydrogen bonds, their lifetimes, and occupancy.

3.4.6 Data Visualization

The XMGrace program was utilized (https://plasma-gate.weizmann.ac.il/Grace/) to process and analyze the simulation trajectories. Gnuplot (http://www.gnuplot.info/) was employed for plotting and preparing high-quality graphical representations of the computed data, enhancing the clarity and presentation of the results (Racine, 2006). 3D visualization and detailed interaction analyses were carried out using the PyMOL molecular graphics system (Schrödinger, LLC, 2015; Yuan et al., 2017). PyMOL served as a vital tool for creating three-dimensional images, illustrating molecular interactions, and exploring spatial arrangements within the system.

CHAPTER 4
RESULTS & DISCUSSION

4.1 Dynamics and Stability of Lipid Bilayer System

In drug pharmacology, the important stage of the mechanism of action is the diffusion of the drug molecule through cellular membranes. This process is critical because it determines how effectively a drug can reach its target site within the body. Cellular membranes, primarily composed of a phospholipid bilayer, act as selective barriers that control the passage of substances in and out of cells. For a drug to exert its therapeutic effect, it must first traverse these membranes to enter the bloodstream, distribute throughout the body, and ultimately reach the target cells or tissues.

Understanding the molecular details of drug permeation and diffusion through cellular membranes is essential for optimizing drug design and delivery. One powerful computational tool that has become increasingly valuable in this context is MD simulation. MD simulations provide a detailed, atomistic view of the interactions between drug molecules and the lipid bilayer, offering insights that are difficult to obtain through experimental methods alone. In this study, MD simulation was employed to investigate the behavior of three kratom alkaloids—mitragynine, 7-hydroxymitragynine, and mitragynine pseudoindoxyl—within lipid bilayer systems.

4.1.1 Area per Lipid and Membrane Thickness

The area per lipid and membrane thickness are fundamental structural properties that characterize the packing and organization of lipids within a bilayer, providing critical insights into membrane dynamics and stability. These analyses are crucial for validating simulations of lipid bilayers, ensuring that the lipid bilayer systems reflect realistic biological behavior. Table 4.1 presents the analyses of the area per lipid and membrane thickness for the alkaloid-DPPC lipid bilayer systems in this study.

The simulation of the pure DPPC lipid bilayer, serving as the control system, yielded an area per lipid of 0.646 ± 0.02 nm^2 and a membrane thickness of 3.895 ± 0.01 nm. These results are consistent with previous computational and experimental studies,

such as the area per lipid range of 0.633-0.729 nm^2 reported by Nagle & Tristram-Nagle (2000) and the 0.655 nm^2 value from MD simulations by Domahski et al. (2004), suggesting that the simulation parameters and force field used in this study are appropriate for modeling DPPC bilayers.

In Model System 1, which contained one molecule of alkaloid embedded in the DPPC bilayer, the area per lipid increased to 0.698 ± 0.03 nm^2 across all three alkaloid systems, indicating that the presence of a single alkaloid molecule slightly disrupts lipid packing and expands the bilayer. Concurrently, the membrane thickness slightly decreased to 3.943 ± 0.02 nm, reflecting minor structural changes induced by the alkaloid. In Model System 2, which contained three molecules of the same type of alkaloid, the effects on the bilayer were more pronounced and varied depending on the specific alkaloid. For mitragynine, the area per lipid decreased to 0.583 ± 0.01 nm^2, and the membrane thickness reduced to 3.796 ± 0.46 nm. For 7-hydroxymitragynine, the area per lipid was 0.629 ± 0.03 nm^2, and the membrane thickness was 3.721 ± 0.49 nm. Similarly, for mitragynine pseudoindoxyl, the area per lipid was 0.645 ± 0.01 nm^2, and the membrane thickness was 3.714 ± 0.44 nm. These results suggest that the incorporation of multiple alkaloid molecules leads to tighter lipid packing and a thinner bilayer, likely due to increased interactions between the alkaloids and the lipid components. In Model System 3, which contained three different alkaloid molecules (mitragynine, 7-hydroxymitragynine, and mitragynine pseudoindoxyl) within the same bilayer, the area per lipid was 0.613 ± 0.08 nm^2, and the membrane thickness was 3.836 ± 0.36 nm. This indicates that the combined presence of multiple alkaloid types results in intermediate structural changes compared to systems with a single type of alkaloid.

Model System 4 contains six alkaloids, including mitragynine, 7-hydroxymitragynine (both penetrated and not penetrated forms), and mitragynine pseudoindoxyl. Mitragynine shows an area per lipid of 0.610 ± 0.01 nm^2, suggesting moderate interaction with the lipid bilayer, while 7-hydroxymitragynine displays two values: 0.615 ± 0.01 nm^2 for the penetrated form, indicating slight bilayer expansion, and 0.583 ± 0.01 nm^2 for the non-penetrated form, reflecting tighter lipid packing. Mitragynine pseudoindoxyl exhibits the highest area per lipid at 0.629 ± 0.02 nm^2, suggesting the greatest expansion or disordering of the bilayer. In terms of membrane thickness, mitragynine and mitragynine pseudoindoxyl result in similar values (3.764 ± 0.35 nm), indicating comparable effects on bilayer integrity. Penetrated 7-hydroxymitragynine shows a reduced thickness (3.710 ± 0.43 nm), suggesting bilayer

thinning upon penetration, while the non-penetrated form maintains a thicker membrane (3.862 ± 0.42 nm). These findings suggest that alkaloid penetration generally leads to bilayer expansion and thinning due to lipid packing disruptions, while non-penetrated states maintain or slightly increase membrane thickness. Such interactions can significantly impact bilayer properties, potentially affecting membrane fluidity and permeability.

The observed changes in area per lipid and membrane thickness across all model systems highlight the sensitivity of lipid bilayers to the presence, type, and concentration of alkaloid molecules. These results provide insights into how alkaloids influence membrane structure and dynamics, which is valuable for understanding drug- membrane interactions and their potential effects on membrane properties, such as fluidity and permeability.

Table 4.1
Area per Lipid and Membrane Thickness for All Alkaloid-DPPC Lipid Bilayer Systems.

Lipid Bilayer Systems	**Area per Lipid** (nm^2)	**Membrane Thickness (nm)**
Pure DPPC	0.646 ± 0.02	3.895 ± 0.01
Model System 1 - 1 Alkaloid	0.698 ± 0.03	3.943 ± 0.02
Model System 2 - 3 Alkaloids		
Mitragynine	0.583 ± 0.01	3.796 ± 0.46
7-hydroxymitragynine Mitragynine	0.619 ± 0.03	3.787 ± 0.29
pseudoindoxyl	0.624 ± 0.01	3.721 ± 0.44
Model System 3 - 3 Different Alkaloids	0.612 ± 0.08	3.836 ± 0.36
Model System 4 - 6 Alkaloids		
Mitragynine		
7-hydroxymitragynine:	0.610 ± 0.01	3.764 ± 0.35
(penetrated)	0.615 ± 0.01	3.710 ± 0.43
(Not penetrated)	0.583 ± 0.01	3.862 ± 0.42
Mitragynine pseudoindoxyl	0.629 ± 0.02	3.764 ± 0.35
Experimental References (Nagle & Tristram-Nagle, 2000)	0.633 - 0.729	3.83
MD references (Pure DPPC) (Patra et al., 2004)	0.600 0.655	3.60

4.1.2 Mass Density Profile and Deuterium Order Parameter of Pure DPPC Lipid Bilayer

The mass density profile is another fundamental property used to characterize the structural organization of lipid bilayers at the molecular level. It provides a spatial distribution of the mass density of different components (e.g., lipid headgroups, tails, water, and embedded molecules) along the axis perpendicular to the bilayer plane (z-axis). This profile is essential for understanding the arrangement and dynamics of lipids and other molecules within the membrane, as well as their interactions with the surrounding environment. In this study, the mass density profile of all model systems was computed during the final 50 ns of the simulations. This is to ensure that the systems already converged and reach stable configuration.

The density profile plot for a pure DPPC lipid bilayer provides a detailed spatial distribution of the various components within the bilayer, offering critical insights into its structural organization and physical properties. The plot reveals a symmetric distribution around the bilayer center, reflecting the equivalence of the two leaflets, which is characteristic of a stable, equilibrated system. Each leaflet consists of hydrophilic headgroups facing the aqueous environment and hydrophobic tails oriented toward the bilayer center, forming a well-defined, lamellar structure. The phosphate groups, part of the lipid headgroups which are around -2.569-2.544 nm, show sharp peaks at a specific distance from the bilayer center, marking the interface between the hydrophobic core and the aqueous environment. The choline groups, also part of the headgroup, exhibit peaks slightly offset from the phosphate groups, closer to the aqueous phase, reflecting the orientation and arrangement of the headgroups. The carbonyl groups of the glycerol backbone appear as smaller peaks between the headgroup and tail regions, indicating the transition zone from the hydrophilic headgroups to the hydrophobic tails. The lipid tails dominate the central region of the bilayer, forming a hydrophobic core with the highest density in the bilayer center, gradually decreasing toward the headgroup region, reflecting the fluid-like nature of the hydrophobic core in the liquid crystalline phase.

The density profile of water shows a sharp increase at the headgroup region, reaching a plateau in the bulk water phase, while dropping to near zero in the hydrophobic core, confirming the bilayer's role as a barrier to water and polar molecules. The limited penetration of water into the headgroup region highlights the bilayer's

ability to maintain compartmentalization. The distance between the peaks corresponding to the phosphate groups in the two leaflets provides an estimate of the bilayer's hydrophobic thickness, typically around 3-4 nm for DPPC bilayers, depending on temperature and hydration conditions. This thickness is a key parameter for understanding the bilayer's mechanical properties and its interactions with embedded proteins or other molecules. The width of the interface between the hydrophobic core and the headgroup region can be inferred from the density profile, with a broader interface suggesting greater disorder or flexibility in the lipid packing, and a sharper interface indicating a more ordered arrangement. For DPPC bilayers in the liquid crystalline phase, the interface is relatively broad, reflecting the dynamic nature of the lipid molecules.

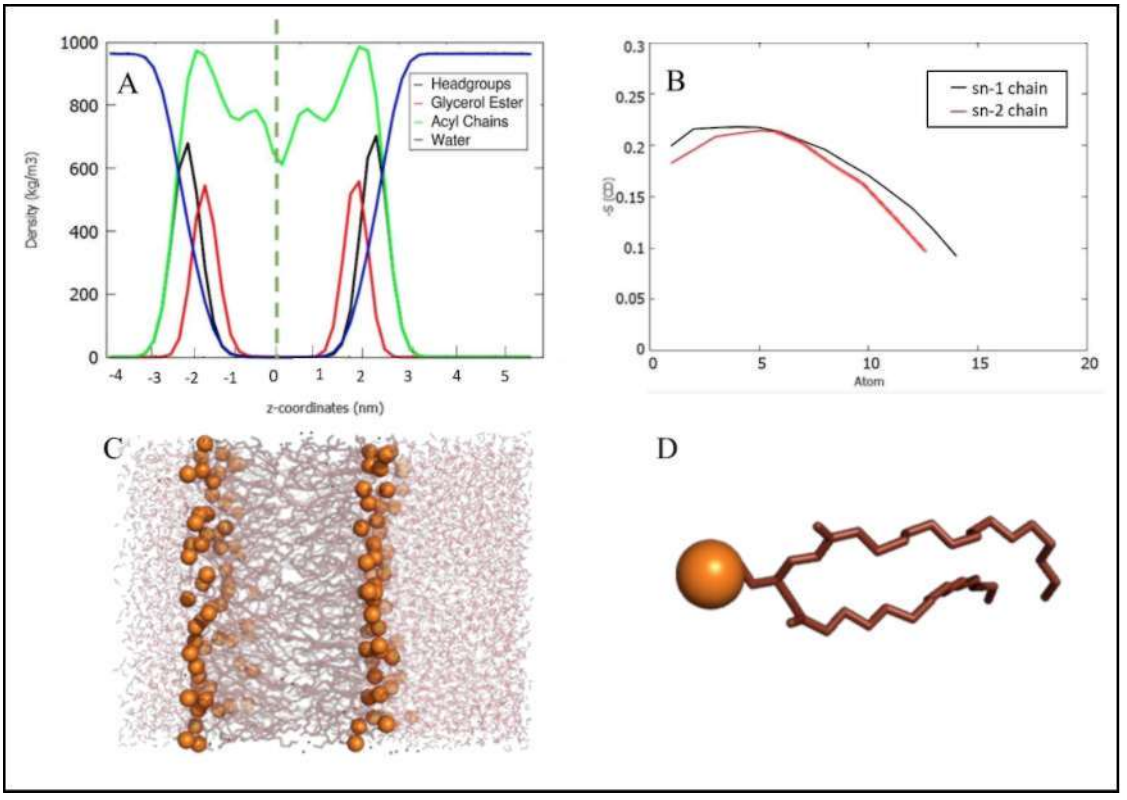

Figure 4.1 Mass Density and Deuterium Order Parameter of Pure DPPC Lipid Bilayer. (A) Mass Density Profile, (B) Deuterium Order Parameter, (C) A Snapshot of 100 ns Simulation of DPPC Bilayer, and (D) A molecule of DPPC lipid.

The lipid tail deuterium order parameter (SCD) serves as an important metric for assessing the ordering and dynamics of lipid acyl chains in a bilayer (Leekumjorn & Sum, 2006). It is a tool for understanding membrane structure, fluidity, and the effects

of external factors, making it essential for both experimental and computational studies of lipid bilayers. SCD profile for the acyl chains of DPPC provides a quantitative measure of the spatial variation in molecular order and dynamics within the lipid bilayer (Figure 4.1). In the region proximal to the headgroup (carbons C2-C5), SCD values are typically elevated (ranging from -0.2 to 0.3), indicative of a highly ordered and rigid structure. This ordering arises from the strong intermolecular interactions between the polar headgroups and the constrained packing of the upper segments of the acyl chains. Progressing toward the mid-chain region (carbons C6-C10), the SCD values exhibit a gradual decline, reflecting increased conformational flexibility and reduced order due to diminished steric constraints and enhanced thermal motion. At the terminal ends of the acyl chains (carbons C11-C16), the SCD values decrease significantly (range of -0.05 to 0.1), approaching near-isotropic behavior. This reduction in order at the chain termini is characteristic of the high degree of motional freedom and dynamic disorder in this region. The observed gradient in SCD values along the acyl chains is a well-documented feature of lipid bilayers, consistent with experimental NMR studies and MD simulations values in the range -0.20 ± 0.02 (Nagle, 1993).

4.2 Model System 1 - Behavior of A Single Molecule of Alkaloid in DPPC Lipid Bilayers

The first model system was designed to initially understand the basic interaction of an alkaloid with the lipid bilayers. Thus, Model System 1 was built to represent a single molecule of kratom alkaloid in a lipid bilayer system for mitragynine, 7-hydroxymitragynine, and mitragynine pseudoindoxyl.

Figure 4.2 presents the interaction of a single molecule of kratom alkaloids—mitragynine, 7-hydroxymitragynine, and mitragynine pseudoindoxyl—with DPPC lipid bilayers over the course of a 100 ns MD simulation. In Model System 1, mitragynine exhibited the most rapid bilayer penetration, integrating into the hydrophobic core within approximately 16 ns, likely due to its small and planar structure that promotes swift interaction with the lipid environment. In contrast, 7- hydroxymitragynine and mitragynine pseudoindoxyl displayed comparable penetration times of around 33 ns and 32 ns, respectively, with their hydroxyl and pseudoindoxyl functional groups potentially forming transient interactions with the polar lipid headgroups, thereby slightly delaying

their insertion compared to mitragynine. Once embedded, all three alkaloids remained stably localized just beneath the lipid headgroup region throughout the remainder of the simulation, suggesting strong hydrophobic interactions with the membrane, which underscores their potential for efficient membrane association and possible implications for their pharmacokinetic behavior and cellular membrane interactions.

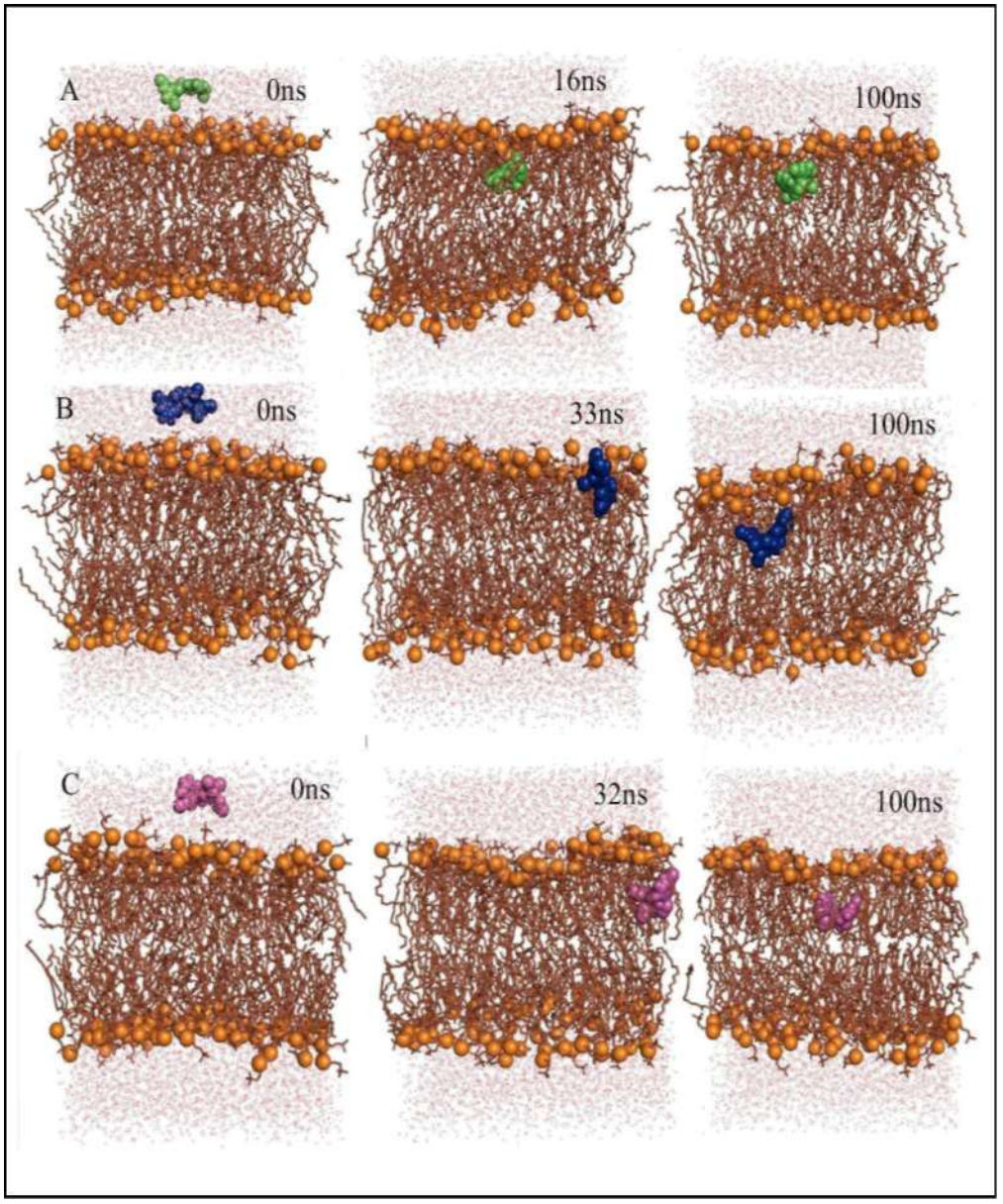

Figure 4.2 Interactions of a Single Kratom Alkaloid with DPPC Lipid Bilayers During 100 ns MD Simulations**.** Snapshots of (A) Mitragynine (Green Spheres), (B) 7-Hydroxymitragynine (Blue Spheres), and (C) Mitragynine Pseudoindoxyl (Magenta Spheres), Lipid Headgroup (Orange Balls), Lipid Tails (Brown Sticks) and Water (Red Sticks).

Distance analysis was conducted in order to evaluate detail interactions between a kratom alkaloids in Model System 1 of mitragynine, 7-hydroxymitragynine, and mitragynine pseudoindoxyl—and the DPPC lipid bilayers. Table 4.2 presents the visualization plots of average distance for alkaloid molecules in each system during the 100 ns of the MD simulations and the average distance based on the final 50 ns. Based on the plots, Model System 1 of mitragynine exhibits the fastest interactions of mitragynine with the lipid bilayer (16 ns). Inline with the simulation trajectories, mitragynine molecules that entered the lipid bilayer region remained in the hydrophobic environment throughout the simulations. The distance analysis of the final 50 ns of the simulations shows the average distance of 1.23 ± 0.71 nm between the mitragynine molecules to lipid headgroups. The result indicates very close and stable interactions of the mitragynine with the polar region of the DPPC lipids. On the other hand, both plots for the 7-hydroxymitragynine and mitragynine pseudoindoxyl displayed similar trends, which is parallel with the insertion time for both molecules as visualized from the simulation trajectories (Figure 4.2). Toward the end of the simulations, mitragynine pseudoindoxyl and 7-hydroxymitragynine formed stable interactions with the lipid headgroups with the average distance of 2.40 ± 0.31 nm and 3.62 ± 0.27 nm, respectively. The finding from Model System 1 shows a single molecule of kratom alkaloid able to rapidly diffuse into the lipid bilayer and reside below the lipid headgroups, which emphasize the amphiphilic nature of these alkaloids.

Table 4.2
The Average Distance of Kratom Alkaloids to The DPPC Lipid Headgroup in Model System 1. The Presented Values are Based on The Final 50 ns of Simulations.

Alkaloids	Distance to membrane	Distance Plot
Mitragynine	1.23 ±0.71 nm	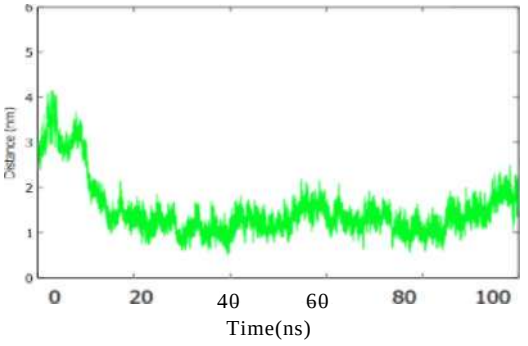

7-hydroxymitragynine	3.62 ± 0.27 nm
Mitragynine pseudoindoxyl	2.40 ± 0.31 nm

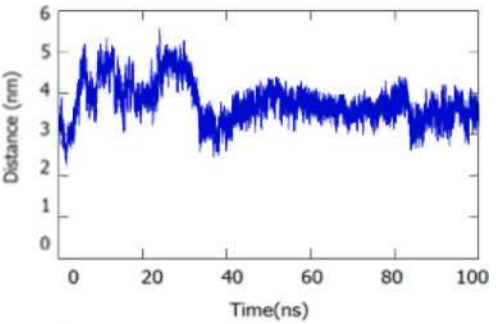

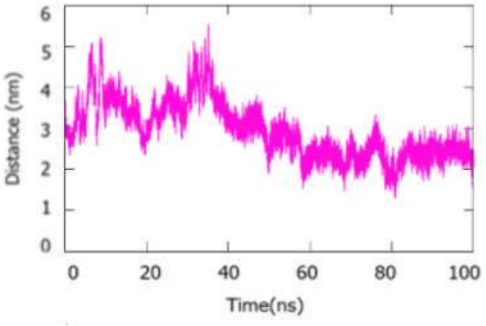

4.2.1 Mass- Density Profile and Deuterium Order Parameter

In Model System 1, the mass density distribution of the major molecules within the lipid bilayer closely matches that observed in simulations of pure DPPC, indicating that the overall structure and organization of the bilayer remain consistent even in the presence of kratom alkaloids. For mitragynine, the density peak was observed at 0.48 ± 0.14 nm, suggesting that this alkaloid tends to regions of the lipid bilayer, near the interface between the hydrophilic headgroups and the hydrophobic core. In contrast, 7- hydroxymitragynine exhibited a density peak at -0.72 ± 0.15 nm, showing that it penetrates deeper into the hydrophobic core of the bilayer. Mitragynine pseudoindoxyl showed a density peak at 0.33 ± 0.18 nm, placing it closer to the center of the bilayer than mitragynine but not as deep as 7-hydroxymitragynine. The results, illustrated in Figure 4.3, provide valuable insights into the behavior of kratom alkaloids in lipid bilayers.

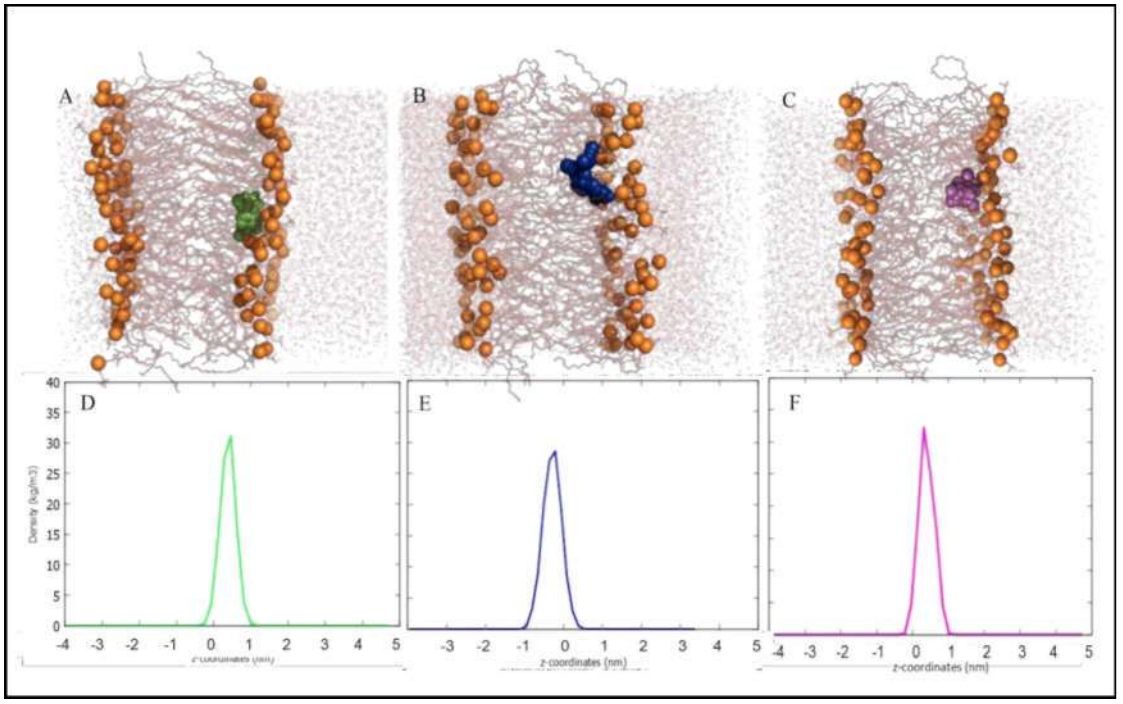

Figure 4.3 The Mass Densities of A Single Kratom Alkaloid in DPPC Lipid Bilayer. (A-C) The Snapshot of 100 ns of Mitragynine (Green Spheres), 7-hydroxymitragynine (Blue Spheres) and Mitragynine Pseudoindoxyl (Magenta Spheres), Lipid Headgroup (Orange Spheres), Lipid Tails (Brown Sticks) and Water (Red Sticks). The Mass Densities Plots of a Kratom Alkaloids in DPPC Lipid Bilayer. (D) Mitragynine (Green), (E) 7-hydroxymitragynine (Blue) and (F) Mitragynine Pseudoindoxyl (Magenta)

ScDfor the sn-1 and sn-2 chains of DPPC in Model System 1, that consist the presence of a single alkaloid molecules—mitragynine, 7-hydroxymitragynine, and mitragynine pseudoindoxyl—are presented in Figure 4.4. The SCD profiles for these systems exhibit trends that are consistent with those observed in pure DPPC bilayers. Specifically, the SCD values are higher near the headgroup region (C2-C5) and decrease progressively toward the tail ends (C11-CI6), reflecting the characteristic gradient of order in lipid bilayers. This indicates that the presence of these alkaloids does not significantly disrupt the overall ordering of the DPPC acyl chains. While minor variations in SCD values are observed at specific carbon positions, particularly in the mid-chain region (C6-C10), these variations are likely due to localized interactions between the alkaloids and the lipid chains and do not alter the fundamental structure of the bilayer. The consistency in SCD profiles across all three alkaloid systems further supports the conclusion that the incorporation of a single molecule of alkaloid does not induce major changes in the structural properties of the DPPC bilayer. Thus, the results

suggest that the DPPC bilayer maintains its structural integrity and dynamic behavior in the presence of these alkaloids, aligning well with the behavior of pure DPPC.

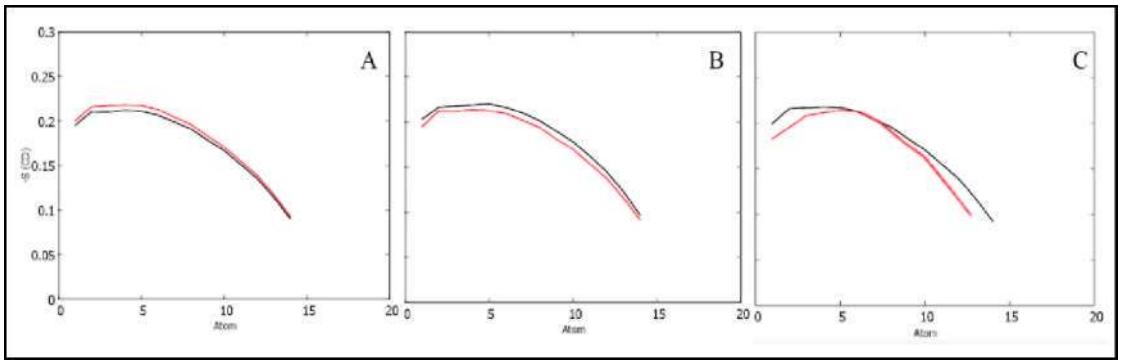

Figure 4.4 Deuterium Order Parameters (SCD) for DPPC in Model System 1. (A) Mitragynine, (B) 7-hydroxymitragynine, (C) and Mitragynine Pseudoindoxyl. The Lines Represent DPPC Acyl Chains: Sn-1 (Black) and Sn-2 (Red).

4.2.2 Hydrogen Bond Interactions

Hydrogen bonding plays a critical role in determining membrane permeability (Desai et al., 2012; Dickson et al., 2019). Figure 4.5 displays the hydrogen bonds interactions of alkaloids between the lipids and water molecules. During the simulation, mitragynine and mitragynine pseudoindoxyl each formed up to 3 hydrogen bonds with lipid headgroups. Inline with the observed close proximity of mitragynine and mitragynine pseudoindoxyl to the lipid headgroup after residing inside the lipid bilayers, the plot shows consistently 2 hydrogen bonds were formed until the end of simulations. Meanwhile, the 7-hydroxymitragynine system shows that 7- hydroxymitragynine occasionally formed one hydrogen bond with the lipid headgroups, particularly after residing inside the lipid bilayer. As observed from the plot, there were durations that the hydrogen bonds were absent, which could indicate the position of the molecule located deep into the hydrophobic core region. This result inline with the mass density profile of the 7-hydroxymitragynine system that displays the density of 7- hydroxymitragynine position at the middle position of bilayer normal (Figure 4.3-E), where the molecule was far from the polar headgroup region. On the other hand, mitragynine, 7-hydroxymitragynine and mitragynine pseudoindoxyl formed hydrogen bonds with lipid

headgroup when entering the lipid bilayer, which shows by the 3D visualization and density plot that its located mostly at lower lipid leaflet (Figure 4.3 D, E and F).

Hydrogen bond interactions between the alkaloids and water molecules of the Model System 1 clearly shows the decrease of interactions with water after the alkaloid diffused into lipid bilayer. Both the 7-hydroxymitragynine and mitragynine pseudoindoxyl system, initially during the location of the molecules in the water phase, strongly formed 7 hydrogen bonds with water molecules. However, when residing inside the bilayer, the number of hydrogen bonds is reduced to one interaction for both alkaloids. Nevertheless, 7-hydroxymitragynine and mitragynine pseudoindoxyl molecules were the most consistent and had the highest number of hydrogen bonds with water compared to the mitragynine in Model System 2. In the mitragynine system, before entering the lipid region, it consistently formed 6 hydrogen bonds with water molecules, and the number reduced to 1-2 interactions obviously shows the location of alkaloids. Moreover, the result illustrates that these alkaloids not only form hydrogen bonds with lipid headgroups, but also form interactions with water molecules at the interface.

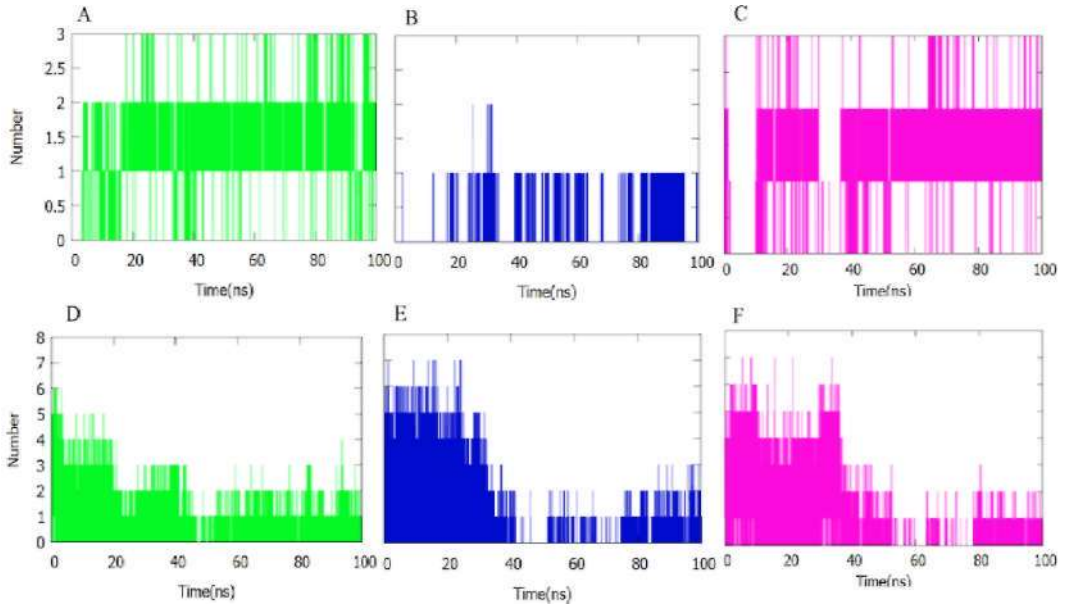

Figure 4.5 Hydrogen Bond Analysis in Model System 1. Hydrogen Bond Interactions Between the Kratom Alkaloid and Lipids (A, B, C), and Water Molecules (D, E, F) During the 100 ns of MD Simulations. Mitragynine (A, D), 7-Hydroxymitragynine (B, E), and Mitragynine Pseudoindoxyl (C, F).

4.3 Model System 2 - Behavior of Three Molecule of Alkaloids in DPPC Lipid Bilayers

In Model System 2, three molecules of the same type of kratom alkaloid were studied within the DPPC lipid bilayer. This system aims to evaluate the behavior of the alkaloids when having several of the same type of molecules. Figure 4.6 shows snapshots of each system at the initial stage (0 ns), the penetration stage, and the final stage (100 ns) of the simulations. During the simulation of the three mitragynine molecules, one of the molecules penetrated the lipid bilayer at approximately 15 ns, while the other two remained in the aqueous environment, forming interactions there. By the end of the simulation, all three mitragynine molecules had entered the lipid bilayer milieu; however, they did not form aggregates within the bilayer. Similarly, for the 7-hydroxymitragynine system, one molecule began interacting with the DPPC bilayer at approximately 10 ns, followed subsequently by the other two molecules. By the final stage of the simulation, all three 7-hydroxymitragynine molecules had positioned themselves below the lipid headgroups of the DPPC bilayer. Among these, two molecules were observed to interact with each other, while the third remained isolated. For the mitragynine pseudoindoxyl system, penetration began at a later stage, approximately 53 ns. Nevertheless, the behavior of the three mitragynine pseudoindoxyl molecules was similar to that observed in the 7-hydroxymitragynine system. Overall, the presence of three alkaloid molecules in the aqueous environment did not lead to rapid aggregation among the molecules. Instead, the alkaloids managed to penetrate the lipid bilayer at an early stage of the simulations. Furthermore, these alkaloids were preferentially localized in the hydrophobic region of the DPPC lipids while still forming polar interactions with the lipid phosphate groups.

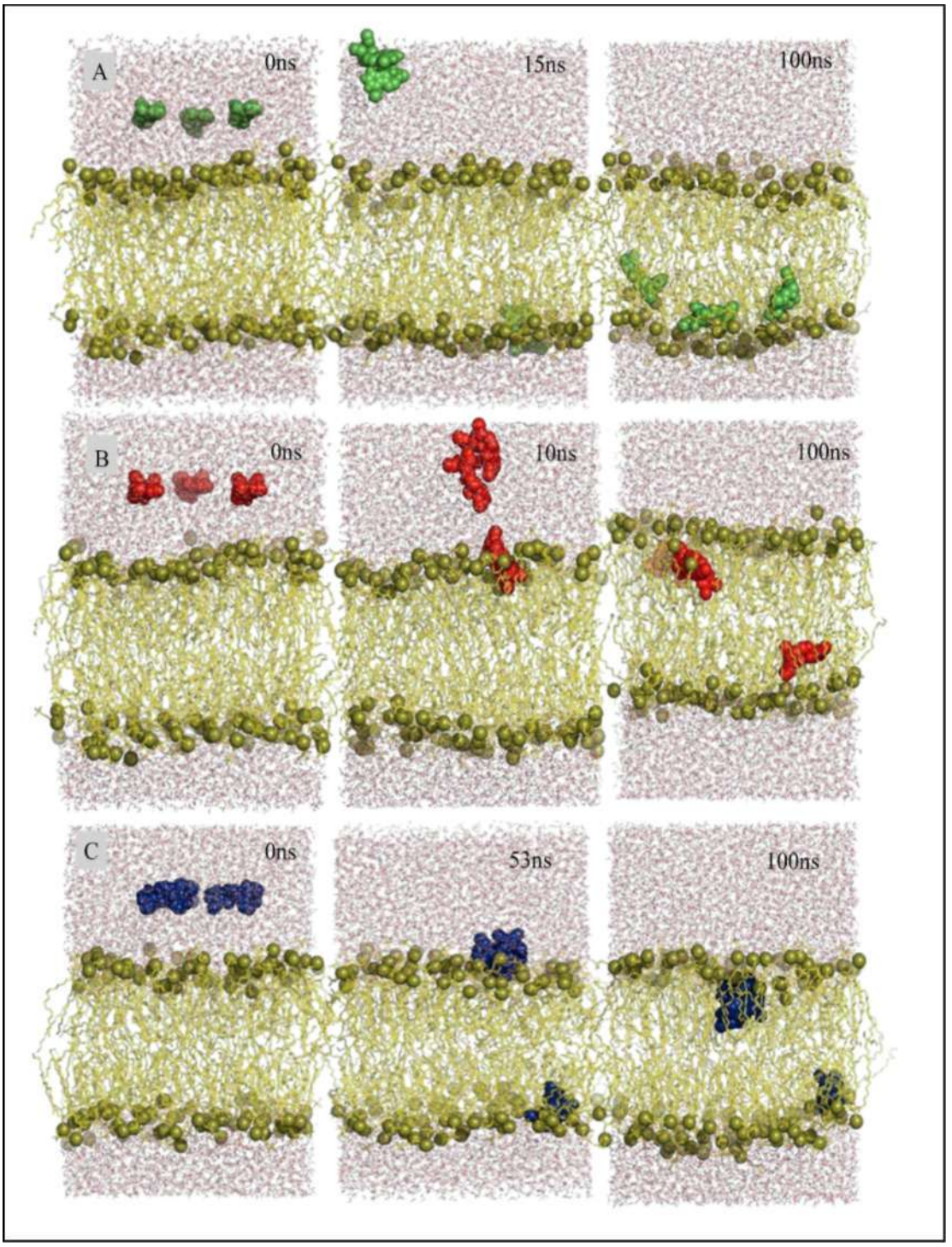

Figure 4.6 Interactions of Three Molecules of Kratom Alkaloids with DPPC Lipid Bilayers During 100 ns MD Simulations. Snapshots of (A) Mitragynine (Green Spheres), (B) 7-Hydroxymitragynine (Red Spheres), and (C) Mitragynine Pseudoindoxyl (Blue Spheres), Lipid Headgroup (Olive Spheres), Lipid Tails (Yellow Sticks) and Water (Red Sticks).

Distance analysis was conducted in order to evaluate detail interactions between the three kratom alkaloids in Model System 2 of mitragynine, 7-hydroxymitragynine,

and mitragynine pseudoindoxyl—and the DPPC lipid bilayers. Table 4.3 presents the visualization plots of average distance for the three alkaloid molecules in each system during the 100 ns of the MD simulations and the average distance based on the final 50 ns. Based on the plots, Model System 2 of 7-hydroxymitragynine exhibits a similar trend of the three molecules starting to interact with the lipid headgroups before 20 ns of the simulation. As observed from the simulation trajectories, 7-hydroxymitragynine molecules that entered the lipid bilayer region remained in the hydrophobic environment throughout the simulations. The distance analysis shows the average range of 1-4 nm (3.256 ± 0.36 nm) between the 7-hydroxymitragynine molecules to lipid headgroups, which indicate the dynamics positions of the molecules inside the lipid bilayer. Similarly, Model System 2 of mitragynine shows the three molecules formed interactions with the lipids approximately at 20 ns and resided in the lipid bilayer region within the same range of distance as the 7-hydroxymitragynine system, averagely 3.052 ± 0.70 nm. The slowest penetration, exhibited by Model System 2 of mitragynine pseudoindoxyl displayed the shortest interactions to the lipids approximately at 30 ns, however the penetration of the first mitragynine pseudoindoxyl happened after 50 ns (Figure 4.6). Although one of the molecules exhibited unstable behavior, the average distance of the mitragynine pseudoindoxyl to the lipid headgroups was the shortest among the Model System 2 (2.891 ± 0.43 nm).

Table 4.3
The Average Distance of Kratom Alkaloids to The DPPC Lipid Headgroup In Model System 2. The Presented Values are Based on The Final 50 ns of Simulations.

Alkaloids	**Distance to membrane**	**Distance Plot**
Mitragynine	3.052 ± 0.70 nm	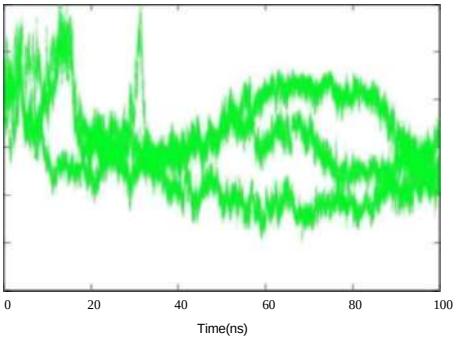

Alkaloids	Distance to membrane	Distance Plot
7-hydroxymitragynine	3.256 ± 0.36 nm	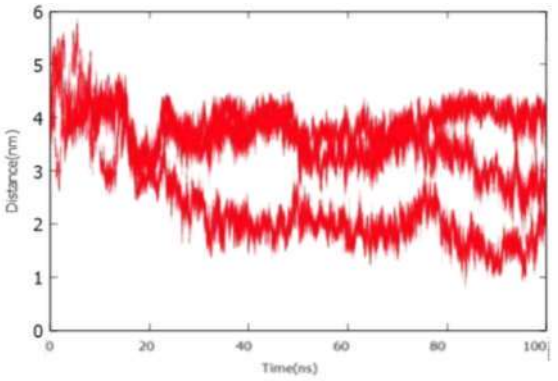
Mitragynine pseudoindoxyl	2.891 ± 0.43 nm	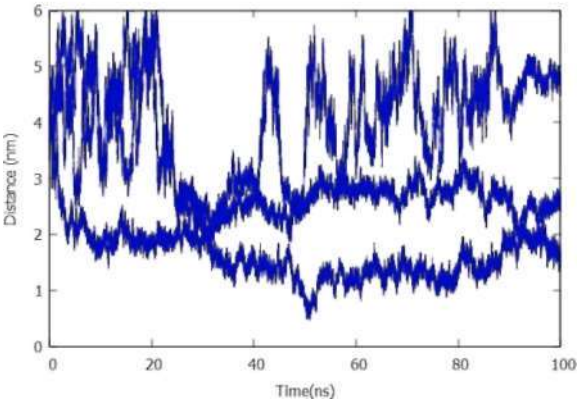

4.3.1 Mass- Density Profile and Deuterium Order Parameter

Figure 4.7 displays the density distribution of three kratom alkaloids in Model System 2 of mitragynine, 7-hydroxymitragynine, and mitragynine pseudoindoxyl within the DPPC lipid bilayer based on the final 50 ns of MD simulations. Mitragynine demonstrated a peak position at -2.3 ± 0.15 nm, indicating its deep penetration into the hydrophobic region of the bilayer. Similarly, mitragynine pseudoindoxyl exhibited peak positions at -1.5 ± 0.20 nm and 1.82 ± 0.18 nm, reflecting its ability to integrate into both leaflets of the bilayer. In contrast, 7-hydroxymitragynine remained closer to the bilayer surface with a peak at 0.45 ± 0.16 nm, suggesting it prefers to interact with the polar headgroup region due to its structural features. These results highlight that mitragynine and mitragynine pseudoindoxyl are well-integrated within the membrane, while 7-hydroxymitragynine predominantly associates with the bilayer surface which representative for the simulation.

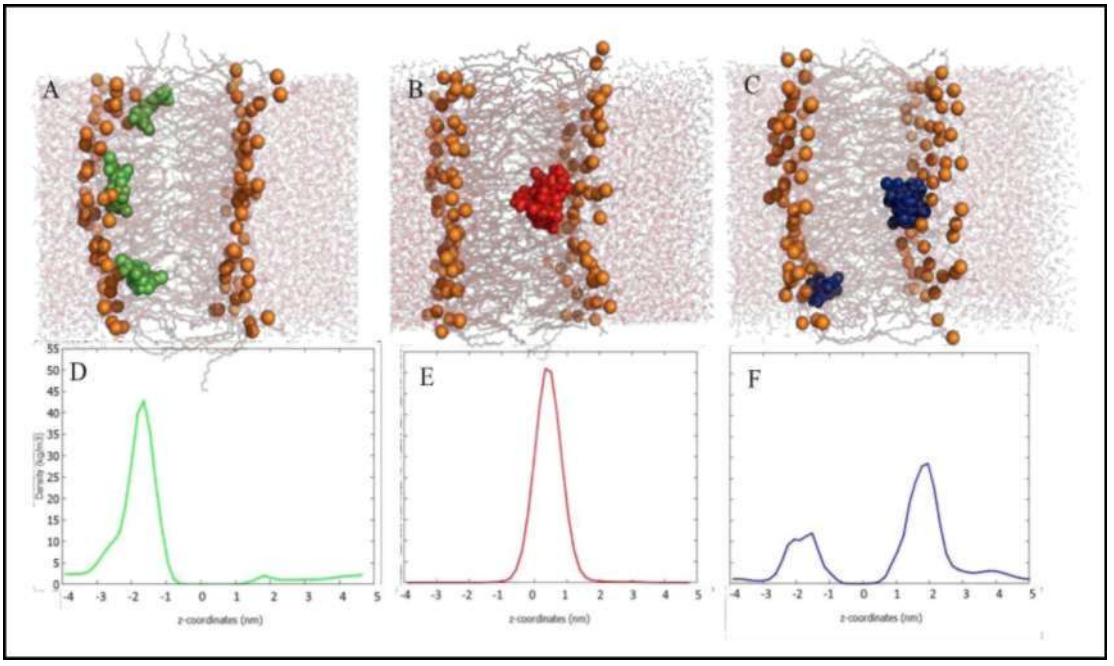

Figure 4.7 The Mass Densities Profile of Alkaloids in Model System 2. Snapshots at 100 ns of Model System 2; (A) Mitragynine (Green Spheres), (B) 7-Hydroxymitragynine (Red Spheres), and (C) Mitragynine Pseudoindoxyl (Blue Spheres), Lipid Headgroup (Orange Spheres), Lipid Tails (Brown Sticks) and Water (Red Sticks). The Mass Densities of Three Kratom Alkaloids in DPPC lipid bilayer for (D) Mitragynine (Green Line), (E) 7-Hydroxymitragynine (Red Line) and (F) Mitragynine Pseudoindoxyl (Blue Line).

Figure 4.8 presents the deuterium order parameters (SCD) for the sn-1 and sn-2 chains of DPPC lipids in the presence of three kratom alkaloids: Mitragynine,7-hydroxymitragynine, and Mitragynine pseudoindoxyl. Across all three systems, the lipid tails show a clear trend of decreasing order from the headgroup region to the terminal end, as seen by the gradual decline in S_{CD} values along the carbon atoms. The sn-1 chain generally exhibits slightly higher order compared to the sn-2 chain, especially in the presence of 7-hydroxymitragynine and mitragynine pseudoindoxyl, suggesting that these alkaloids may influence lipid tail organization. The absence of sharp changes in SCD values suggests that the membranes remained in the fluid phase throughout the simulations, indicating that none of the alkaloids induced a transition to a gel phase. This is significant because the presence of alkaloids did not rigidify the bilayer structure, maintaining typical DPPC fluidity levels despite interactions with the lipid environment.

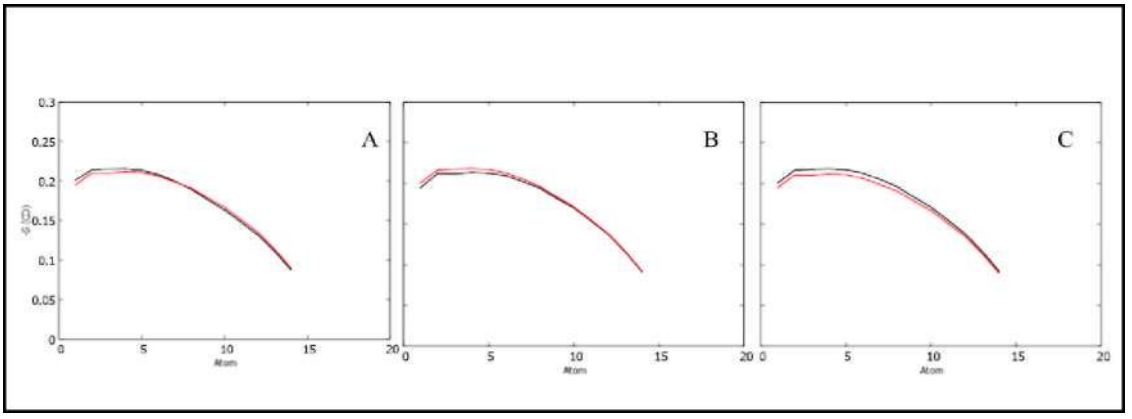

Figure 4.8 Deuterium Order Parameters (SCD) for DPPC in Model System 2. (A) Mitragynine, (B) 7-hydroxymitragynine, (C) and Mitragynine Pseudoindoxyl. The Lines Represent DPPC Acyl Chains: Sn-1 (Black) and Sn-2 (Red).

4.3.2 Hydrogen Bond Interactions

Figure 4.9 displays the hydrogen bond interactions between the alkaloids and DPPC lipid bilayers during the 100 ns MD simulation for the three molecules of the same alkaloid. In the mitragynine system, all three mitragynine molecules occasionally formed up to 3 hydrogen bonds with the lipid headgroups. Inline with the observed close proximity of mitragynine to the lipid headgroup after residing inside the lipid bilayer, the plot shows consistently 2 hydrogen bonds were formed till the end of the simulations. Meanwhile, the 7-hydroxymitragynine system shows that each 7-hydroxymitragynine molecule consistently formed only one hydrogen bond with the lipid headgroups, particularly after residing in the lipid bilayer. As observed from the plot, there were durations that the hydrogen bonds were absent, which could indicate the position of the molecules located deep into the hydrophobic core region. This result is inline with the mass density profile of the 7-hydroxymitragynine system that displays the density of 7-hydroxymitragynine at the middle position of bilayer normal (Figure 4.7-E), where the molecules were far from the polar headgroup regions. On the other hand, the mitragynine pseudoindoxyl system demonstrates a similar trend as the mitragynine system for the two molecules. The other molecule exhibited only one hydrogen bond formed with the lipid headgroup when entering the lipid bilayer, which shows by the 3D visualization and the density plot that its location mostly at the lower lipid leaflet (Figure 4.7-C and F).

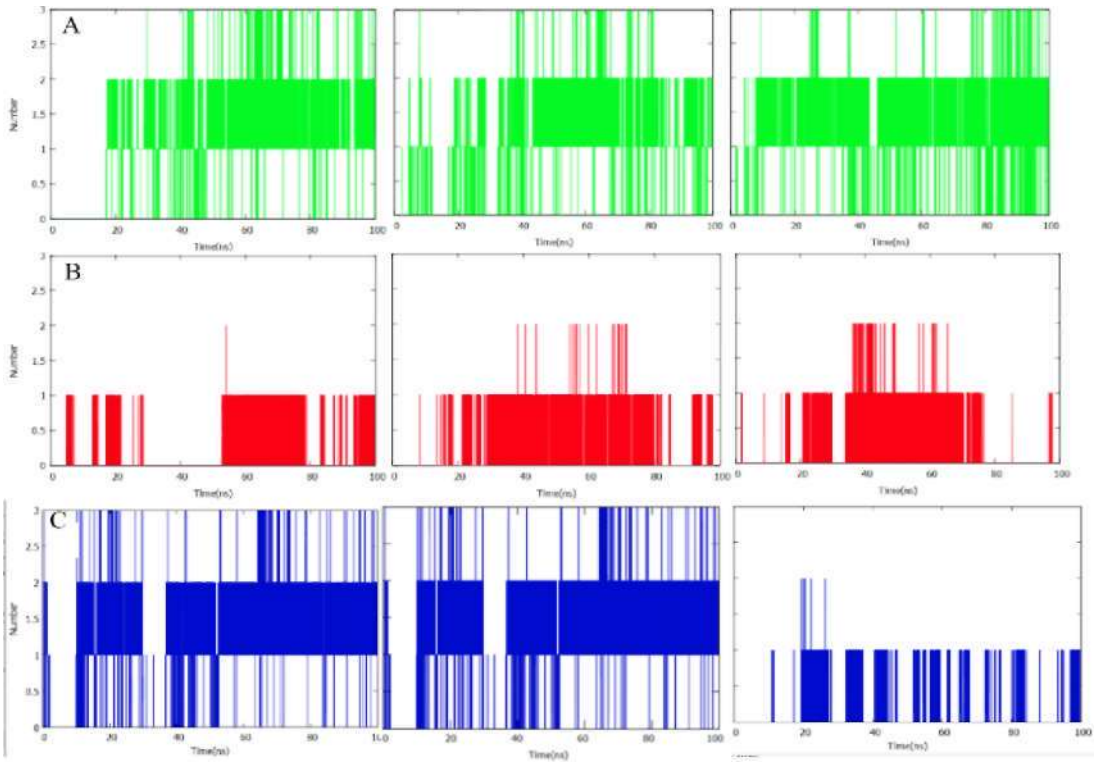

Figure 4.9 Hydrogen Bond Analysis Between Alkaloids and Lipids in Model System 2. Hydrogen Bond Interactions Between the Kratom Alkaloids and DPPC Lipids During the 100 ns MD Simulations of (A) Mitragynine (Green), (B), 7-Hydroxymitragynine (Red) and (C) Mitragynine Pseudoindoxyl (Blue).

Hydrogen bond analysis with water molecules of Model System 2 clearly shows the decrease of interactions with water after the alkaloids diffused into the lipid bilayer. In the mitragynine system, initially during the location of the molecules in the water phase, they strongly formed 5 hydrogen bonds with water molecules. However, when residing inside the bilayer, the number of hydrogen bonds reduced to two interactions for two mitragynine molecules, and the other formed only one. Nevertheless, mitragynine molecules were the most consistent and had the highest number of hydrogen bonds with water compared to the other alkaloids in Model System 2. Both the 7-hydroxymitragynine and mitragynine pseudoindoxyl systems exhibited similar interaction patterns with the water molecules. Before entering the lipid region, they consistently formed 5-6 hydrogen bonds with water molecules, and the number reduced to 1-2 interactions when located inside the lipid bilayer region. The reduction of hydrogen bond interactions obviously shows the location of these alkaloids. Moreover, the results illustrate that these alkaloids not only form hydrogen bonds with the lipid headgroups, but also form interactions with water molecules at the interface.

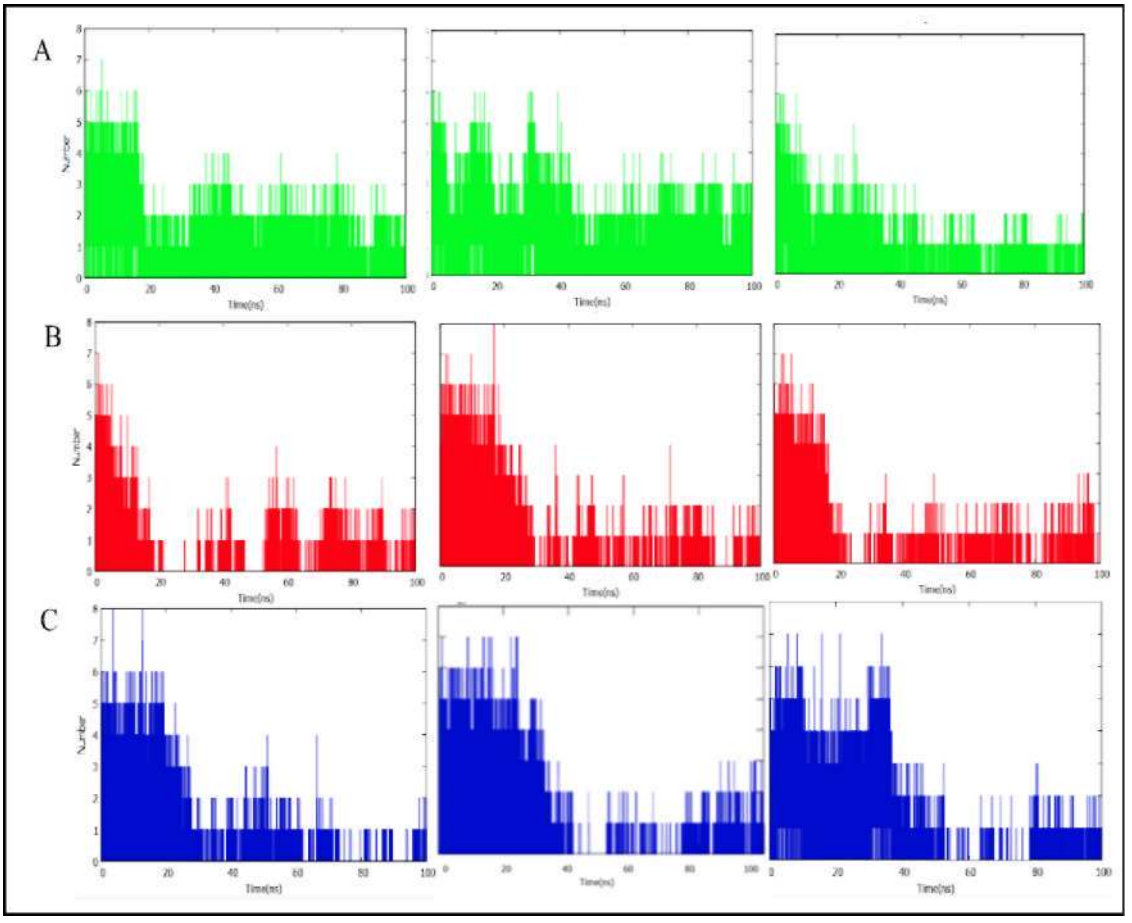

Figure 4.10 Hydrogen Bond Analysis Between Alkaloids and Water Molecules in Model System 2. Hydrogen Bond Interactions Between the Kratom Alkaloids and Water Molecules During the 100 ns MD Simulations of (A) Mitragynine (Green), (B), 7-Hydroxymitragynine (Red) and (C) Mitragynine Pseudoindoxyl (Blue).

4.4 Model System 3 - Behavior of Three Different Alkaloids in DPPC Lipid Bilayers

Model System 3 represents three different types of kratom alkaloid in the lipid bilayer. The aim is to study the behavior of different types of kratom alkaloids when they co-exist together. Figure 4.11 shows the snapshots from the MD simulation trajectories of this system representing the initial stage, (0 ns), 2nd stage: when the first molecule penetrates the lipid bilayer, 3rd stage: when all the molecules entered the bilayer, and the final stage (100 ns). The same as the other model systems, all three alkaloid molecules were positioned in the aqueous environment above the lipid bilayer as the starting point for the simulation. As the simulation progressed, mitragynine was the first molecule that began to interact with and penetrate the lipid bilayer approximately at 10 ns. This was followed by the gradual entry of the remaining alkaloid

molecules. By approximately 50 ns of the simulation, all three alkaloids had successfully entered the lipid bilayer, positioning themselves within the hydrophobic region of the DPPC lipids and remained throughout the end of the simulation. Similar to the other model systems, the alkaloids exhibited a preference for localizing near the lipid headgroups, where they could form polar interactions with the phosphate groups while remaining embedded in the hydrophobic core. This dual behavior highlights the amphiphilic nature of the alkaloids, allowing them to interact with both the polar and nonpolar regions of the lipid bilayer. Additionally, no significant aggregation among the alkaloids was observed, suggesting that the presence of multiple alkaloid types does not promote clustering but rather allows for independent interactions with the lipid bilayer.

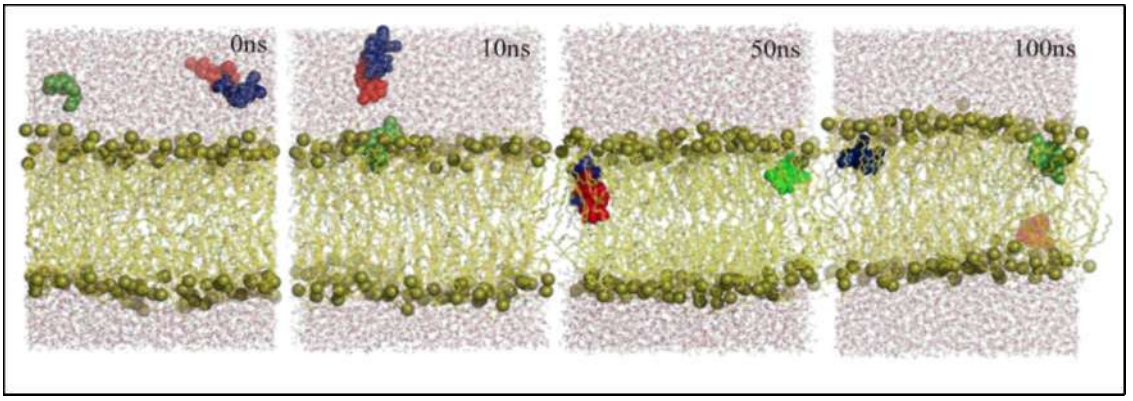

Figure 4.11 Interactions of Three Different Molecules of Kratom Alkaloids with DPPC Lipid Bilayers During 100 ns MD Simulations. Snapshots of (A) Mitragynine (Green Spheres), (B) 7-Hydroxymitragynine (Red Spheres), and (C) Mitragynine Pseudoindoxyl (Blue Spheres), Lipid Headgroup (Olive Spheres), Lipid Tails (Yellow Sticks) and Water (Red Sticks).

Distance analysis was conducted to evaluate the detailed interactions between the three kratom alkaloids in Model System 3—mitragynine, 7-hydroxymitragynine, and mitragynine pseudoindoxyl—and the DPPC lipid bilayers. Table 4.4 presents the visualization plots of the average distance for the three alkaloid molecules in each system during the 100 ns of the MD simulations, along with the average distance based on the final 50 ns. Based on the plots, Model System 3 of mitragynine exhibits a trend where the molecules begin to interact with the lipid headgroups before 20 ns of the simulation. As observed from the simulation trajectories, mitragynine molecules that entered the lipid bilayer region remained in the hydrophobic environment throughout

the simulations. The distance analysis shows an average range of 1-4 nm (2.852 ±0.51 nm) between the mitragynine molecules and the lipid headgroups, indicating their dynamic positions within the lipid bilayer. Similarly, Model System 3 of 7-hydroxymitragynine shows that the three molecules formed interactions with the lipids approximately at 20 ns and resided in the lipid bilayer region within a similar range of distance as the mitragynine system, averaging 3.092 ± 0.13 nm. The slowest penetration was exhibited by Model System 3 of mitragynine pseudoindoxyl, which displayed interactions with the lipids starting at approximately 30 ns. However, the penetration of the first mitragynine pseudoindoxyl molecule occurred after 50 ns. Although one of the molecules exhibited unstable behavior, the average distance of mitragynine pseudoindoxyl to the lipid headgroups was 3.194 ± 0.12 nm, reflecting its slower and less stable penetration into the lipid bilayer.

Table 4.4
The Average Distance of Kratom Alkaloids to The DPPC Lipid Headgroup in Model System 3. The Presented Values are Based on The Final 50 ns of Simulations.

Alkaloids	Distance to membrane	Distance Plot
Mitragynine	2.852 ± 0.51 nm	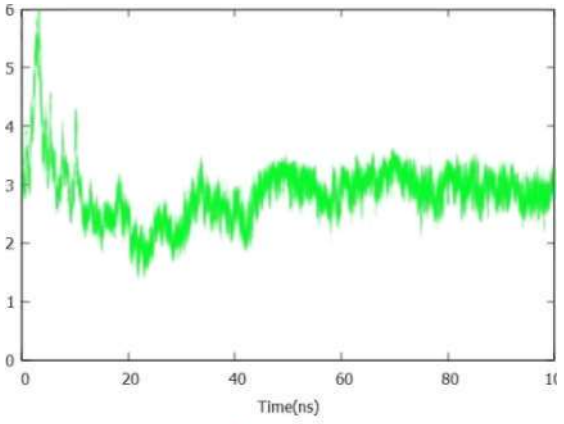
7-hydroxymitragynine	3.092 ±0.13 nm	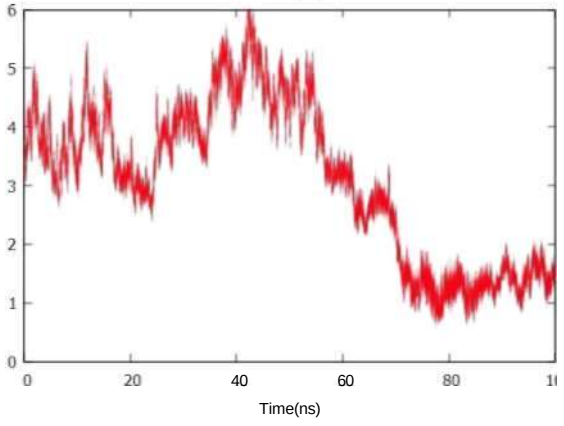

Alkaloids	Distance to membrane	Distance Plot
Mitragynine pseudoindoxyl	3.194±0.12nm	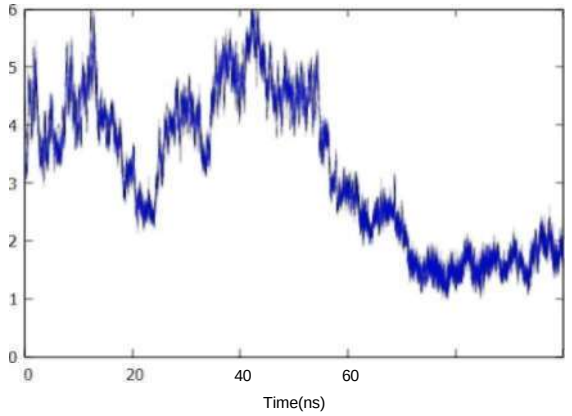

4.4.1 Mass- **Density Profile and Deuterium Order Parameter**

Figure 4.12 (A) illustrates the mass densities of the DPPC lipid-water system along the z-axis of the simulation box for the Model System 3 that consist of three different kratom alkaloids—mitragynine, 7-hydroxymitragynine, and mitragynine pseudoindoxyl—within the lipid bilayer environment. The zoomed density for each alkaloid is shown in Figure 4.12 (D). The density profile highlights the positioning of all alkaloids inside the lipid bilayer hydrophobic region.

Mitragynine is localized near the center of the lipid bilayer with an average position of 1.582 ± 0.41 nm, indicating a strong affinity for the hydrophobic core region of the membrane. This suggests that mitragynine interacts stably within the lipid environment, possibly embedding itself within the nonpolar tails of the lipids. 7-hydroxymitragynine is positioned at an average of-1.896 ± 0.87 nm, placing it closer to the lipid headgroups and the interface between the lipid and water phases. The broader standard deviation indicates that this molecule may exhibit some movement or fluctuation between the polar headgroup region and the water phase, reflecting its amphiphilic nature. Mitragynine pseudoindoxyl shows two distinct peaks at -1.294 ± 0.51 nm and 0.658 ± 0.24 nm, indicating that it is distributed across both the lipid headgroup region and slightly into the aqueous phase. This suggests that mitragynine pseudoindoxyl may have a dynamic interaction, oscillating between the lipid bilayer and the surrounding water, which could be significant for its permeability and transport across the membrane.

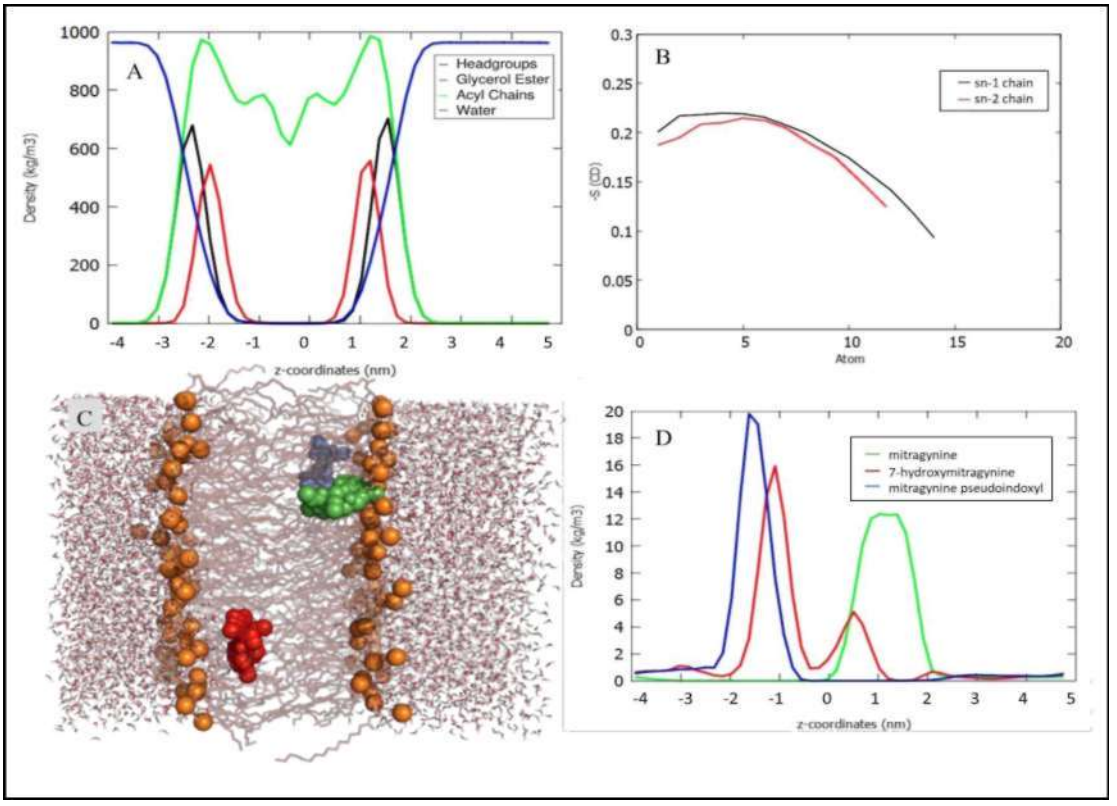

Figure 4.12 Mass Density and Deuterium Order Parameter for Model System 3. (A) Mass Density Profile, (B) Deuterium Order Parameter, (C) A Snapshot of 100 ns Simulation of DPPC Bilayer, and (D) The Mass Densities of Different Kratom Alkaloid in DPPC Lipid Bilayer.

Figure 4.12 (B) displays the deuterium order parameters (SCD) for the sn-1 and sn-2 acyl chains of DPPC lipid bilayers in the presence of different alkaloids during the MD simulation. In this figure, both the sn-1 and sn-2 chains follow a similar pattern, with relatively higher (SCD) values near the lipid head group region (atoms 1 to 5), signifying a more ordered structure. As the chain length increases, the order parameters decrease gradually, reflecting increased flexibility and reduced order in the mid and terminal regions of the lipid tails. The sn-1 chain consistently shows higher (S_{CD}) values compared to the sn-2 chain, indicating that the sn-1 chain remains more rigid and ordered throughout the simulation. In contrast, the sn-2 chain exhibits slightly lower order parameters, suggesting greater flexibility, particularly in the mid-chain and terminal regions. This difference is typical in lipid bilayers due to the intrinsic structural asymmetry between the two chains. The results show that the embedded alkaloids minimally influence the order parameters, as seen from the varying slopes and values along the chain length, which represent a similar pattern of acyl chain in the pure DPPC simulations.

4.4.2 Hydrogen Bond Interactions

Figure 4.14 illustrates the hydrogen bond interactions between the three alkaloids—mitragynine, 7-hydroxymitragynine, and mitragynine pseudoindoxyl—with lipids and water molecules. Both the mitragynine and mitragynine pseudoindoxyl systems exhibited similar interaction patterns with the lipids headgroups, each forming up to 3 hydrogen bonds with lipid headgroups. In line with the observed close proximity of mitragynine and mitragynine pseudoindoxyl to the lipid headgroups after residing inside the lipid bilayers, the plot shows consistently 2 hydrogen bonds were formed until the end of simulations. Meanwhile, the 7-hydroxymitragynine system plot shows occasionally formed one hydrogen bond with lipid headgroups, particularly after residing inside the lipid bilayer. As observed from the plot, there were durations that the hydrogen bonds were absent, which could indicate the position of the molecule located deep into the hydrophobic core of the region. This result inline with the mass density profile of the 7-hydroxymitragynine system that display the density of 7-hydroxymitragynine position at the middle position of bilayer normal (Figure 4.12-E), where the molecule was far from the polar headgroup region.

Hydrogen bond interactions between the three different alkaloids and water molecules of the Model System 3 clearly shows the decrease of interactions with water after the alkaloid diffused into lipid bilayer. The mitragynine, 7-hydroxymitragynine, and mitragynine pseudoindoxyl system, initially during the location of the molecules in the water phase, occasionally formed 7 hydrogen bonds with water molecules. However, when residing inside the bilayer, the number of hydrogen bonds is reduced to one interaction for all alkaloids. Moreover, the result illustrates that these alkaloids not only form hydrogen bonds with lipid headgroups, but also form interactions with water molecules at the interface.

Figure 4.13 Hydrogen Bond Analysis Between Kratom Alkaloids with Lipids and Water Molecules in Model System 3. Interactions Between the Kratom Alkaloids and Lipids (A, B, C) and Water Molecules (D, E, F) During the 100 ns. MD Simulations of (A, D) Mitragynine (Green), (B, E), 7-Hydroxymitragynine (Red) and (C, F) Mitragynine Pseudoindoxyl (Blue).

4.5 Model System 4 - Behavior of Six Molecule of Alkaloids in DPPC Lipid Bilayers

The final model system in this study, Model System 4, builds on the findings from Model Systems 2 and 3, where the behavior of three alkaloid molecules in the DPPC lipid bilayer was studied. Since no significant differences were observed in the behavior of three molecules, Model System 4 was designed to investigate the effects of a higher number of alkaloid molecules. Specifically, six molecules of the same type of alkaloid were added to the DPPC lipid bilayer, allowing for an examination of how increased alkaloid concentration influences their interactions and distribution within the bilayer.

The snapshots capture the initial stage, penetration process, and final distribution of the alkaloids within the lipid bilayer. For the mitragynine model system, the six molecules initially diffused independently in the aqueous environment without forming interactions with one another. Each molecule entered the hydrophobic region of the lipid bilayer individually. By 50 ns, most of the mitragynine molecules had already entered the lipid region, while the remaining two began to penetrate. At approximately 100 ns, all six mitragynine molecules had fully entered the lipid region, positioning themselves

below the lipid phosphate groups. Over the 100-200 ns period, interactions between the mitragynine molecules were observed, although they remained localized below the lipid phosphate groups. In contrast, mitragynine pseudoindoxyl exhibited a different behavior. Before entering the lipid bilayer, assembly among several molecules was observed in the aqueous environment. Approximately 50 ns during the simulation, four assembled mitragynine pseudoindoxyl molecules had formed interactions with the lipid interface, while the remaining two molecules formed a pair and were halfway through penetrating the DPPC lipids. By approximately 100 ns, the assembled groups of mitragynine pseudoindoxyl had entered the hydrophobic region of the DPPC bilayer. Throughout the 100-200 ns, some molecules continued to interact as assemblies, while others interacted as a single molecule with the lipid phosphate groups.

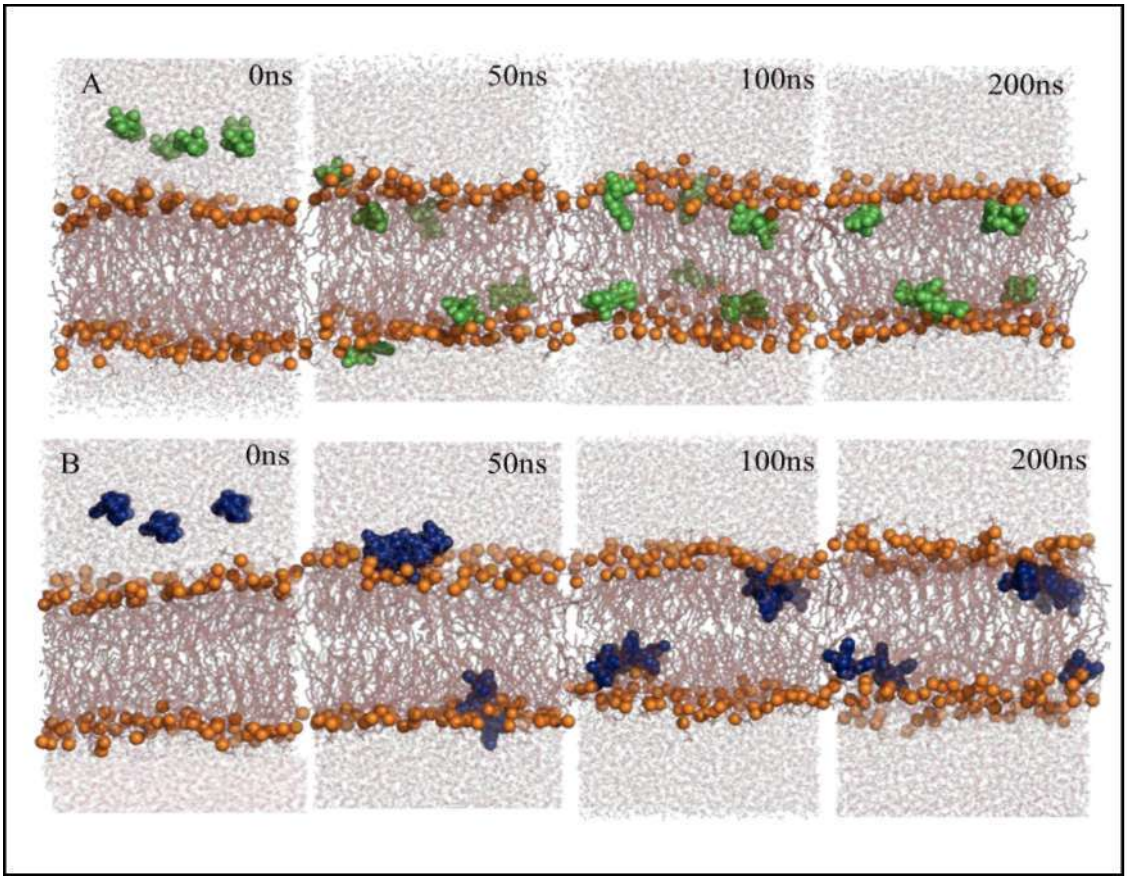

Figure 4.14 Interactions of Six Molecules Kratom Alkaloid with DPPC Lipid Bilayers During 200 ns MD Simulations. Snapshots of (A) Mitragynine (Green Spheres), (B), and (B) Mitragynine Pseudoindoxyl (Blue Spheres), Lipid Headgroup (Orange Balls), Lipid Tails (Brown Sticks) and Water (Red Sticks).

Distance analysis was performed to evaluate the detailed interactions between the six kratom alkaloids—mitragynine and mitragynine pseudoindoxyl—in Model System 4 and the DPPC lipid bilayers. Table 4.5 provides visualization plots of the average distance for the six alkaloid molecules in each system during the 200 ns MD simulations, along with the average distance calculated from the final 50 ns. According to the plots, Model System 4 of mitragynine shows a similar trend, with all six molecules beginning to interact with the lipid headgroups before 50 ns of the simulation. The simulation trajectories reveal that mitragynine molecules that penetrate into the lipid bilayer region remain in the hydrophobic environment throughout the simulations. The distance analysis indicates an average range of 3.358 ± 0.69 nm between the mitragynine molecules and the lipid headgroups, reflecting the dynamic positions of the molecules within the lipid bilayer. In contrast, Model System 4 of mitragynine pseudoindoxyl demonstrates that the six molecules formed interactions with the lipids at approximately 50 ns (Figure 4.14) and has an average distance of 2.462±0.132nm, showing that it is closer to the lipid headgroup than Mitragynine. The finding from Model 4 shows six molecules of kratom alkaloids able to diffuse into the lipid bilayer and settle below the lipid headgroups, highlighting the amphiphilic characteristics of these alkaloids.

Table 4.5
The Average Distance of Kratom Alkaloids to The DPPC Lipid Headgroup in Model System 4. The Presented Values are Based on The Final 50 ns of Simulations.

Alkaloids	Distance to membrane	Distance Plot
Mitragynine	3.358 ± 0.69 nm	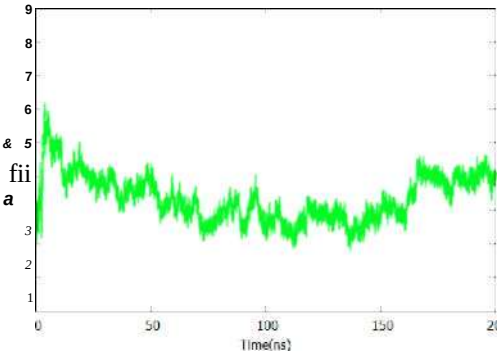

Alkaloids	Distance to membrane	Distance Plot
Mitragynine pseudoindoxyl	2.462 ±0.132 nm	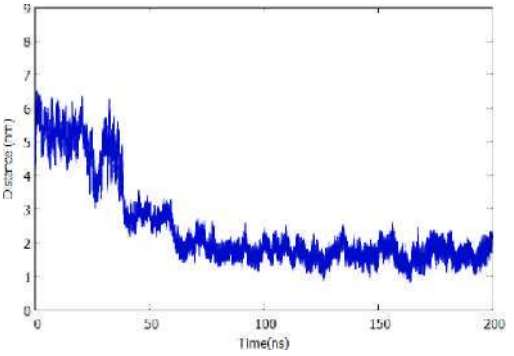

4.5.1 Mass Density Profile and Deuterium Order Parameter

Figure 4.16 shows the mass density profiles of the Model System 4 for the mitragynine and mitragynine pseudoindoxyl system.The mass density profile of mitragynine represents the six molecules of mitragynine distribution across the bilayer, showing distinct peaks at 0.13 ± 0.29 nm and 2.85 ± 0.42 nm, indicating its preferred localization near the lipid headgroups. This profile reflects mitragynine's significant interaction with the bilayer surface, where it associates primarily with the polar headgroups while also displaying a gradual insertion into the hydrophobic core. The two density peaks suggest that mitragynine molecules are distributed throughout the bilayer, with some molecules penetrating deeper into the other lipid leaflet while still localizing near the bilayer surface. In the mitragynine pseudoindoxyl system, the six alkaloids distributed evenly in both lipid bilayer leaflets, which is represented by the two similar peaks in the plot at 0.44 ± 0.26 nm and 2.72 ± 0.29 nm. Similar to the mitragynine system, the six mitragynine pseudoindoxyl molecules are primarily localized near the lipid headgroups.

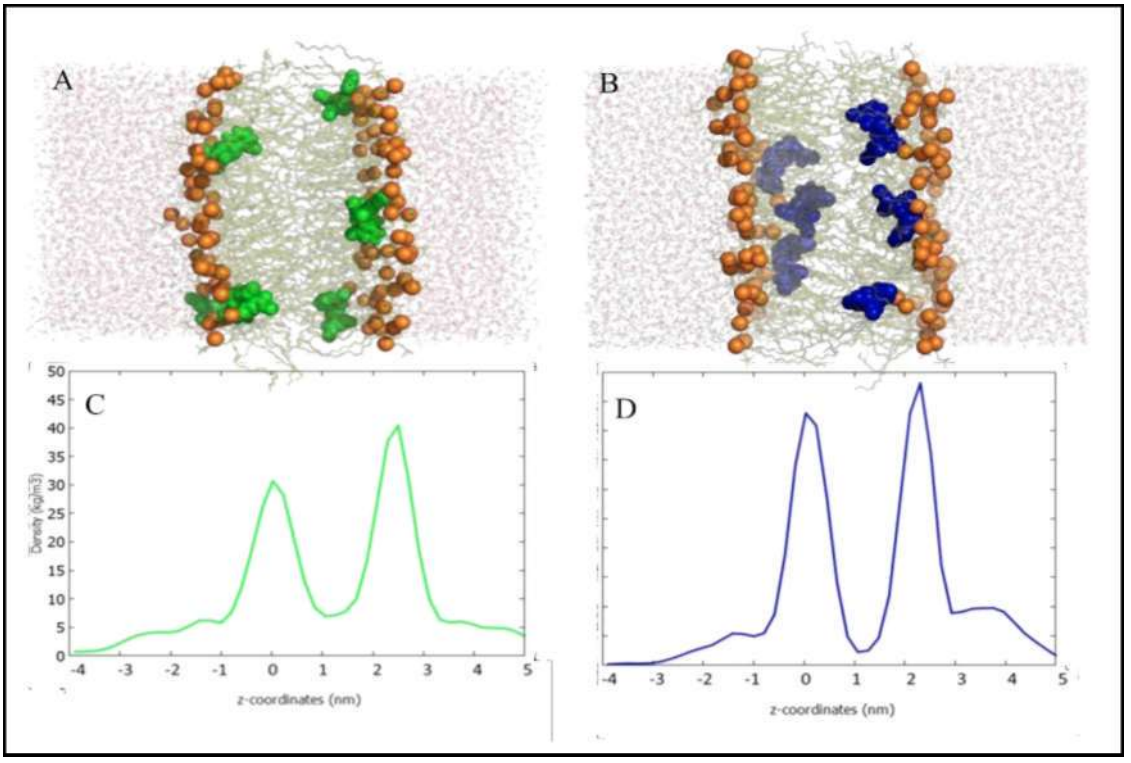

Figure 4.15 The Mass Densities Profile of Alkaloids in Model System 4. Snapshots at 200 ns of Model System 4: (A) Mitragynine (Green Spheres), and (B) Mitragynine Pseudoindoxyl (Blue Spheres), Lipid Headgroup (Orange Spheres), Lipid Tails (Brown Sticks) and Water (Red Sticks). The Mass Densities of Six Kratom Alkaloids in DPPC lipid bilayer for (C) Mitragynine (Green Line), and (D) Mitragynine Pseudoindoxyl (Blue Line).

Figure 4.17 presents the deuterium order parameters for the sn-1 and sn-2 acyl chains of DPPC bilayers in the presence of mitragynine and mitragynine pseudoindoxyl. The order parameter (SCD) provides insights into the rigidity and flexibility of lipid tails, with higher values indicating more ordered and rigid lipid chains, and lower values suggesting increased flexibility and disorder.

Mitragynine's presence results in a slight decrease in the order of both sn-1 and sn-2 chains as the atomic number increases, particularly in the bilayer core region. The order parameters of both chains follow a similar trend, indicating that mitragynine interacts moderately with the lipid bilayer, maintaining relatively balanced lipid tail flexibility across both chains. This suggests that mitragynine integrates into the bilayer without significantly altering lipid tail dynamics, aligning with its observed partial insertion into the bilayer from previous figures.

However, the effect of mitragynine pseudoindoxyl shows a more significant impact on the lipid tails, especially in the sn-2 chain. The sn-2 chain displays

consistently higher order parameters across most atom positions compared to the sn-1 chain, suggesting that mitragynine pseudoindoxyl enhances the stability of the lipid tails more effectively, particularly within the hydrophobic core of the bilayer. This observation is consistent with the previous figure, where mitragynine pseudoindoxyl exhibited deeper and more stable integration into the bilayer, leading to increased lipid order and potentially reducing membrane fluidity.

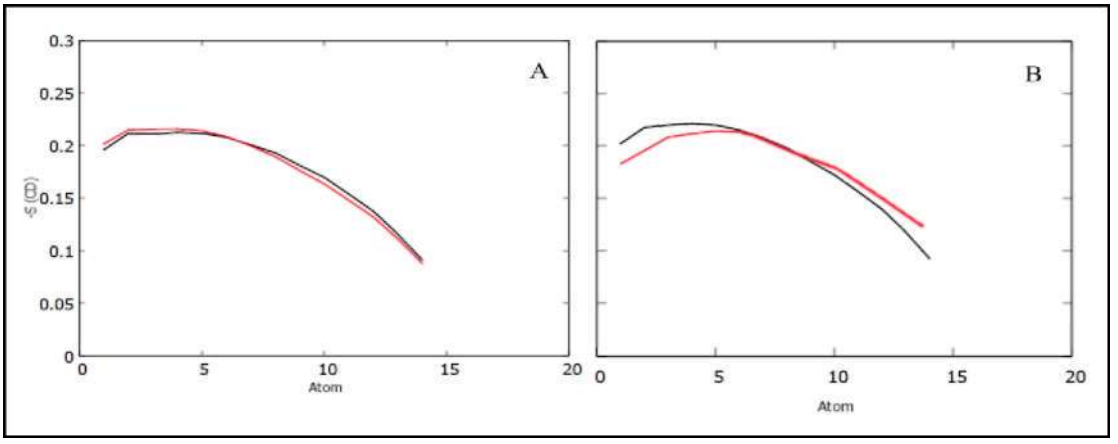

Figure 4.16 Deuterium Order Parameters (SCD) for DPPC in Model System 4. (A) Mitragynine, (B) and Mitragynine Pseudoindoxyl. The Lines Represent DPPC Acyl Chains: Sn-1 (Black) and Sn-2 (Red).

4.5.2 Hydrogen Bond Interactions

Figure 4.17 displays the hydrogen bonds interactions between mitragynine and mitragynine pseudoindoxyl with lipids and water molecules. During the simulation, mitragynine formed up to 3 hydrogen bonds with lipid headgroups. Inline with the observed close proximity of mitragynine to the lipid headgroups after residing inside the lipid bilayers, the plot consistently 2 hydrogen bonds were formed until the end of simulation. Meanwhile, the mitragynine pseudoindoxyl system shows that mitragynine pseudoindoxyl occasionally formed one hydrogen bond with the lipid headgroups, particularly after residing inside the lipid bilayer. As observed from the plot, there were durations that the hydrogen bonds were absent, which could indicate the position of the molecule located deep into the hydrophobic core region. This result is inline with mass density mitragynine pseudoindoxyl at the middle position of bilayer normal (Figure 4.15-D), where the molecule was far from the polar headgroups region.

Hydrogen bonds analysis with water molecules of Model System 4 clearly shows the decrease of interactions with water after alkaloids diffused into the lipid bilayers. In the mitragynine system, initially during the location of molecules in the water phase, they formed 6 hydrogen bonds with water molecules. However, when residing inside the lipid bilayer, the number of hydrogen bonds is reduced to one hydrogen bond. Nevertheless, mitragynine pseudoindoxyl molecules show that mitragynine pseudoindoxyl occasionally formed 7 hydrogen bonds with water molecules. Before entering the lipid region, mitragynine and mitragynine pseudoindoxyl systems consistently formed 5-6 numbers of hydrogen bonds with water molecules, and the number reduced to 1-2 interactions when located inside the lipid bilayer.

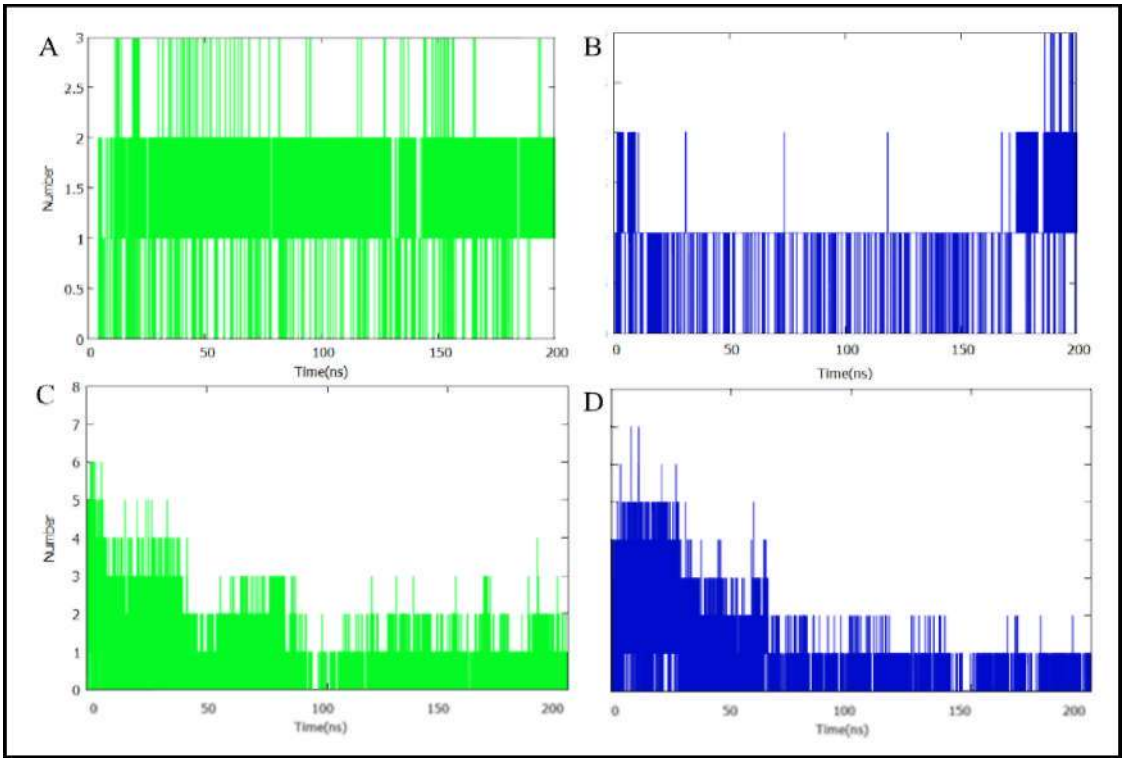

Figure 4.17 Hydrogen Bond Analysis Between Kratom Alkaloids with Lipids and Water Molecules in Model System 4. Hydrogen Bond Interactions Between the Kratom Alkaloids and Lipid (A, B), and Water Molecules (C, D) During the 200 ns MD Simulations. (A,C) Mitragynine (Green), and (B, D) Mitragynine Pseudoindoxyl (Blue).

4.6 Behavior of Six Molecules of 7-hydroxymitragynine with Lipid Bilayer

The behavior of 7-hydroxymitragynine in lipid bilayers was further investigated in Model System 4, which involved six molecules of 7-hydroxymitragynine in a DPPC lipid bilayer. This system was analyzed separately due to the unique and variable behaviors observed across the three replicate simulations (Figure 4.19). A consistent pattern of molecular assembly among the 7-hydroxymitragynine molecules was observed across all replicates, though the penetration dynamics into the lipid bilayer varied significantly. In Replicate 1, interactions among the 7-hydroxymitragynine molecules led to the formation of an assembly in the aqueous environment. Around 100 ns, an assembly of five molecules began to penetrate the lipid bilayer, while one molecule entered independently. By approximately 150 ns, the assembly of five molecules had successfully entered the hydrophobic region of the bilayer. Interestingly, towards the end of the simulation (150-200 ns), the molecules broke away from the assembly and interacted as individual molecules within the lipid bilayer, localizing near the lipid phosphate groups. In contrast, Replicate 2 was the only replicate where none of the 7-hydroxymitragynine molecules entered the lipid bilayer during the 200 ns simulation. Similar to Replicate 1, an assembly of six molecules formed in the aqueous environment from the initial stage. Around 100 ns, the assembly interacted with the phosphate groups of the DPPC lipids from the aqueous side but failed to penetrate further into the hydrophobic region. This interaction persisted until the end of the simulation, with the molecules remaining in the aqueous environment. Replicate 3 also exhibited assembly behavior in the aqueous environment. Between 100-150 ns, one molecule successfully entered the hydrophobic region of the lipid bilayer, while the remaining five molecules stayed assembled in the aqueous phase. Surprisingly, during the final 50 ns (150-200 ns), the assembled group of five molecules managed to penetrate the hydrophobic region and remained there until the end of the simulation.

The simulation for the Model System 4: 7-hydroxymitragynine reveals the consistent formation of molecular assemblies among 7-hydroxymitragynine molecules in systems containing six molecules. This assembly behavior appears to play a critical role in the penetration dynamics of the molecules into the lipid bilayer, particularly for 7-hydroxymitragynine. The cause is highly likely due to the high energy barrier required for a large system such as the aggregate molecules to disrupt the lipid bilayer, which leads to slower or incomplete penetration. These findings suggest that molecular

assembly and aggregation can be one of the key factors influencing the interactions of 7-hydroxymitragynine with lipid bilayers, which may have implications for its pharmacological behavior and membrane permeability.

Figure 4.18 Interactions of Six Molecules of 7-hydroxymitragynine with DPPC Lipid Bilayers During 200 ns MD Simulations. Snapshots of (A) First replicate (B) Second replicate and (C) Third replicate, 7-hydroxymitragynine (Red Spheres), Lipid Headgroup (Orange Spheres), Lipid Tails (Brown Sticks) and Water (Red Sticks).

Distance analysis was conducted in order to evaluate detailed interaction between the kratom alkaloids in Model System 4 of 7-hydroxymitragynine-and the

DPPC lipid bilayers. Table 4.6 presents the visualization plots of average distance for six alkaloids in each system during 200 ns of the MD simulations and the average distance based on the final 50 ns. Based on the plots, Replicate 3 exhibits the fastest interactions of 7-hydroxymitragynine with the lipid bilayers around 50 ns. Inline with the simulation trajectories, in Replicate 3 that entered the lipid bilayer region remained in a hydrophobic environment throughout the simulations. The distance analysis of the final 50 ns simulations shows the average distance of 2.949 ± 0.39 nm between six 7-hydroxymitragynine molecules to lipid headgroups. However, plot for the Replicate 1 displayed similar trends with Replicate 3, with is insertion time for both replicate as visualized from the trajectories (Figure 4.18). Towards the end of the simulations, Replicate 1 formed interaction with lipid headgroups with the average distance of 3.038 ± 0.13 nm. Surprisingly, for six 7-hydroxymitragynine in Replicate 2 shows only interactions with water molecules throughout the end of simulations. The result indicates that Replicate 2 is more favourable with hydrophilic regions, with the average distance 3.725 ± 0.74 nm.

Table 4.6
The Average Distance of Kratom Alkaloids to The DPPC Lipid Headgroup In Model System 4 of 7-hydroxymitragynine. The Presented Values are Based on The Final 50 ns of Simulations.

Alkaloids	**Distance to membrane**	**Distance Plot**
Replicate 1	3.038 ± 0.13 nm	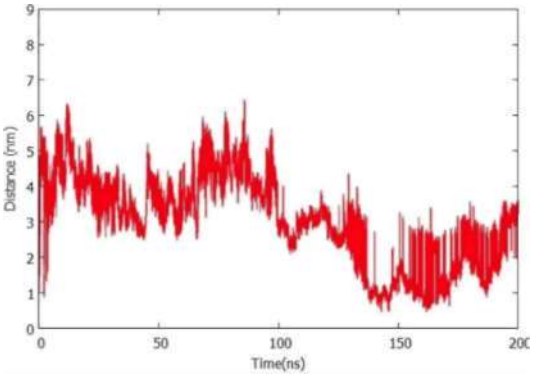

Alkaloids	Distance to membrane	Distance Plot
Replicate 2	3.725 ± 0.74 nm	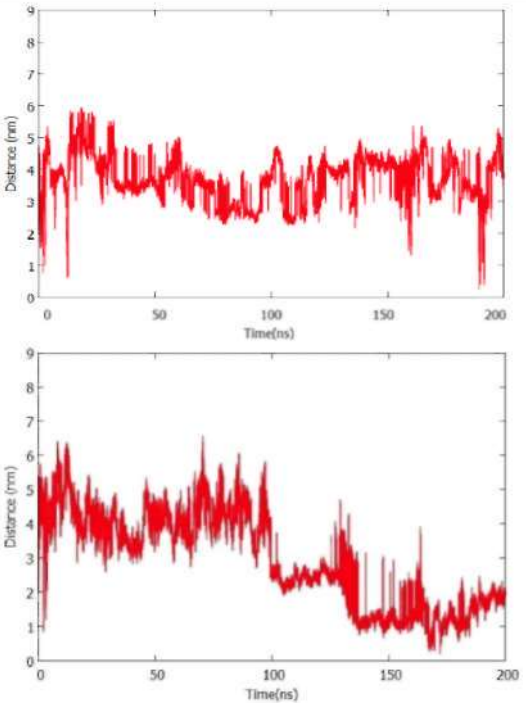
Replicate 3	2.949 ± 0.39 nm	

4.6.1 Mass Density Profile and Deuterium Order Parameter

Figure 4.20 presents the mass densities profile of the Model System 4 of the 7-hydroxymitragynine system. The plot only shows the mass density for the 6 7-hydroxymitragynine molecules along the z-axis for the three simulation replicates. In Replicate 1, the 7-hydroxymitragynine molecules maintain an average position of 1.714 ± 0.27 nm from the lipid headgroups with a bell-shaped peak that illustrate the distribution of the six molecules of 7-hydroxymitragynine positioned in both lipid leaflets. In contrast, Replicate 2 of the 7-hydroxymitragynine system that exhibited the failures of the six 7-hydroxymitragynine molecules displayed the mass density of the molecules position between 2-4 nm (average position of 3.324 ± 0.45 nm) along the bilayer normal. This is consistent with the observed 3D visualization from the simulation trajectory showing the interactions of the 7-hydroxymitragynine assembly with lipid headgroups at the water phase throughout the simulations. Meanwhile, Replicate 3 that shows similar behavior as Replicate 1 display the mass density of 7-hydroxymitragynine molecules at 0-2 nm (average position of 1.961 ± 0.17 nm), which

literally illustrate the assembly of the 7-hydroxymitragynine molecules positioned between below the lipid headgroup to the core region of acyl chain.

Replicate 3 shows an average distance of 1.961 ± 0.17 nm, with the molecules remaining near the bilayer, reflecting stable interactions comparable to Replicate 1, albeit at a slightly increased distance from the headgroups. These results emphasize the variability in molecular positioning across the three replicates, highlighting differences in the strength and stability of interactions between the 7-hydroxymitragynine molecules and the DPPC lipid bilayer.

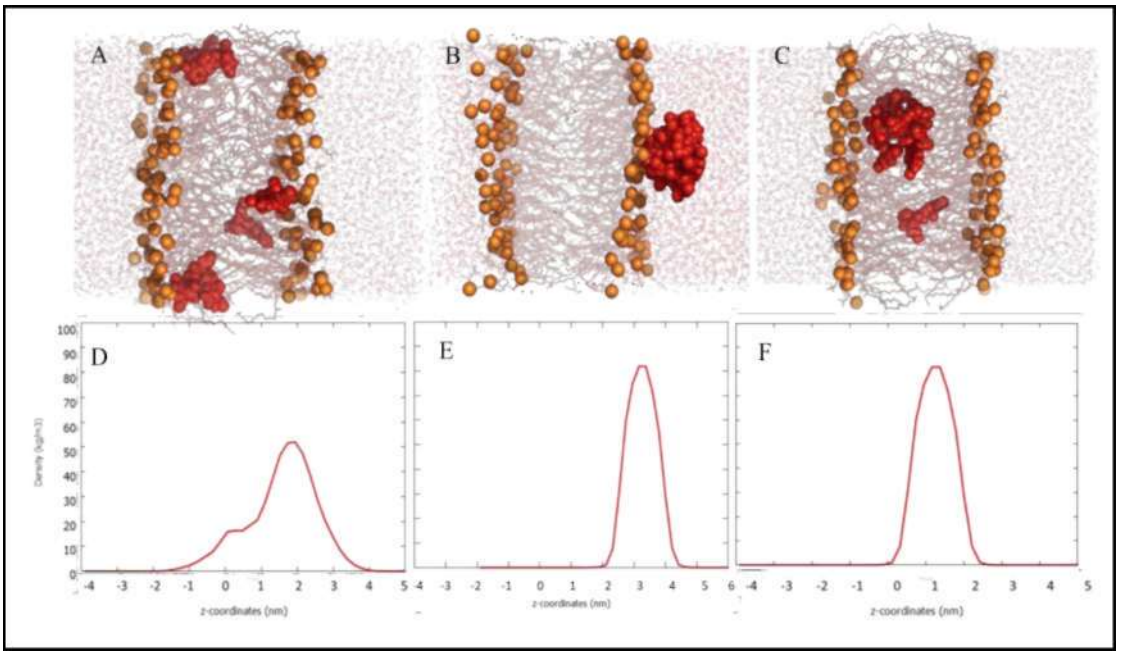

Figure 4.19 The Mass Densities Profile of Alkaloids in Model System 4. Snapshots at 200 ns of Model System 4: (A) First Replicate, (B) Second Replicate and (C) Third Replicate, 7-hydroxymitragynine (Red Spheres), Lipid Headgroup (Orange Spheres), Lipid Tails (Brown Sticks) and Water (Red Sticks). The Mass Densities of Kratom Alkaloids in DPPC lipid bilayer for (D-E) 7-Hydroxymitragynine (Red Line).

Figure 4.21 presents the deuterium order parameters for the sn-1 and sn-2 chains of the DPPC lipid bilayer across three replicates of the simulation involving the same six molecules of 7-hydroxymitragynine. In Replicate 1, the order parameters of both chains show a similar trend, with slight differences in values, indicating consistent lipid chain ordering. Replicate 2 displays a comparable pattern, with both sn-1 and sn-2 chains maintaining similar levels of order, though minor deviations between the two chains are observed along the lipid tails. In Replicate 3, the trend remains consistent, with the sn-2 chain slightly more ordered than the sn-1 chain across most of the lipid

atoms. Overall, the figure shows that the presence of 7-hydroxymitragynine molecules affects the lipid bilayer's order parameters consistently across all three replicates, with the sn-2 chain generally maintaining a slightly higher level of order compared to the sn-1 chain, reflecting the influence of the alkaloid molecules on the lipid membrane structure.

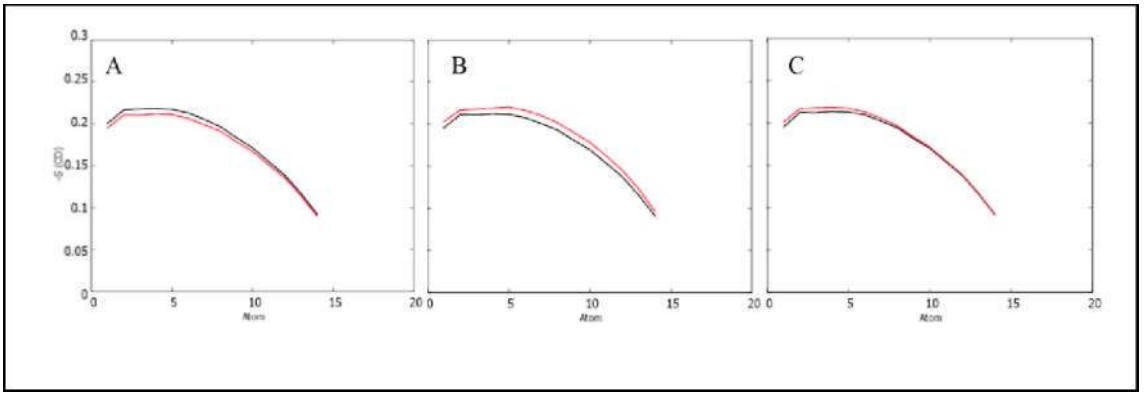

Figure 4.20 Deuterium Order Parameters (SCD) for DPPC in Model System 4: 7-hydroxymitragynine. (A) First Replicate, (B) Second Replicate, and (C) Third Replicate. The Lines Represent DPPC Acyl Chains: Sn-1 (Black) and Sn-2 (Red).

4.6.2 Hydrogen Bond Interactions

Figure 4.21 presents the hydrogen bonds analysis between the 7-hydroxymitragynine molecules of Model System 4. Due to the assembly of the six molecules of 7-hydroxymitragynine in the water phase, polar interactions with the lipids were significantly reduced as compared to the other model systems. The most hydrogen bond interactions were represented by Replicate 1, which was able to penetrate as an assembly, and some molecules were subsequently separated during the simulations. As observed from the other model systems, individual alkaloids prefer localization near the lipid headgroups in order to form polar interactions as displayed by the consistent hydrogen bond formation during the 120-200 ns timeframe. In contrast to Replicate 2, hydrogen bond interactions of 7-hydroxymitragynine with the lipid headgroups are mostly absent throughout the simulations except between 50-80 ns timeframe. Interestingly, Replicate 3 exhibited the least number of hydrogen bonds between the 7-hydroxymitragynine and the lipids, although the molecules were able to penetrate into the lipid bilayer region. The persistent interactions of 7-hydroxymitragynine molecules as an assembly in the bilayer might explain this result. The polar functional group of the

7-hydroxymitragynine highly likely interacts with other 7-hydroxymitragynine molecules in forming the assembly, which causes the assembled molecules to expose their on-polar groups, and comfortably interact with the lipid tail region as shown in the mass density profile (Figure 4.19).

Consistent with the location of the 7-hydroxymitragynine molecules, the amount of hydrogen bonds with the lipids is the opposite to the water. The common trend can be observed in Replicate 1 and 3, where the number of hydrogen bonds during the molecules in water phase were strongly 5 interactions and was sometimes up to 8. Conversely, when the assembly of 7-hydroxymitragynine enters the bilayer, the hydrogen bonds with the lipids reduce between 1-2 interactions. As expected for Replicate 2 that remained in the aqueous phase, the assembly of 7-hydroxymitragynine formed at least 8 hydrogen bonds with the surrounding water molecules. This finding reveals the consequences when the alkaloids that form aggregation failed to penetrate the lipid bilayer region. Although, there is possibility that the assembly molecules may be able to penetrate the lipid bilayer in a longer timescale of molecular dynamics simulations.

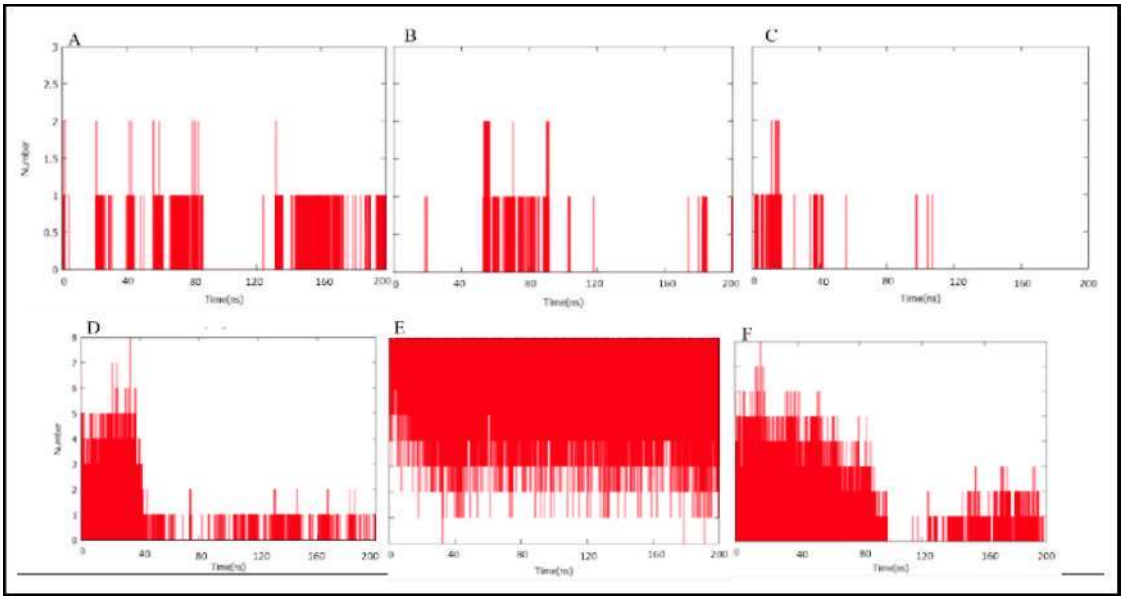

Figure 4.21 Hydrogen Bond Analysis in Model System 4: 7-hydroxymitragynine. Hydrogen Bond Interactions Between the Kratom Alkaloid and Lipids (A, B, C), and Water Molecules (D, E, F) During the 200 ns of MD Simulations. Replicate 1 (A, D), Replicate 2 (B, E), and Replicate 3 (C, F).

4.7 Discussion

MD simulations have become an indispensable tool for studying drug-membrane interactions, offering atomic-level insights into the behavior of drug molecules within lipid bilayers. Unlike experimental techniques, MD simulations allows researchers to observe dynamic processes such as drug penetration, localization, and aggregation in real-time (Dror et al., 2013). This is particularly valuable for understanding the behavior of amphiphilic drugs that exhibit complex interactions with lipid bilayers due to their dual affinity for polar and nonpolar environments (Bennett & Tieleman, 2013). Based on the simulations, predictions can be made for drug bioavailability, membrane permeability, and potential pharmacological effects, providing a foundation for rational drug design and optimization (Dror et al., 2013).

Kratom alkaloids, particularly mitragynine and its derivatives (7-hydroxymitragynine and mitragynine pseudoindoxyl) have garnered significant attention as potential alternatives to classical opioids for pain management and other therapeutic applications. Mitragynine, the primary alkaloid in kratom, has been shown to exhibit analgesic effects through partial agonism at u-opioid receptors, while displaying a lower risk of respiratory depression compared to traditional opioids like morphine (Hassan et al., 2013; Kruegel & Grundmann, 2018; Varadi et al., 2016). Similarly, 7-hydroxymitragynine, a potent metabolite of mitragynine, has demonstrated enhanced analgesic activity, making it a promising candidate for pain relief (Kruegel & Grundmann, 2018; Matsumoto et al., 2004; Takayama et al., 2002). Mitragynine pseudoindoxyl, another derivative, has shown potential as a biased agonist at opioid receptors, offering a pathway to develop safer and more effective analgesics (Yamamoto et al., 1999). These three alkaloids are shown to be more potent than morphine, while exhibit less addiction effects, thus making them attractive compounds for therapeutics usage.

The physicochemical properties of these alkaloids play a critical role in their pharmacological behavior. According to Lipinski's Rule of Five, mitragynine, 7-hydroxymitragynine, and mitragynine pseudoindoxyl exhibit favorable drug-like properties, including moderate molecular weights (<500 Da), balanced hydrophobicity (logP values ranging from 2.5 to 4.0), and the ability to form hydrogen bonds (Hassan et al., 2013; Kruegel & Grundmann, 2018; Varadi et al., 2016). These properties contribute to their amphiphilic nature, enabling them to interact with both the polar

headgroups and hydrophobic core of lipid bilayers. For instance, the presence of polar functional groups (e.g., hydroxyl and methoxy groups) allows these alkaloids to form hydrogen bonds with lipid phosphate or carbonyl oxygen groups, while their hydrophobic indole and pseudoindoxyl moieties facilitate embedding in the lipid tail region (Kruegel & Grundmann, 2018; Váradi et al., 2016). This dual behavior is consistent with studies on other amphiphilic drugs, such as fentanyl and buprenorphine, which also exhibit membrane localization near lipid headgroups (Sutcliffe et al., 2022; Váradi et al., 2016). Fentanyl was reported to orient itself parallel to the headgroups while forming interactions with the water molecules at the interface that lead to disruption of lipid ordering, while propofol, a general anesthetic, prefers to interact with the carbonyl oxygen groups, exhibited minimal changes to the lipid bilayer (Faulkner et al 2020).

In this study, the findings from MD simulations revealed distinct yet consistent behaviors among the kratom alkaloids, highlighting their interactions with DPPC lipid bilayers. Mitragynine, 7-hydroxymitragynine, and mitragynine pseudoindoxyl all exhibited amphiphilic behavior, localizing near the lipid headgroups while embedding in the hydrophobic core. These amphiphilic molecules formed hydrogen bonds with the polar headgroups of DPPC lipids as well as with the water molecules at the lipid-water interface.

In every model system, mitragynine and mitragynine pseudoindoxyl exhibit the highest number of hydrogen bond interactions with lipids, with each forming up to 3 hydrogen bonds. Whereas 7-hydroxymitragynine has the lowest interaction with lipids by forming 1. However, in the interaction with water molecules, 7- hydroxymitragynine exhibits the highest and most stable hydrogen bonding, particularly in System Model 4, where it forms 8 hydrogen bonds.

Nevertheless, the penetration dynamics of these alkaloids varied significantly. For example, in Model System 1 (single molecule), all three alkaloids penetrated the bilayer relatively fast (in less than 50 ns), with mitragynine showing the fastest diffusion. In Model System 2 (three molecules of the same type), both mitragynine and 7-hydroxymitragynine were rapidly diffused into the lipid bilayer (during 10-15 ns) compared to the mitragynine pseudoindoxyl (approximately ~50 ns). Meanwhile for the Model System 3 (three different types of alkaloids), mitragynine again diffused the fastest (10 ns), while both 7-hydroxymitragynine and mitragynine pseudoindoxyl formed as a couple when entering the lipid hydrophobic region at ~50 ns, which then

caused its position towards the core hydrophobic region and larger distances to the lipid headgroups However, the separations of the 7-hydroxymitragynine and mitragynine pseudoindoxyl couple (-70 ns) led to a stable localization of both alkaloids that interact with the polar region of the lipid headgroups till end of the simulations.

When comparing the simulations for a single and a higher number of alkaloids (Model Systems 2-4), we observed that an increased amount of alkaloid molecules in the lipid bilayer system led to an aggregation in the aqueous phase, which delayed or hindered penetration. For instance, in Model System 4 (six molecules of 7-hydroxymitragynine), the formation of large aggregates created an energy barrier that prevented full penetration in one replicate (Replicate 2), while slower penetration occurred in others (Replicates 1 and 3). This behavior aligns with studies on curcumin and doxorubicin, where aggregation was shown to reduce membrane permeability by increasing the effective size of the drug molecules (Kunwar et al., 2006; Tacar et al., 2013; Wang et al, 1997). During the 50-100 ns timeframe, all 6 molecules of mitragynine interact with the DPPC lipid bilayer as a single compound, demonstrating stable and consistent penetration into the membrane. In contrast, mitragynine pseudoindoxyl shows the first 2 molecules enter the lipid bilayer individually within the first -50 ns, while the remaining 4 molecules penetrate individually over the full 100 ns simulation.

The behavior of 7-hydroxymitragynine in Model System 4 (six molecules) provides valuable insights into the role of molecular assembly in drug-membrane interactions. Unlike Model Systems 1 and 2, where 7-hydroxymitragynine exhibited consistent penetration, the high concentration in Model System 4 led to the formation of large aggregates that either delayed penetration or completely prevented it. This can be attributed to the high energy barrier required for large aggregates to disrupt the lipid bilayer, as well as the increased steric hindrance at the lipid-water interface (Bennett & Tieleman, 2013; Kunwar et al., 2006). The assembly of 7-hydroxymitragynine molecules increases their effective size, making it energetically unfavorable for them to enter the hydrophobic core. This behavior is consistent with studies on fentanyl, where molecular aggregation was shown to reduce membrane permeability and alter pharmacological activity (Vuckovic et al., 2009). Additionally, the localization of 7-hydroxymitragynine aggregates near the lipid headgroups mirrors the behavior of morphine, which also interacts strongly with lipid phosphate groups while embedding in the hydrophobic region (Kruegel & Grundmann, 2018; Varadi et al., 2016). These

behaviors describe the result of Yusof et al that observed the lower permeation rate of 7-hydroxymitragynine than mitragynine in *in vitro* blood-brain-barrier model (Yusof et al., 2018). These findings highlight the importance of considering molecular aggregation in the design of the drug delivery system as it can significantly impact drug bioavailability and efficacy.

CHAPTER 5
CONCLUSION

Mitragynine demonstrates moderate membrane penetration, gradually embedding into the bilayer overtime. Its localization near the lipid headgroups, coupled with partial insertion into the bilayer core, suggests a balanced membrane permeability that likely contributes to its controlled bioavailability and sustained pharmacological effects. This interaction profile aligns with mitragynine's known pharmacological behavior, where a slower onset of action is observed, potentially leading to more prolonged therapeutic effects. 7-hydroxymitragynine exhibits more dynamic and variable interactions with the bilayer. Its amphiphilic nature and strong water affinity limit its ability to deeply penetrate the membrane, often resulting in the molecule remaining near the membrane surface or only partially inserted into the bilayer. These interactions suggest limited membrane permeability, which may affect its bioavailability and indicate that alternative transport mechanisms—such as active transport—could contribute to its potent pharmacological effects despite its superficial membrane interactions. In contrast, mitragynine pseudoindoxyl displays the deepest and most stable bilayer integration among the three alkaloids. Its high lipophilicity drives rapid and consistent penetration into the bilayer core, suggesting enhanced membrane permeability. This behavior may insertion facilitate faster systemic absorption, correlating with its greater potency and stronger pharmacological effects compared to its parent compound, mitragynine.

MD simulations provide key insights into how the structural differences among mitragynine, 7-hydroxymitragynine, and mitragynine pseudoindoxyl influence their membrane interactions, thereby affecting permeability, bioavailability, and pharmacological potency. Mitragynine pseudoindoxyl's deep and stable bilayer penetration aligns with its heightened opioid activity, while mitragynine and 7-hydroxymitragynine exhibit more nuanced behaviors that balance solubility and membrane affinity. These findings offer valuable perspectives on the biophysical underpinnings of kratom alkaloids' pharmacokinetics and could inform the design of safer and more effective therapeutics derived from these natural compounds.

In conclusion, reveals that although three alkaloids consist of amphiphilic properties, they exhibit higher preference toward lipophilicity, which enable them to rapidly diffuse into the hydrophobic core of the lipid bilayer while localizing near the lipid phosphate groups. This preferred localization allows the alkaloids to form hydrogen bonds with both lipid headgroups and water molecules at the interface, facilitating their integration into the membrane. Among the alkaloids, mitragynine demonstrated the fastest penetration into the bilayer, followed by 7-hydroxymitragynine and mitragynine pseudoindoxyl, which exhibited slower diffusion rates. In systems with multiple molecules, the penetration dynamics were influenced by molecular aggregation in the aqueous environment. For instance, in systems with higher concentrations of 7-hydroxymitragynine, the formation of large aggregates created an energy barrier that either delayed or prevented penetration into the bilayer. This behavior highlights the critical role of molecular assembly in modulating membrane interactions and provides valuable insights into the factors influencing the bioavailability and pharmacological efficacy of kratom alkaloids.

This work paves the way for further research into the development of safer and more effective opioid analogs. Strategies to mitigate aggregation, such as nanoformulation or co-administration with surfactants, could improve the membrane permeability of kratom alkaloids and enhance their therapeutic efficacy. Additionally, the dual localization of these alkaloids near lipid headgroups warrants further investigation into their interactions with membrane proteins, such as u-opioid receptors, which play a critical role in their pharmacological effects. For future outlook, integrating computational and experimental approaches will be essential to unlock the full therapeutic potential of kratom alkaloids and address the ongoing need for alternatives to classical opioids in pain management and addiction treatment.

REFERENCES

Ahmad, K., & Aziz, Z. (2012). Mitragyna speciosa use in the northern states of Malaysia: A cross-sectional study. *Journal of Ethnopharmacology, 141,* 446-450. https://doi.org/10.1016/jjep.2012.03.009

Allen, M. P., Frenkel, D., & Talbot, J. (1989). Molecular dynamics simulation using hard particles. *Computer Physics Reports,* 9(6), 301-353. https://doi. org/10.1016/0167-7977(89)90009-9

Allen, W. J., Lemkul, J. A., & Bevan, D. R. (2009). GridMAT-MD: A grid-based membrane analysis tool for use with molecular dynamics. *Journal of Computational Chemistry, 30(12),* 1952-1958. https://doi.org/10.1002/jcc.21172

Amrianto, Ishak, S. S. O., Putra, N., Salsabila, S., & Muqarrabun, L. M. R. A. (2021). Mitragynine: A review of its extraction, identification, and purification methods. *Current Research on Biosciences and Biotechnology,* 3(1), Article 1. https://doi.Org/10.5614/crbb.2021.3.l/TMPNSA4H

Anand, A., & Hosanagar, A. (2022). The Addictive Potential and Challenges with Use of the "Herbal Supplement" Kratom: A Case Report and Literature Review. *Pain Medicine (Maiden, Mass.), 23(1),* 4-9. https://doi.org/10.1093/pm/pnabl26

Annuar, N. A. K., Azlan, U. K., Mediani, A., Tong, X., Han, R., Al-Olayan, E., Baharum, S. N., Bunawan, H., Sarian, M. N., Hamezah, H. S., & Jantan, I. (2024). An insight review on the neuropharmacological effects, mechanisms of action, pharmacokinetics and toxicity of mitragynine. *Biomedicine & Pharmacotherapy, 171,* 116134. https://doi.Org/10.1016/j.biopha.2024.116134

Babu, K. M., McCurdy, C. R., & Boyer, E. W. (2008). Opioid receptors and legal highs: Salvia divinorum and Kratom. *Clinical Toxicology (Philadelphia, Pa.), 46(2),* 146-152. https://doi.org/10.1080/15563650701241795

Benson, N. C, & Daggett, V. (2012). A Comparison of Multiscale Methods for the Analysis of Molecular Dynamics Simulations. *The Journal of Physical Chemistry B, 116(29),* 8722-8731. https://doi.org/10.1021/jp302103t

Berendsen, H. J. C, Postma, J. P. M., van Gunsteren, W. F., DiNola, A., & Haak, J. R (1984). Molecular dynamics with coupling to an external bath. *The Journal of Chemical Physics,* 57(8), 3684-3690. https://doi.org/10.1063/L448118

Berneche, S., & Roux, B. (2001). Energetics of ion conduction through the K+ channel. *Nature, 414(6859), 13-11.* https://doi.org/10.1038/35102067

Borhani, D. W., & Shaw, D. E. (2012). The future of molecular dynamics simulations in drug discovery. *Journal ofComputer-Aided Molecular Design, 26(1),* 15-26. https://doi.org/10.1007/sl0822-011-9517-y

Bothun, G. D. (2008). Hydrophobic silver nanoparticles trapped in lipid bilayers: Size distribution, bilayer phase behavior, and optical properties. *Journal of Nanobiotechnology,* (5(1), 13. https://doi.org/10.1186/1477-3155-6-13

Brown, P. N., Lund, J. A., & Murch, S. J. (2017). A botanical, phytochemical and ethnomedicinal review of the genus Mitragyna korth: Implications for products sold as kratom. *Journal of Ethnopharmacology, 202,* 302-325. https://doi.org/10.1016/jjep.2017.03.020

Bruininks, B. M. H., Wassenaar, T. A., & Vattulainen, I. (2023). Unbreaking Assemblies in Molecular Simulations with Periodic Boundaries. *Journal of Chemical Information and Modeling, 63(11),* 3448-3452. https://doi.org/10.1021/acs.jcim.2c01574

Charoenratana, S., Anukul, C, & Aramrattana, A. (2021). Attitudes towards Kratom use, decriminalization and the development of a community-based Kratom control mechanism in Southern Thailand. *International Journal of Drug Policy,95,* 103197. https://doi.org/10.32890/uumjls. 11.1.2020.6928

Chen, L., Fei, S., & Olatunji, O. J. (2022). LC/ESI/TOF-MS Characterization, Anxiolytic and Antidepressant-like Effects of Mitragyna speciosa Korth Extract in Diabetic Rats. *Molecules, 27(1),* 2208. https://doi.org/10.3390/molecules27072208

Chittrakarn, S., Radenahmad, N., Kaewsara, S., Udomuksorn, W., Keawpradub, N., & Phukpattaranont, P. (2018). *Gastroprotective effects of methanolic extract of kratom leaves on gastric ulcer and reflux esophagitis in rats.*

Chodera, J. D., Mobley, D. L., Shirts, M. R., Dixon, R. W., Branson, K., & Pande, V. S. (2011). Alchemical free energy methods for drug discovery: Progress and challenges. *Current Opinion in Structural Biology, 21(2),* 150-160. https://doi.Org/10.1016/j.sbi.2011.01.011

Clark, A. J., Tiwary, P., Borrelli, K., Feng, S., Miller, E. B., Abel, R., Friesner, R A., & Berne, B. J. (2016). Prediction of Protein-Ligand Binding Poses via a Combination of Induced Fit Docking and Metadynamics Simulations. *Journal of Chemical Theory and Computation, 12(6),* 2990-2998. https://doi.org/10.1021/acs.jctc.6b00201

Cohen, P. (2002). Protein kinases—The major drug targets of the twenty-first century? *Nature Reviews. Drug Discovery,* 7(4), 309-315. https://doi.org/10.1038/nrd773

Darden, T., York, D., & Pedersen, L. (1993). Particle mesh Ewald: AnN-log(N) method for Ewald sums in large systems. *The Journal of Chemical Physics,* 95(12), 10089-10092. https://doi.org/10.1063/L464397

Davidson, L., Rawat., M., Stojanovski., S., & Chandrasekharan., P. (2019). Natural drugs, not so natural effects: Neonatal abstinence syndrome secondary to "kratom." Journal of Neonatal-Perinatal Medicine, 12(1), 109-112. https://doi.org/10.3233/npm-1863

Dolinsky, T. J., Nielsen, J. E., McCammon, J. A., & Baker, N. A. (2004). PDB2PQR: An automated pipeline for the setup of Poisson-Boltzmann electrostatics calculations. *Nucleic Acids Research,* 32(suppl_2), W665-W667. https://doi. org/10.1093/nar/gkh3 81

Domnic, G., Jeng-Yeou Chear, N., Abdul Rahman, S. F., Ramanathan, S., Lo, K.-W., Singh, D., & Mohana-Kumaran, N. (2021). Combinations of indole-based alkaloids from Mitragyna speciosa (Kratom) and cisplatin inhibit cell proliferation and migration of nasopharyngeal carcinoma cell lines. *Journal of Ethnopharmacology, 279,* 114391. https://doi.org/10.1016/jjep.2021.114391

Dowhan, W. (1997). Molecular basis for membrane phospholipid diversity: Why are there so many lipids? *Annual Review of Biochemistry, 66,* 199-232. https://doi.org/10.1146/annurev.biochem.66.1.199

Dror, R. O., Green, H. F., Valant, C, Borhani, D. W., Valcourt, J. R., Pan, A. C, Arlow,

D. H., Canals, M., Lane, J. R., Rahmani, R., Baell, J. B., Sexton, P. M., Christopoulos, A., & Shaw, D. E. (2013). Structural basis for modulation of a G-protein-coupled receptor by allosteric drugs. *Nature, 503(7475),* 295-299. https://doi.org/10.1038/naturel2595

Durrant, J. D., & McCammon, J. A. (2011). Molecular dynamics simulations and drug discovery. *BMC Biology, 9,* 71. https://doi.org/10.1186/1741-7007-9-71

Eggleston, W., Stoppacher, R, Suen, K., Marraffa, J. M., & Nelson, L. S. (2019). Kratom Use and Toxicities in the United States. *Pharmacotherapy, 39(7),* 775-777. https://doi.org/10.1002/phar.2280

Ellis, C. R., Racz, R, Kruhlak, N. L., Kim, M. T., Zakharov, A. V., Southall, N., Hawkins, E. G., Burkhart, K., Strauss, D. G., & Stavitskaya, L. (2020). Evaluating kratom alkaloids using PHASE. *PLOS ONE,* 75(3), e0229646. https://doi.org/10.1371/journal.pone.0229646

E. N., Angelini, A., Waghray, D., Dror, R O., Ploegh, H. L., & Garcia, K. C. (2015). Structural basis for chemokine recognition and activation of a viral G protein-coupled receptor. *Science (New York, NY.), 347(6226),* 1113-1117. https://doi.org/10.1126/science.aaa5026

Escriba, P. V., Gonzalez-Ros, J. M., Gofii, F. M., Kinnunen, P. K. J., Vigh, L., Sanchez-Magraner, L., Fernandez, A. M., Busquets, X., Horvath, I., & Barcelo-Coblijn,

Essmann, U., Perera, L., Berkowitz, M. L., Darden, T., Lee, H., & Pedersen, L. G. (1995). A smooth particle mesh Ewald method. *Journal of Chemical Physics, 103,* 8577-8593. https://doi.org/10.1063/L470117

Faulkner, C, Santos-Carballal, D., Plant, D. F., & de Leeuw, N. H. (2020). Atomistic Molecular Dynamics Simulations of Propofol and Fentanyl in Phosphatidylcholine Lipid Bilayers. *ACS Omega,* 5(24), 14340-14353. https://doi.org/10.1021/acsomega.0c00813

Farkas, D. L, Foss, J. D., Ward, S. J., & Rawls, S. M. (2022). Kratom alkaloid mitragynine: Inhibition of chemotherapy-induced peripheral neuropathy in mice is dependent on sex and active adrenergic and opioid receptors. *IBRO NeuroscienceReports, 13,* 198-206. https://doi.Org/10.1016/j.ibneur.2022.08.007

Feller, S. E., Venable, R. M., & Pastor, R. W. (1997). Computer Simulation of aDPPC Phospholipid Bilayer: Structural Changes as a Function of Molecular Surface Area. *Langmuir, 13(24),* 6555-6561. https://doi.org/10.1021/la970746j

Feng, L.-Y., Battulga, A., Han, E., Chung, H, & Li, J.-H. (2017). New psychoactive substances of natural origin: A brief review. *Journal of Food and Drug Analysis, 25(3),* 461-471. https://doi.org/10.1016/jjfda.2017.04.001

Foss, J. D., Nayak, S. U., Tallarida, C. S., Farkas, D. J., Ward, S. I, & Rawls, S. M. (2020). Mitragynine, bioactive alkaloid of kratom, reduces chemotherapy-induced neuropathic pain in rats through a-adrenoceptor mechanism. *Drug and Alcohol Dependence, 209,* 107946. https://doi.Org/10.1016/j.drugalcdep .2020.107946

Gutridge, A. M., Chakraborty, S., Varga, B. R., Rhoda, E. S., French, A. R., Blaine, A. T., Royer, Q. H., Cui, H., Yuan, J., Cassell, R. I, Szabo, M., Majumdar, S., & van Rijn, R M. (2021). Evaluation of Kratom Opioid Derivatives as Potential Treatment Option for Alcohol Use Disorder. *Frontiers in Pharmacology, 12,* 764885. https://doi.org/10.3389/fphar.2021.764885

Hanapi, N. A., Chear, N. J.-Y, Azizi, J., & Yusof, S. R. (2021). Kratom Alkaloids: Interactions With Enzymes, Receptors, and Cellular Barriers. *Frontiers in Pharmacology, 12,* https://www.firontiersin.org/articles/10.3389/fphar.2021.751656

Hassan, Z., Muzaimi, M., Navaratnam, V., Yusoff, N. H. M., Suhaimi, F. W., Vadivelu, R., Vicknasingam, B. K., Amato, D., von Horsten, S., Ismail, N. I. W., Jayabalan, N., Hazim, A. I, Mansor, S. M., & Muller, C. P. (2013). From Kratom to mitragynine and its derivatives: Physiological and behavioural effects related to use, abuse, and addiction. *Neuroscience & Biobehavioral Reviews, 37(2),* 138-151. https://doi.0rg/lO.lOl6/j.neubiorev.2Oi2.ll.Oi2

Henningfield, J. E. (2018). *The abuse potential of kratom according the 8 factors of the controlled substances act: Implications for regulation and research.*

Hollingsworth, S. A., & Dror, R. O. (2018). Molecular dynamics simulation for all. *Neuron, 99(6),* 1129-1143.https://doi.org/10.1016/j.neuron.2018.08.011

Hossain, S. I., Saha, S. C, & Deplazes, E. (2021). Phenolic compounds alter the ion permeability of phospholipid bilayers via specific lipid interactions. *Physical Chemistry Chemical Physics, 23(39),* 22352-22366. https://doi.org/10.1039/DlCP03250J

Hou, T., Wang, J., Li, Y., & Wang, W. (2011). Assessing the performance of the MM/PBS A and MM/GBSA methods: I. The accuracy of binding free energy calculations based on molecular dynamics simulations. *Journal of Chemical Information and Modeling,* 57(1), 69-82. https://doi.org/10.1021/cil00275a

Hurst, D. P., Grossfield, A., Lynch, D. L., Feller, S., Romo, T. D., Gawrisch, K., Pitman, M. C, & Reggio, P. H. (2010). A Lipid Pathway for Ligand Binding Is Necessary for a Cannabinoid G Protein-coupled Receptor *. *Journal of BiologicalChemistry,285(23),\7954-\7964.* https://doi.org/10.1074/jbc.M109.041590

Idayu, N. F., Hidayat, M. T., Moklas, M. a. M., Sharida, F., Raudzah, A. R N., Shamima, A. R, & Apryani, E. (2011). Antidepressant-like effect of mitragynine isolated from Mitragyna speciosa Korth in mice model of depression. *Phytomedicine: International Journal of Phytotherapy and Phytopharmacology*, 75(5), 402-407. https://doi.Org/10.1016/j.phymed. 2010.08.011

Innok, W., Hiranrat, A., Chana, N., Rungrotmongkol, T., & Kongsune, P. (2021). In silico and in vitro anti-AChE activity investigations of constituents from Mytragyna speciosa for Alzheimer's disease treatment. *Journal of Computer-AidedMolecular Design, 35(3),* 325-336. https://doi.org/10.1007/sl0822-020-00372-4

Ismail, N. A., & Jusoh, S. A. (2017). Molecular Docking and Molecular Dynamics Simulation Studies to Predict Flavonoid Binding on the Surface of DENV2 E Protein. *Interdisciplinary Sciences: Computational Life Sciences,* 9(4), 499-511. https://doi.org/10.1007/sl2539-016-0157-8

Jasim, R. K., Hassan, Z., Singh, D., Boyer, E., & Gam, L.-H. (2022). Characterization of urinary protein profile in regular kratom (Mitragyna speciosa korth.) users in Malaysia. *Journal of Addictive Diseases, 40(2),* 235-246. https://doi.org/10.1080/10550887.2021.1981122

Jentsch, M. J., & Pippin, M. M. (2024). Kratom. In *StatPearls.* StatPearls Publishing. http://www.ncbi.nlm.nih.gov/books/NBK585120/

Juanda, E., Andayani, S., & Maftuch, M. (2019). Phytochemical Screening and Antibacterial Activity of Kratom Leaf (Mitragyna speciosa Korth.) Against Aeromonas hydrophilla. *The Journal of Experimental Life Science, 9(3),* Article 3. https://doi.org/10.21776/ub.jels.2019.009.03.02

Jusoh, S. A., & Helms, V. (2011). Helical integrity and microsolvation of transmembrane domains from Flaviviridae envelope glycoproteins. *Biochimica et Biophysica Acta (BBA) - Biomembranes, 1808(4),* 1040-1049. https://doi.Org/10.1016/j.bbamem.2011.01.004

Karami, L. (2023). Interaction of neutral and protonated Tamoxifen with the DPPC lipid bilayer using molecular dynamics simulation. *Steroids, 194*, 109225. https://doi.Org/10.1016/j.steroids.2023.109225

Karplus, M., & McCammon, J. A. (2002). Molecular dynamics simulations of biomolecules. *Nature Structural Biology*, 9(9), 646-652. https://doi. org/10.103 8/nsb0902-646

Khafizov, K., Perez, C, Koshy, C, Quick, M., Fendler, K., Ziegler, C, & Forrest, L.R. (2012). Investigation of the sodium-binding sites in the sodium-coupled betaine transporter BetP. *Proceedings of the National Academy of Sciences of the United States of America, 109(44),* E3035-E3044. https://doi.org/10.1073/pnas.1209039109

Knobloch, J., Suhendro, D. K., Zieleniecki, J. L., Shapter, J. G., & Koper, I. (2015). Membrane-drug interactions studied using model membrane systems. *Saudi Journal of Biological Sciences, 22(6),* 714-718. https://doi.Org/10.1016/j.sjbs.2015.03.007

Koehl, A., Hu, H., Maeda, S., Zhang, Y., Qu, Q., Paggi, J. M., Latorraca, N. R., Hilger, D., Dawson, R., Matile, H., Schertler, G. F. X., Granier, S., Weis, W. I., Dror, R. O., Manglik, A, Skiniotis, G, & Kobilka, B. K. (2018). Structure of the *[i* Opioid Receptor-Gi Protein Complex. *Nature*, 555(7711), 547-552. https://doi.org/10.1038/s41586-018-0219-7

Kopec, W., Telenius, J., & Khandelia, H. (2013). Molecular dynamics simulations of the interactions of medicinal plant extracts and drugs with lipid bilayer membranes. *The FEBS Journal, 280(12),* 2785-2805. https://doi.org/10.1111/febs. 12286

Kruegel, A. C, Gassaway, M. M., Kapoor, A., Varadi, A., Majumdar, S., Filizola, M., Javitch, J. A., & Sames, D. (2016). Synthetic and Receptor Signaling Explorations of the Mitragyna Alkaloids: Mitragynine as an Atypical Molecular Framework for Opioid Receptor Modulators. *Journal of the American Chemical Society, 138(21),* 6754-6764. https://doi.org/10.1021/jacs.6b00360

Kruegel, A. C, & Grundmann, O. (2018). The medicinal chemistry and neuropharmacology of kratom: A preliminary discussion of a promising medicinal plant and analysis of its potential for abuse. *Neuropharmacology, 134,* 108-120. https://doi.Org/10.1016/j.neuropharm.2017.08.026

Kruegel, A. C, Uprety, R., Grinnell, S. G., Langreck, C, Pekarskaya, E. A., LeRouzic, V., Ansonoff, M., Gassaway, M. M., Pintar, J. E., Pasternak, G. W., Javitch, J. A., Majumdar, S., & Sames, D. (2019). 7-Hydroxymitragynine Is an Active Metabolite of Mitragynine and a Key Mediator of Its Analgesic Effects. *ACS Central Science,* 5(6), 992-1001. https://doi.org/10.1021/acscentsci.9b00141

Latorraca, N. R., Fastman, N. M., Venkatakrishnan, A. J., Frommer, W. B., Dror, R O., & Feng, L. (2017). Mechanism of substrate translocation in an alternating access transporter. *Cell, 169(1),* 96-107.el2. https://doi.Org/10.1016/j.cell.2017.03.010

La-Up, A., Saengow, U, & Aramrattana, A. (2021). High serum high-density lipoprotein and low serum triglycerides in Kratom users: A study of Kratom users in Thailand. *Heliyon,* 7(4), e06931. https://doi.Org/10.1016/j.heliyon.2021.e06931

Leong Bin Abdullah, M. F. I., Tan, K. L., Mohd Isa, S., Yusoff, N. S., Chear, N. J. Y., & Singh, D. (2020). Lipid profile of regular kratom (Mitragyna speciosa Korth.) users in the community setting. *PloS One, 15(6),* e0234639. https://doi.org/10.1371/journal.pone.0234639

Li, J., Shaikh, S. A, Enkavi, G, Wen, P.-C, Huang, Z., & Tajkhorshid, E. (2013). Transient formation of water-conducting states in membrane transporters. *Proceedings of the National Academy of Sciences of the United States of America, 110(19),* 7696-7701. https://doi.org/10.1073/pnas.1218986110

Limcharoen, T., Pouyfung, P., Ngamdokmai, N, Prasopthum, A., Ahmad, A. R., Wisdawati, W., Prugsakij, W., & Warinhomhoun, S. (2022). Inhibition of a-Glucosidase and Pancreatic Lipase Properties of Mitragyna speciosa (Korth.) Havil. (Kratom) Leaves. *Nutrients, 14(19),* 3909. https://doi.org/10.3390/nul4193909

Mackay, L., & Abrahams, R. (2018). Novel case of maternal and neonatal kratom dependence and withdrawal. *Canadian Family Physician, 64(2),* 121-122.

Malde, A. K., Zuo, L., Breeze, M., Stroet, M., Poger, D., Nair, P. C, Oostenbrink, C, & Mark, A. E. (2011). An Automated Force Field Topology Builder (ATB) and Repository: Version 1.0. *Journal of Chemical Theory and Computation,* 7(12), 4026.

Manabe, S., Miyano, K., Fujii, Y., Ohshima, K., Yoshida, Y., Nonaka, M., Uzu, M., Matsuoka, Y., Sato, T., Uezono, Y., & Morimatsu, H. (2019). Possible biased analgesic of hydromorphone through the G protein-over P-arrestin-mediated pathway: cAMP, CellKey™, and receptor internalization analyses. *Journal of Pharmacological Sciences, 140(2), Ill-Ill.* https://doi.org/10.1016/jjphs.2019.06.005

Mark, P., & Nilsson, L. (2002). Structure and dynamics of liquid water with different long-range interaction truncation and temperature control methods in molecular dynamics simulations. *Journal of Computational Chemistry,* 23(13), 1211-1219. https://doi.org/10.1002/jcc.10117

Matsumoto, K., Horie, S., Ishikawa, H., Takayama, H., Aimi, N, Ponglux, D., & Watanabe, K. (2004). Antinociceptive effect of 7-hydroxymitragynine in mice: Discovery of an orally active opioid analgesic from the Thai medicinal herb Mitragyna speciosa. *Life Sciences, 74(11),* 2143-2155. https://doi.Org/10.1016/j.lfs.2003.09.054

Matsumoto, K., Mizowaki, M., Suchitra, T., Takayama, H., Sakai, S., Aimi, N., & Watanabe, H. (1996). Antinociceptive action of mitragynine in mice: Evidence for the involvement of supraspinal opioid receptors. *Life Sciences,* 59(14), 1149-1155. https://doi.org/10.1016/0024-3205(96)00432-8

McLure, J. A., Miners, J. O., & Birkett, D. J. (2000). Nonspecific binding of drugs to human liver microsomes. *British Journal of Clinical Pharmacology, 49(5),* 453-461. https://doi.Org/10.1046/j.1365-2125.2000.00193.x

Michaud-Agrawal, N., Denning, E. I, Woolf, T. B., & Beckstein, O. (2011). MDAnalysis: A toolkit for the analysis of molecular dynamics simulations. *Journal of Computational Chemistry,* 32(10), 2319-2327. https://doi. org/10.1002/j cc.21787

Michot, J.-M., Serai, C, VanBambeke, F., Mingeot-Leclercq, M.-P., & Tulkens, P. M. (2005). Influence of Efflux Transporters on the Accumulation and Efflux of Four Quinolones (Ciprofloxacin, Levofloxacin, Garenoxacin, and Moxifloxacin) in J774 Macrophages. *Antimicrobial Agents and Chemotherapy, 49(6),* 2429-2437. https://doi.Org/10.1128/AAC.49.6.2429-2437.2005

Mirjalili, V., & Feig, M. (2013). Protein Structure Refinement through Structure Selection and Averaging from Molecular Dynamics Ensembles. *Journal of Chemical Theory and Computation,* 9(2), 1294-1303. https://doi. org/10.102 l/ct3 00962x

Mobley, D. L., & Dill, K. A. (2009). Binding of Small-Molecule Ligands to Proteins: "What You See" Is Not Always "What You Get." *Structure (London, England : 1993), 17(4),* 489-498. https://doi.Org/10.1016/j.str.2009.02.010

Mousa, M. S., Sephien, A., Gutierrez, J., & O'Leary, C. (2018). N-Acetylcysteine for Acute Hepatitis Induced by Kratom Herbal Tea. *American Journal of Therapeutics,* 25(5), e550-e551. https://doi.org/10.1097/MJT. 0000000000000631

Nagar, S., & Korzekwa, K. (2012). Commentary: Nonspecific protein binding versus membrane partitioning: it is not just semantics. *Drug Metabolism and Disposition: The Biological Fate of Chemicals, 40(9),* 1649-1652. https://doi.org/10.1124/dmd. 112.046599

Obeng, S., Kamble, S. H., Reeves, M. E., Restrepo, L. F., Patel, A., Behnke, M., Chear, N. J.-Y., Ramanathan, S., Sharma, A., Leon, F., Hiranita, T., Avery, B. A., McMahon, L. R., & McCurdy, C. R (2020). Investigation of the Adrenergic and Opioid Binding Affinities, Metabolic Stability, Plasma Protein Binding Properties, and Functional Effects of Selected Indole-Based Kratom Alkaloids. *Journal of Medicinal Chemistry, 63(1),* 433-439. https://doi.org/10.1021/acs.jmedchem. 9b01465

Overbeek, D. L., Abraham, I, & Munzer, B. W. (2019). Kratom (Mitragynine) Ingestion Requiring Naloxone Reversal. *Clinical Practice and Cases in Emergency Medicine,* 3(1), 24-26. https://doi.org/10.5811/cpcem.2018.ll.40588

Peetla, C, Stine, A., & Labhasetwar, V. (2009). Biophysical interactions with model lipid membranes: Applications in drug discovery and drug delivery. *Molecular Pharmaceutics, 6(5),* 1264-1276. https://doi.org/10.1021/mp9000662

Perez, A., Morrone, J. A., Simmerling, C, & Dill, K. A. (2016). Advances in free-energy-based simulations of protein folding and ligand binding. *Current Opinion in Structural Biology, 36,* 25-31. https://doi.Org/10.1016/j.sbi.2015. 12.002

Philipp, A. A., Wissenbach, D. K., Weber, A. A, Zapp, J., & Maurer, H. H. (2011). Metabolism studies of the Kratom alkaloids mitraciliatine and isopaynantheine, diastereomers of the main alkaloids mitragynine and paynantheine, in rat and human urine using liquid chromatography-linear ion trap-mass spectrometry. *Journal of Chromatography. B, Analytical Technologies in the Biomedical and Life Sciences*, 579(15-16), 1049-1055. https://doi.org/10.1016/jjchromb.2011.03.005

Poghosyan, A. H., Gharabekyan, H. H., & Shahinyan, A. A. (2007). MOLECULAR DYNAMICS SIMULATIONS OF DMPC/DPPC MIXED BILAYERS. *International Journal of Modern Physics C*, 75(01), 73-89. https://doi.org/10.1142/S0129183107010267

Prates Ramalho, J. P., Gkeka, P., & Sarkisov, L. (2011). Structure and Phase Transformations of DPPC Lipid Bilayers in the Presence of Nanoparticles: Insights from Coarse-Grained Molecular Dynamics Simulations. *Langmuir*, 27(7), 3723-3730. https://doi.org/10.1021/la200236d

Prevete, E., Kuypers, K. P. C, Theunissen, E. L., Corazza, O., Bersani, G., & Ramaekers, J. G (2022). A systematic review of (pre)clinical studies on the therapeutic potential and safety profile of kratom in humans. *Human Psychopharmacology*, 37(1), e2805. https://doi.org/10.1002/hup.2805

Prozialeck, W. C, Jivan, J. K., & Andurkar, S. V. (2012). Pharmacology of kratom: An emerging botanical agent with stimulant, analgesic and opioid-like effects. *The Journal of the American Osteopathic Association*, 772(12), 792-799.

Ramanathan, S., Leon, F., Chear, N. J. Y., Yusof, S. R., Murugaiyah, V., McMahon, L. R., & McCurdy, C. R. (2021). Kratom *(Mitragyna speciosa* Korth.): A description on the ethnobotany, alkaloid chemistry, and neuropharmacology. In Atta-ur-Rahman (Ed.), *Studies in Natural Products Chemistry* (Vol. 69, pp. 195-225). Elsevier. https://doi.org/10.1016/B978-0-12-819487-4.00003-3

Raval, A., Piana, S., Eastwood, M. P., Dror, R O., & Shaw, D. E. (2012). Refinement of protein structure homology models via long, all-atom molecular dynamics simulations. *Proteins*, 50(8), 2071-2079. https://doi.org/10.1002/prot.24098

Rech, M. A., Donahey, E., Cappiello Dziedzic, J. M., Oh, L., & Greenhalgh, E. (2015). New drugs of abuse. *Pharmacotherapy, 35(2)*, 189-197. https://doi.org/10.1002/phar. 1522

Salim, H. M., Choirotussanijjah, Awwalia, E. S., & Alam, I. P. (2022). Anti-inflammatory effects and potential mechanisms of Mitragyna speciosa methanol extract on X-karagenan-induced inflammation model. *Bali Medical Journal,* 77(3), Article 3. https://doi.org/10.15562/bmj.vlli3.3535

Saref, A., Suraya, S., Singh, D., Grundmann, O., Narayanan, S., Swogger, M. T., Prozialeck, W. C, Boyer, E., & Balasingam, V. (2020). Self-Report Data on Regular Consumption of Illicit Drugs and HIV Risk Behaviors after Kratom (Mitragyna Speciosa korth.) Initiation among Illicit Drug Users in Malaysia. *Journal of Psychoactive Drugs, 52(2),* 138-144. https://doi.org/10.1080/02791072.2019.1686553

Saref, A., Suraya, S., Singh, D., Grundmann, O., Narayanan, S., Swogger, M. T., Prozialeck, W. C, Boyer, E., Chear, N. J. Y., & Balasingam, V. (2019). Self-reported prevalence and severity of opioid and kratom (Mitragyna speciosa korth.) side effects. *Journal of Ethnopharmacology, 238,* 111876. https://doi.org/10.1016/jjep.2019.111876

Schmid, N., Eichenberger, A. P., Choutko, A., Riniker, S., Winger, M., Mark, A. E., & van Gunsteren, W. F. (2011). Definition and testing of the GROMOS force-field versions 54A7 and 54B7. *European Biophysics Journal: EBJ, 40(1),* 843-856. https://doi.org/10.1007/s00249-011-0700-9

Singer, S. J., & Nicolson, G. L. (1972). The fluid mosaic model of the structure of cell membranes. *Science (New York, N.Y.),* 775(4023), 720-731. https://doi.org/10.1126/science.175.4023.720

Singh, D., Muller, C. P., & Vicknasingam, B. K. (2014). Kratom (Mitragyna speciosa) dependence, withdrawal symptoms and craving in regular users. *Drug and Alcohol Dependence, 139,* 132-137. https://doi.Org/10.1016/j.drugalcdep. 2014.03.017

Singh, D., Muller, C. P., Vicknasingam, B. K., & Mansor, S. M. (2015). Social Functioning of Kratom *(Mitragyna speciosa)* Users in Malaysia. *Journal of Psychoactive Drugs, 47(2),* 125-131. https://doi.org/10.1080/02791072.2015. 1012610

Singh, D., Murugaiyah, V., Hamid, S. B. S., Kasinather, V., Chan, M. S. A., Ho, E. T. W., Grundmann, O., Chear, N. J. Y., & Mansor, S. M. (2018). Assessment of gonadotropins and testosterone hormone levels in regular Mitragyna speciosa (Korth.) users. *Journal of Ethnopharmacology, 221,* 30-36. https://doi.org/10.1016/jjep.2018.04.005

Singh, D., Narayanan, S., Vicknasingam, B., Corazza, O., Santacroce, R, & Roman-Urrestarazu, A. (2017). Changing trends in the use of kratom *(Mitragyna speciosa)* in Southeast Asia. *Human Psychopharmacology, 32(3).* https://doi.org/10.1002/hup.2582

S.Khalil, Ahmad, R, & John Abdullah, S. A. (2020). ENFORCEMENT STATUS OF THE POISON ACT 1952 AGAINST OFFENCES RELATED TO KRATOM (MITRAGYNA SPECIOSA KORTH) MISUSE IN MALAYSIA. *UUM Journal of Legal Studies, 11*. https://doi.org/10.32890/uumjls.ll.L2020.6928

Smith, D. A., Di, L., & Kerns, E. H. (2010). The effect of plasma protein binding on in vivo efficacy: Misconceptions in drug discovery. *Nature Reviews. Drug Discovery, 9(12),* 929-939. https://doi.org/10.1038/nrd3287

Spahn, V., Del Vecchio, G., Labuz, D., Rodriguez-Gaztelumendi, A., Massaly, N., Temp, J., Durmaz, V., Sabri, P., Reidelbach, M., Machelska, H, Weber, M., & Stein, C. (2017). A nontoxic pain killer designed by modeling of pathological receptor conformations. *Science (New York, N.Y.),* 355(6328), 966-969. https://doi.org/10.1126/science.aai8636

Stolt, A.-C, Schroder, H., Neurath, H., Grecksch, G, Hollt, V., Meyer, M. R., Maurer, H. H., Ziebolz, N., Havemann-Reinecke, U., & Becker, A. (2014). Behavioral and neurochemical characterization of kratom (Mitragyna speciosa) extract. *Psychopharmacology, 231(1),* 13-25. https://doi.org/10.1007/s00213-013-3201-y

Suhaimi, F. W., Yusoff, N. H. M., Hassan, R., Mansor, S. M., Navaratnam, V., Muller, C. P., & Hassan, Z. (2016). Neurobiology of Kratom and its main alkaloid mitragynine. *Brain Research Bulletin, 126(Pt* 1), 29-40. https://doi.Org/10.1016/j.brainresbull.2016.03.015

Sutcliffe, K. J., Corey, R A., Alhosan, N., Cavallo, D., Groom, S., Santiago, M., Bailey, C, Charlton, S. I, Sessions, R. B., Henderson, G, & Kelly, E. (2022). Interaction With the Lipid Membrane Influences Fentanyl Pharmacology. *Advances in Drug and Alcohol Research, 2,* 10280. https://doi.org/10.3389/adar.2022.10280

Swift, R. V., Jusoh, S. A., Offutt, T. L., Li, E. S., & Amaro, R. E. (2016). Knowledge-Based Methods To Train and Optimize Virtual Screening Ensembles. *Journal of Chemical Information and Modeling, 56(5),* 830-842. https://doi.org/10.1021/acs.jcim.5b00684

Swogger, M. T., Hart, E., Erowid, F., Erowid, E., Trabold, N., Yee, K., Parkhurst, K. A., Priddy, B. M., & Walsh, Z. (2015). Experiences of Kratom Users: A Qualitative Analysis. *Journal of Psychoactive Drugs, 47(5),* 360-367. https://doi.org/10.1080/02791072.2015.1096434

Sztain, T., Amaro, R., & McCammon, J. A. (2021). Elucidation of Cryptic and Allosteric Pockets within the SARS-CoV-2 Main Protease. *Journal of Chemical Information and Modeling,6I(7),3495-350*\. https://doi.org/10.1021/acs.jcim. Ic00140

Takayama, H., Ishikawa, H., Kurihara, M., Kitajima, M., Aimi, N., Ponglux, D., Koyama, F., Matsumoto, K., Moriyama, T., Yamamoto, L. T., Watanabe, K., Murayama, T., & Horie, S. (2002). Studies on the Synthesis and Opioid Agonistic Activities of Mitragynine-Related Indole Alkaloids: Discovery of Opioid Agonists Structurally Different from Other Opioid Ligands. *Journal of Medicinal Chemistry, 45(9),* 1949-1956. https://doi.org/10.1021/jm010576e

Tang, H, Demir, O., Kurniawan, F., Brown, W. L., Shi, K., Moeller, N. H., Carpenter, M. A., Belica, C, Orellana, K., Du, G, LeBeau, A. M., Amaro, R. E., Harris, R. S., & Aihara, H. (2021). Structural Characterization of a Minimal Antibody against Human APOBEC3B. *Viruses, 13(4),* Article 4. https://doi.org/10.3390/vl3040663

Todd, D. A., Kellogg, J. J., Wallace, E. D., Khin, M., Flores-Bocanegra, L., Tanna, R. S., Mcintosh, S., Raja, H. A., Graf, T. N., Hemby, S. E., Paine, M. F., Oberlies, N. H., & Cech, N. B. (2020). Chemical composition and biological effects of kratom *(Mitragyna speciosa):* In vitro studies with implications for efficacy and drug interactions. *Scientific Reports, 10(1),* Article 1. https://doi.org/10.1038/s41598-020-76119-w

Trakulsrichai, S., Sathirakul, K., Auparakkitanon, S., Krongvorakul, I, Sueajai, J., Noumjad, N., Sukasem, C, & Wananukul, W. (2015). Pharmacokinetics of mitragynine in man. *Drug Design, Development and Therapy, 9,* 2421-2429. https://doi.org/10.2147/DDDT.S79658

Udier-Blagovic, M., Tirado-Rives, J., & Jorgensen, W. L. (2003). Validation of a model for the complex of HIV-1 reverse transcriptase with nonnucleoside inhibitor TMC125. *Journal of the American Chemical Society,* 725(20), 6016-6017. https://doi.org/10.1021/ja034308c

Varadi, A., Marrone, G. F., Palmer, T. C, Narayan, A., Szabo, M. R., Le Rouzic, V., Grinnell, S. G, Subrath, J. J., Warner, E., Kalra, S., Hunkele, A., Pagirsky, J., Eans, S. O., Medina, J. M., Xu, J., Pan, Y.-X., Borics, A., Pasternak, G. W., McLaughlin, J. P., & Majumdar, S. (2016). Mitragynine/Corynantheidine Pseudoindoxyls as Opioid Analgesics with Mu Agonism and Delta Antagonism, Which Do Not Recruit P-Arrestin-2. *Journal of Medicinal Chemistry,* 59(18), 8381-8397. https://doi.org/10.1021/acs.jmedchem.6b00748

Vazquez Lopez, J. L., Schild, L., Giinther, T., Schulz, S., Neurath, H., & Becker, A. (2017). The effects of kratom on restraint-stress-induced analgesia and its mechanisms of action. *Journal of Ethnopharmacology, 205,* 178-185. https://doi.org/101016/jjep.2017.05.008

Vicknasingam, B., Chooi, W. T., Rahim, A. A., Ramachandram, D., Singh, D., Ramanathan, S., Yusof, N. S. M., Zainal, H., Murugaiyah, V., Gueorguieva, R., Mansor, S. M., & Chawarski, M. C. (2020). Kratom and Pain Tolerance: A Randomized, Placebo-Controlled, Double-Blind Study. *The Yale Journal of Biology and Medicine, 93(2),* 229-238.

Vicknasingam, B., Narayanan, S., Beng, G T., & Mansor, S. M. (2010). The informal use of ketum (Mitragyna speciosa) for opioid withdrawal in the northern states of peninsular Malaysia and implications for drug substitution therapy. *International Journal of Drug Policy, 21(4),* 283-288. https://doi.Org/10.1016/j.drugpo.2009.12.003

Vijeepallam, K., Pandy, V., Kunasegaran, T., Murugan, D. D., & Naidu, M. (2016). Mitragyna speciosa Leaf Extract Exhibits Antipsychotic-Like Effect with the Potential to Alleviate Positive and Negative Symptoms of Psychosis in Mice. *Frontiers in Pharmacology, 7,* 464. https://doi.org/10.3389/fphar.2016.00464

Vo, Q. N., Mahinthichaichan, P., Shen, J., & Ellis, C. R. (2021). How u-opioid receptor recognizes fentanyl. *Nature Communications, 12(1),* Article 1. https://doi.org/10.1038/s41467-021-21262-9

Wang, B., Zhang, L., Bae, S. C, & Granick, S. (2008). Nanoparticle-induced surface reconstruction of phospholipid membranes. *Proceedings of the National Academy of Sciences, 105(47),* 18171-18175. https://doi.org/10.1073/pnas.0807296105

Wang, L., Wu, Y., Deng, Y., Kim, B., Pierce, L., Krilov, G., Lupyan, D., Robinson, S., Dahlgren, M. K., Greenwood, J., Romero, D. L., Masse, C, Knight, J. L., Steinbrecher, T., Beuming, T., Damm, W., Harder, E., Sherman, W., Brewer, M., ... Abel, R. (2015). Accurate and reliable prediction of relative ligand binding potency in prospective drug discovery by way of a modern free-energy calculation protocol and force field. *Journal of the American Chemical Society, 137(1),* 2695-2703. https://doi.org/10.1021/ja512751q

Wantana, R., Niwat, K., & Sawangjaroen, K. (2007). Effects of the extracts from Mitragyna speciosa Korth. Leaves on analgesic and behavioral activities in experimental animals. *Songklanakarin Journal of Science and Technology, 29.*

Wilson, L. L., Harris, H. M., Eans, S. O., Brice-Tutt, A. C, Cirino, T. I, Stacy, H. M., Simons, C. A., Leon, F., Sharma, A., Boyer, E. W., Avery, B. A., McLaughlin, J. P., & McCurdy, C. R (2020). Lyophilized Kratom Tea as a Therapeutic Option for Opioid Dependence. *Drug and Alcohol Dependence, 216,* 108310. https://doi.Org/10.1016/j.drugalcdep.2020.108310

Yamamoto, L. T., Horie, S., Takayama, H, Aimi, N, Sakai, S., Yano, S., Shan, J., Pang, P. K. T., Ponglux, D., & Watanabe, K. (1999). Opioid receptor agonistic characteristics of mitragynine pseudoindoxyl in comparison with mitragynine derived from Thai medicinal plant Mitragyna speciosa. *General Pharmacology: The Vascular System,* 33(1), 73-81. https://doi.org/10.1016/S0306-3623(98)00265-1

Yildirim, M. A., Goh, K.-L, Cusick, M. E., Barabasi, A.-L., & Vidal, M. (2007). Drug-target network. *Nature Biotechnology,* 25(10), 1119-1126. https://doi. org/10.103 8/nbtl 33 8

Yusof, S. R., Mohd Uzid, M., Teh, E., Hanapi, N. A., Mohideen, M., Mohamad Arshad, A. S., Mordi, M. N., Loryan, I., & Hammarlund-Udenaes, M. (2018). Rate and extent of mitragynine and 7-hydroxymitragynine blood-brain barrier transport and their intra-brain distribution: The missing link in pharmacodynamic studies. *Addiction Biology, 24(5),* 935-945. https://doi.org/10.llll/adb.12661

APPENDICES

APPENDIX A

Trajectory Analysis of RMSD of 100 ns MD Simulation of Mitragynine, 7-hydroxymitragynine and mitragynine pseudoindoxyl. Run 1 (blue), Run2 (black) and Run 3 (red)

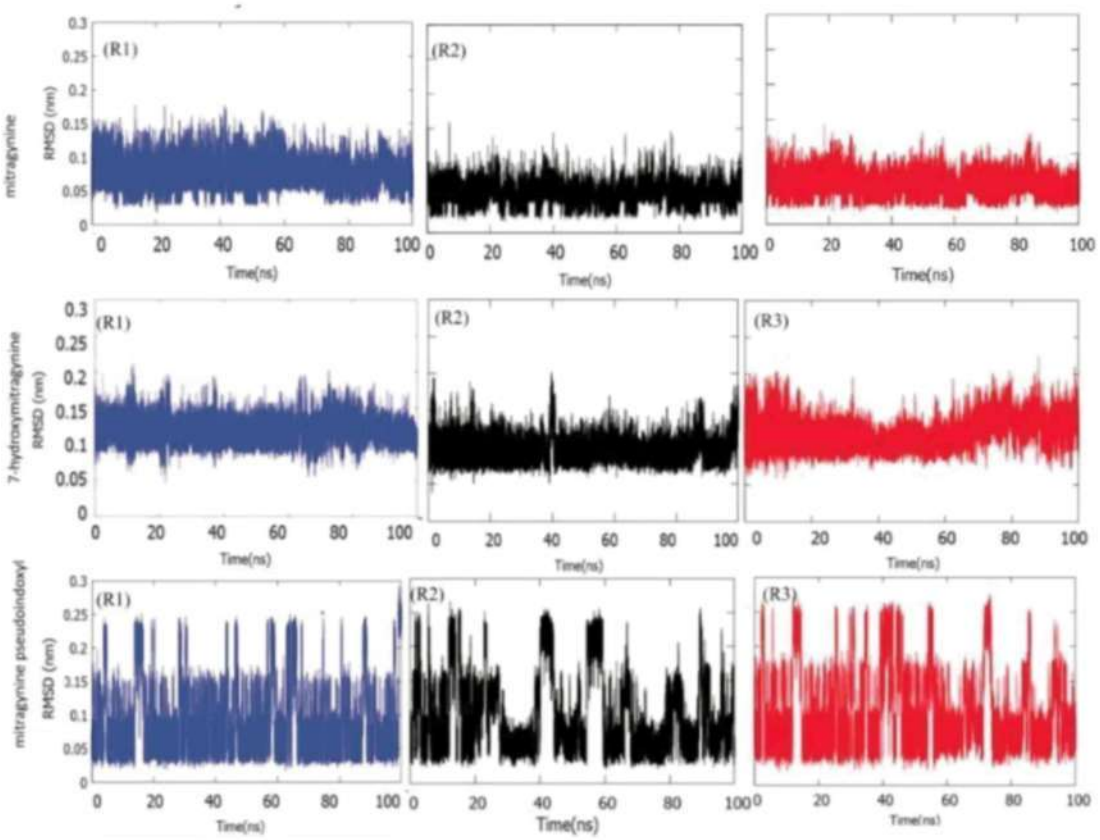

APPENDIX B

Trajectory Analysis of hydrogen bond of 100 ns MD Simulation of Mitragynine, 7- hydroxymitragynine and mitragynine pseudoindoxyl between water. Run 1 (blue), Run2 (black) and Run 3 (red)

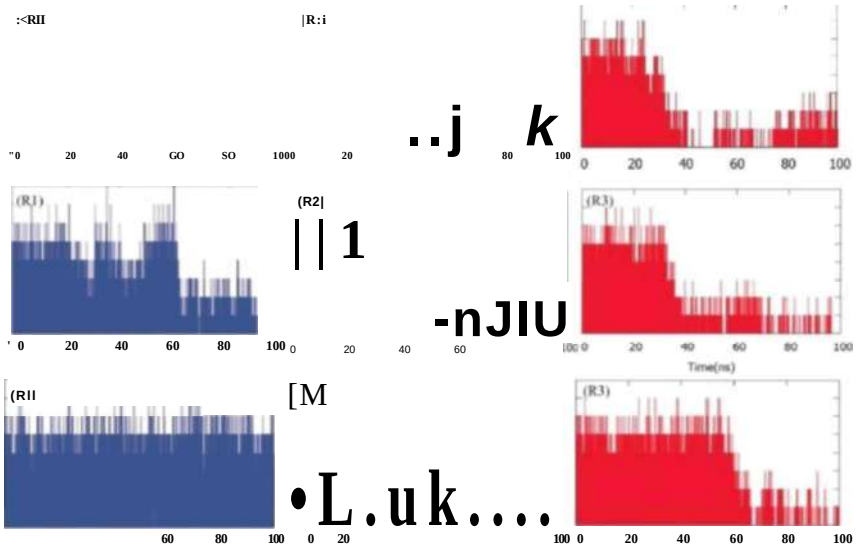

APPENDIX C

Trajectory Analysis of hydrogen bond between alkaloids and lipids. Run 1 (blue), Run2 (black) and Run 3 (red)

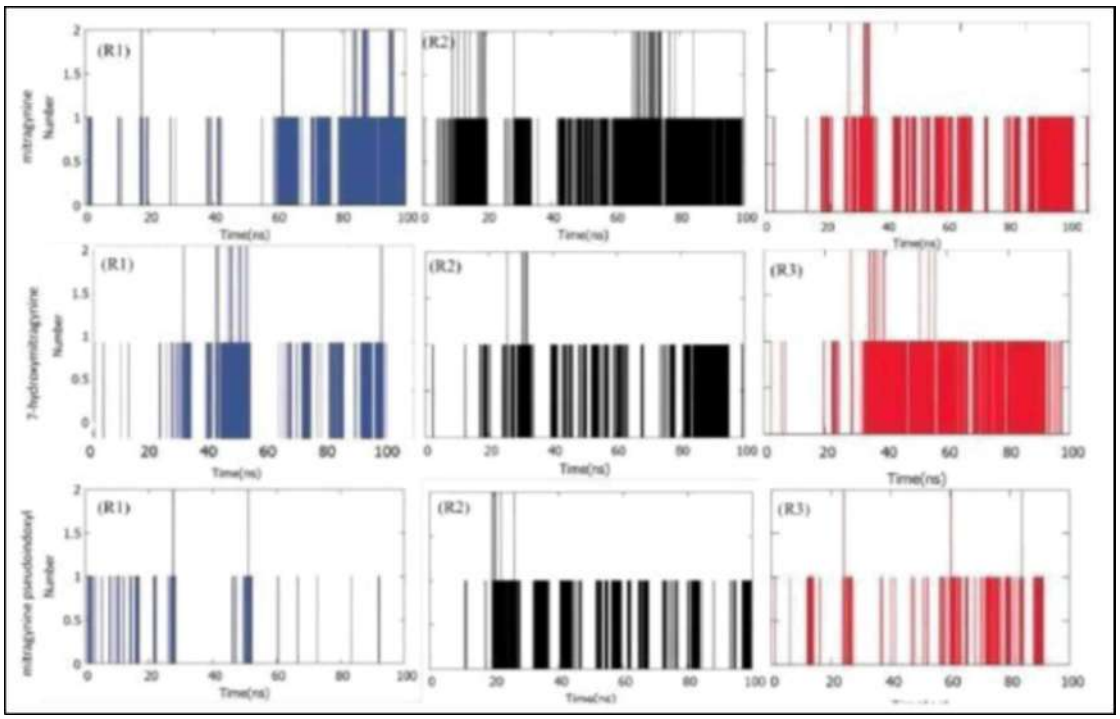

APPENDIX D

Root mean square deviation (RMSD) of the alkaloids during the 100 ns MD simulations. Replicate 1 (blue), replicate 2 (black) and replicate 3 (red).

Mean (nm) *l*± std deviation								
Mitragynine			7-hydroxymitragynine			Mitragynine pseudoindoxyl		
Rl	R2	R3	Rl	R2	R3	Rl	R2	R3
0.08/ ±0.02	0.06/± 0.02	0.06/± 0.02	0.12/± 0.02	0.10/± 0.02	0.12/ ±0.02	0.09/ ±0.05	0.10/± 0.06	0.10/ ±0.06

AUTHOR'S PROFILE

Nur Syahirunelisa Mohd Zubri obtained her Bachelor of Science in Biology (Hons.) in 2022 from Universiti Teknologi MARA (UiTM), Shah Alam. She is currently pursuing her Master of Science (MSc) at the Faculty of Pharmacy under the supervision of Dr. Siti Azma Jusoh. During her MSc studies. She is passionate about MD simulations, particularly in studying the interactions of alkaloids with lipid bilayers. Her research focuses on drug- membrane interactions, computational modeling of biomolecules.

LIST OF PUBLICATIONS

Mohd Zubri, N. S., Amirah Azhar, N. A., Amran, N. A., Weng, S. I. S., Awal, A., & Jusoh, S. A. (2025). Interactions of Kratom Alkaloids-Mitragynine, 7-Hydroxymitragynine, and Mitragynine Pseudoindoxyl with Lipid Bilayers: A Molecular Dynamics Study. International Journal of Pharmaceuticals, Nutraceuticals and Cosmetic Science, 8(1), 124-139. https://doi.org/10.24191/ijpnacs.v8il.09